Towards large-scale accurate Kohn-Sham DFT for the cost of tight-binding

Tiago Jose Remisio Marinheiro

Newcastle University

Newcastle upon Tyne, UK.

A thesis submitted to the School of Engineering for the degree of

Doctor of Philosophy

June 2019

Dedicado aos meus pais sem eles nada disto seria possivel.

And to Carmen and Alelo who have always been there and to whom I am eternally grateful,

Sete anos de pastor Jacob servia
Labão, pai de Raquel, serrana bela;
mas não servia ao pai, servia a ela,
e a ela só por prémio pretendia.

Os dias na esperança de um só dia
passava, contentando-se com vê-la;
porém o pai, usando de cautela,
em lugar de Raquel, lhe dava Lia.

Vendo o triste pastor que por enganos
lhe fora assi negada sua pastora,
como se a não tivera merecida,

Começa a servir outros sete anos,
dizendo: Mais servira, se não fora
para tão longo amor tão curta vida.

Luis Vaz de Camões

Acknowledgements:

First I would like to thank my supervisor Mark Rayson for giving me this opportunity. I have benefited immensely not only from his knowledge but from his ability to explain things at a fundamental level, this is what has always drawn me to Physics and I feel lucky to have had a supervisor who had the patience to do so. Thanks must also go to Patrick Briddon who helped me when I needed and from whom I have also learned much, I stand in awe at the breath of his knowledge and his ability to impart it.

I must also extend thanks to John Goss who always had an open door and a willingness to answer any questions. Further, I must thank all the people who made these 4 years less stressful, particularly Faiz. A big thanks also to James, Johan and Luke.

I would like to sincerely thank my parents who made all this possibly, their patience and help knows no bounds. They both went beyond what anybody could reasonably ask and nothing could ever repay what they did. I only hope that one day Alelo will look at me and feel the same level of love and admiration as I do for them. Finally, my greatest thanks must go to my wife, Carmen, who has endured by my side "though thick and thin" and listened to my lamentations. I could never thank you enough and I will spend the rest of my life trying. Serendipity brought us together and love pulled us through. We now go on to better things. And of course I must thank Alelo for his patience even if he didn't realize it. Grow beautiful and true. It is to them who I dedicate this thesis.

Abstract

Density functional theory (DFT) is a widely used *ab initio* quantum mechanical method to study the properties of materials. Over the past 20 years a huge amount of work has been done developing codes that are able to tackle calculations containing large numbers of atoms. `AIMPRO`, a DFT code which uses Gaussian type orbitals (GTO) as a basis set, uses a filtration methodology which makes calculations with a few thousand atoms routinely possible on desktop machines. Previous implementations of filtration have focused on the time saving aspect of the methodology and performed calculations on structures containing only atoms from a small subset of the periodic table.

In this thesis a novel basis set generation routine is presented and the filtration methodology is modified and expanded to include most of the atoms in the periodic table. The focus of this work lies in demonstrating the potential gains in *accuracy*, in *addition* to efficiency, available through use of the filtration algorithm and shows that results comparable to codes using systematic basis set can be achieved for each of the elements considered across the periodic table. Two huge advantages present themselves using this scheme; firstly, the time to solution is essentially decoupled from the basis size; secondly, basis sets that would be unstable in a conventional calculation can be used allowing for more accurate calculations.

The work presented here is assessed using a recently developed benchmark, the Δ-test. This, together with the increases in speed previously demonstrated, shows that a filtered basis calculation can now achieve the accuracy of a plane wave calculation at the asymptotic cost, with respect to system size, of a tight-binding calculation, enabling Kohn-Sham calculations of unprecedented size to be performed at the basis set limit.

Contents

List of Figures

List of Tables

Chapter 1

Introduction

Density Functional Theory (DFT) has emerged as one of the significant developments in applying quantum mechanics. From just the position of a group of atoms one can calculate many of its ground state properties without a need for any empirical input. DFT results have been widely used accompanying experimental data for the past 50 years, often as a type of validation. With the increase in accuracy and scope of DFT more calculations become feasible allowing for different applications. In addition to accompanying experiments it is not uncommon nowadays to encounter research where DFT has been used in a predictive capacity to model properties inaccessible to experiment or even novel compounds, as yet not seen experimentally.

As a byproduct of it's success at predicting many material properties, DFT has been increasingly adopted in a growing number of research fields, which often necessitate tailored or particular types of implementation which then drives research into DFT theory and methodology. Out of this symbiotic relationship a need for efficient (i.e. fast) and accurate calculations has emerged. It is not hard to fathom the possibilities that codes which can tackle more than 1000 atoms have to offer, and although calculations on that range and higher are now possible it is often at the behest of accuracy.

`AIMPRO` a Kohn-Sham DFT (KSDFT) code which uses Gaussian Type Orbitals (GTO) has recently implemented a filtration methodology where small contracted (filtered) basis sets are constructed during the DFT calculation from the underlying primitive basis set. This method has been used to reduce the computational time of a regular KSDFT calculation to that of a semi-empirical implementation [5], which allows for systems with 1,000-10,000 atoms to be studied routinely on a computer with moderate power. In this thesis the possiblity to use of the filtration methodology to perform calculations with very large basis sets, which would otherwise be infeasible in regular `AIMPRO` calculations, is explored for the first time. This, we will show, allows for calculations with an accuracy close to that of well converged plane wave implementations at the cost of a convetional `AIMPRO` calculation.

A new method to generate basis set is introduced here, which produces very accurate basis sets with large numbers of functions. A new robust routine is introduced which uses a discrete variable representation code to converge the energy of a pseudo-atom, so that the GTO basis set is generated based on the accurate minimization of the pseudo-atomic energy. Furthermore the basis set are generated with properties that suit their usage with the filtration methodology. This large basis sets will then be tailored *in situ* using filtration for the environment at hand, this allows for a great degree of transferability and user friendliness by using only one basis set and having the calculation accuracy controlled by one parameter (set by the filtration methodology), both these charachteristics are typically missing from any GTO implementation.

A modified filtration methodology is presented here to handle the large basis sets that are used in this thesis. Unlike previous versions of the filtration methodology, the one used in this work produces an atomic filtered basis sets by contracting functions only from the respective atom's undelying primitive basis set. This allows the large basis sets to be used which yields a good level of tranferability, and an unprecedented accuracy for filtration calculations. Whereas before [5] filtration calculations were compared with standard `AIMPRO` ones, in this work we will be comparing directly to very well converged plane wave results. A comprehensive benchmark [6] is used to ensure a periodic-table-wide applicability of our method.

It is shown in this thesis, that we can obtain PW accuracy at a cost of an efficient GTO calculation. Furthermore this accuracy is approached systematically in `AIMPRO` using the same large primitive basis set. Although an impressive result on it's own, the work presented here sets the stage for an astounding future work: Large scale calculations with an accuracy of plane waves at the cost of tight-binding.

1.1 Summary of the thesis

The work presented here can be broadly subdivided into four parts, theoretical background, implementation of a new basis set and on-site filtration, results and finally conclusion and future works. Below follows a summary of the individual chapters.

Chapter 2: Reviews some basic ideas in the theory of quantum mechanics, with particular emphasis on topics which underlie the foundations of this work, and which will be mentioned throughout this thesis. In addition, some early methods which solve the interacting many-body quantum Hamiltonian are briefly summarized.

Chapter 3: Reviews the basic tenets of density functional theory, such as the Hohenberg-Kohn theorems and the Kohn-Shams equation. Methodologies to handle fractional occu-

pation and spin polarization are reviewed here too. In the last part of this chapter a brief discussion on boundary conditions is presented.

Chapter 4: Presents a brief overview of code specific details in different KSDFT implementations. Our discussion here is focused on the different basis set and the introduction of pseudopotentials. Finally an efficient Hamiltonian and overlap matrix construction used in `AIMPRO` is outlined.

Chapter 5: Introduces our novel basis set generation which produces a large uncontracted even-tempered basis set. This is used to generate basis sets for the 70 elements used in the benchmark considered in chapter 8. These basis sets would be too large for regular `AIMPRO` calculations were it not for filtration.

Chapter 6: Presents a revised filtration methodology which contracts the large primitive basis on-site to produce a contracted filtered basis. This together with the basis set generated in the previous chapter lays the groundwork for very accurate calculations.

Chapter 7: Summarizes a recently developed benchmark, which can be taken to be the best pass/fail indicator of the quality of a code. Results obtained using the new basis sets and filtration methodology for the set of elements in this benchmark are presented. A slightly modified version of the benchmark is introduced and used which, we show, assess the quality of our basis set and filtration more accurately than the standard version.

Chapter 8: Presents results for ideal vacancy formation energies calculated using the basis sets and filtration and compares them with results obtained using a PW implementation.

Chapter 9: Presents our conclusion and outlines the possible avenues of research for future work.

1.2 Abbreviations

Although care has been taken to ensure that the abbreviations used throughout this thesis is clear, the following list includes the most common ones to help the reader.

- **DFT**: Density Functional Theory
- **KSDFT**: Kohn-Sham Density Functional Theory
- **GTO**: Gaussian Type Orbital

- **PW**: Plane Wave
- **HK**: Hohenberg-Kohn
- **STO**: Slater-type orbital
- **GGA**: Generalized Gradient Approximation
- **PBE**: Perdew-Burke-Ernzerhof exchange-correlation
- **DVR**: Discrete Variable Representation
- **EOS**: Equation Of State
- **r.m.s.**: root-mean-square
- **GEP**: Generalized Eigenvalue Problem
- **OEP**: Ordinary Eigenvalue Problem

Chapter 2

Quantum Mechanics

2.1 Introduction

In this chapter we will briefly review the quantum mechanic formalism that serves as the foundation for later chapters. The equations which describe the behaviour of a system of electrons under the potential originating from a group of nucleus are introduced and some of the first solutions developed to tackle such a problem are summarized.

2.1.1 The Single particle Hamiltonian

Most quantum mechanics problems involve solving what is known as the Schrödinger equation. In this thesis we are concerned with static properties, for this we only need to solve the time-independent Schrödinger equation which can be written as:

$$\Big[\frac{-\hbar^2}{2m}\bigtriangledown^2 + V(\mathbf{r})\Big]\psi(\mathbf{r}) = E\psi(\mathbf{r}) \tag{2.1}$$

where $\hbar$ is Planck's constant, $V(\mathbf{r})$ is the potential and $\psi(\mathbf{r})$ is the particle's wave function. Equation (2.1) can be rewritten as:

$$H(\mathbf{r})\psi(\mathbf{r}) = E\psi(\mathbf{r}) \tag{2.2}$$

where:

$$H(\mathbf{r}) = V(\mathbf{r}) + T \tag{2.3}$$

in which T is the kinetic energy and $H(\mathbf{r})$ is known as the Hamiltonian. This formalism is widely used in Hamiltonian mechanics a reformulation of classical mechanics. In classical mechanics, and similarly in quantum mechanics, the Hamiltonian is a function (in the case of classical mechanics) which represents the total energy of a system.

The established classical Hamiltonian "corresponds" to a quantum Hamiltonian under

the following canonical substitution:

$$\mathbf{p} \rightarrow -i\hbar \frac{d}{d\mathbf{r}} \tag{2.4}$$

Solving equation (2.2), a non-linear partial differential equation, amounts to finding the eigenfunctions (wave functions) and eigenvalues (energies) of H so that:

$$H(\mathbf{r})\psi_n(\mathbf{r}) = E_n\psi_n(\mathbf{r}) \tag{2.5}$$

where $\psi_n(\mathbf{r})$ are the eigenstates of $H(\mathbf{r})$ with an associated eigenvalue E_n.

The set of eigenfunction $\psi_n(\mathbf{r})$ forms a complete basis for the representation of the system i.e. any state $\Psi(\mathbf{r})$ under the influence of the potential $V(\mathbf{r})$ can be represented by one of the eigenstates or, most commonly, by a linear combination of eigenstates.

$$\Psi(\mathbf{r}) = \sum_n c_n\psi_n(\mathbf{r}) \tag{2.6}$$

where c_n are known as the coefficients of expansion. Typically each ψ_n is normalized.

$$\int \psi_i^*(\mathbf{r})\psi_i(\mathbf{r})d\mathbf{r} = 1 \tag{2.7}$$

where $\psi^*(\mathbf{r})$ is the complex conjugate of $\psi(\mathbf{r})$. In addition, since ψ_n are the eigenfunctions of $H(\mathbf{r})$, which is Hermitian, they must be mutually orthogonal:

$$\int \psi_i^*(\mathbf{r})\psi_k(\mathbf{r})d\mathbf{r} = \delta_{ik} \tag{2.8}$$

It is often simpler, and more common, to express the previous equations and most quantum mechanical operations in the Dirac bra-ket notation. A vector-function $\psi_i(\mathbf{r})$ is represented as ket ($|\psi_i\rangle$) and the co-vector $\psi_i^*(\mathbf{r})$ as a bra ($\langle\psi_i|$). In this notation the Hamiltonian $H(\mathbf{r})$ is expressed as an operator, typically denoted by the hat symbol $\hat{H}$. Using the bra-ket notation equation (2.7) can be retyped as:

$$\langle\psi_i|\psi_i\rangle = \int \psi_i^*(\mathbf{r})\psi_i(\mathbf{r})d\mathbf{r} = 1 \tag{2.9}$$

similarly for eq. (2.1)

$$\hat{H}\,|\psi_n\rangle = E_n\,|\psi_n\rangle \tag{2.10}$$

Where appropriate throughout this thesis the bra-ket notation is used.

2.2 Operators

In quantum mechanics, physical properties of a particle that are functions of either the coordinates or momentum are represented by linear operators ($\hat{O}$). These operators act on the wave function and yield a set of results with an associated probability of measuring said result. The average result one would obtain by performing a physical measurement of $\hat{O}$ in a state $\Psi(\mathbf{r})$ is known as the *expectation* value of the operator. The expectation value of $\hat{O}$ is given by:

$$\langle \hat{O} \rangle = \int \Psi^*(\mathbf{r}) \hat{O} \Psi(\mathbf{r}) d\mathbf{r} = \langle \Psi | \hat{O} | \Psi \rangle \tag{2.11}$$

Given that $\langle \hat{O} \rangle$ must be real valued - since it has to correspond the average measured value of an observable - the operator $\hat{O}$ must be Hermitian, $\hat{O} = \hat{O}^*$ or:

$$\langle \hat{O} \rangle = \int \Psi^*(\mathbf{r}) \left(\hat{O} \Psi(\mathbf{r}) \right) d\mathbf{r} = \int \left(\hat{O} \Psi(\mathbf{r}) \right)^* \Psi(\mathbf{r}) d\mathbf{r} \tag{2.12}$$

A linear operator with the properties described above has an associated spectrum of eigenvectors. In quantum mechanics it is assumed that this spectrum is complete and therefore forms a representation of the system [7]. Thus if $\psi_i(\mathbf{r})$ are the eigenvectors associated with $\hat{O}$ any state $\Psi(\mathbf{r})$ can be expanded as follows:

$$\Psi(\mathbf{r}) = \sum_i^\infty c_i \psi_i(\mathbf{r}) \tag{2.13}$$

The expectation value equation (2.12) can then be recast:

$$\langle \hat{O} \rangle = \int \Psi^* \hat{O} \Psi = \int \Big(\sum_i^\infty c_i \psi_i^* \Big) \hat{O} \Big(\sum_i^\infty c_i \psi_i \Big) = \sum_i^\infty o_i c_i^2 \tag{2.14}$$

where o_i are the eigenvalues of the respective eigenfuctions ψ_i and the previous derivation used the orthonormality of the eigenfunctions. The Hamiltonian is itself an operator with the eigenvalues being the range of energies the system can take.

2.2.1 Finite space

When dealing with linear operators in a finite space it is preferable to use the language of linear algebra and represent the operators as matrices and the eigenfunctions as vectors (eigenvectors, ψ_n).

Let $\Psi = \sum_n c_n \psi_n$ be a wavefunction expanded in a complete set of functions,ψ_n. For any linear operator $\hat{O}$ the expectation value can be written (in similar fashion to eq (2.14))

as :

$$\langle \hat{O} \rangle = \int \Psi^*(\mathbf{r}) \hat{O} \Psi(\mathbf{r}) d\mathbf{r} = \sum_n \sum_m c_m c_n O_{mn} \tag{2.15}$$

However, in contrast to eq. (2.14), where $\psi_i(\mathbf{r})$ were the eigenfunctions of $\hat{O}$, the $\psi_i(\mathbf{r})$ in the previous equation are not necessarily eigenvalues of the operator $\hat{O}$. So we have,

$$O_{mn} = \int \psi_m^*(\mathbf{r}) \hat{O} \psi_n(\mathbf{r}) d\mathbf{r} \tag{2.16}$$

and,

$$O_{mn} \neq \delta_{mn} o_n \tag{2.17}$$

where O_{mn} is the matrix formulation of the operator $\hat{O}$ in the representation we chose and o_n are the eigenvalues $\hat{O}$. Throughout this thesis when dealing with matrices, and similarly for vectors, bold letters are used, i.e. the matrix representation of $\hat{O}$ is written as $\mathbf{O}$ and $\Psi(\mathbf{r}) = \sum c_n \psi_n = \mathbf{\Psi}$ (where the vector entries would be the expansion coefficients c_n).

Expanding the expectation value equation (written in matrix form as $\mathbf{O\Psi} = o\mathbf{\Psi}$) we have:

$$\sum_m c_m (\hat{O} \psi_m) = o \sum_m c_m \psi_m \tag{2.18}$$

Multiplying both sides of the equation by ϕ_n^* and integrating, we have (given that the ϕ_n are normalized and orthogonal):

$$\sum_m c_m (\psi_n^* \hat{O} \psi_m) = o \sum_m c_m \phi_n^* \phi_m \tag{2.19}$$

This is simply:

$$\sum_m c_m O_{mn} = o c_n \tag{2.20}$$

Here $\sum c_m$ can be taken as a vector, rearranging the previous equation:

$$\sum_m (O_{mn} - o\delta_{mn}) c_m = 0 \tag{2.21}$$

This is just a regular eigenvalue problem from linear algebra ($\mathbf{Mv} = v\mathbf{v}$) which has a non zero solution if and only if the following determinant is equal to zero:

$$|O_{mn} - o\delta_{mn}| = 0 \tag{2.22}$$

In summary, once a representation is set, solving the Schrödinger equation can be transformed into a linear algebra problem, very suitable for implementation on a modern computer.

2.2.2 The variational principle

The expectation value of the Hamiltonian can be seen as a functional of the wave function $|\Psi\rangle$, $\langle E\rangle = \langle\Psi|\,\hat{H}\,|\Psi\rangle = E[\Psi]$. From this perspective, one can apply a powerful mathematical method from the calculus of variations, known as the variational principle. Let us now slightly perturb the wave function $|\Psi\rangle \to |\Psi\rangle + |\delta\Psi\rangle$, the change in $E[\Psi]$ is given by:

$$\begin{aligned}\delta E[\Psi+\delta\Psi] &= E[\Psi+\delta\Psi] - E[\Psi] \\ &= \frac{\langle\Psi+\delta\Psi|\hat{H}|\Psi+\delta\Psi\rangle}{\langle\Psi+\delta\Psi|\Psi+\delta\Psi\rangle} - \frac{\langle\Psi|\hat{H}|\Psi\rangle}{\langle\Psi|\Psi\rangle} \\ &= \frac{1}{\langle\Psi|\Psi\rangle}\left[\langle\delta\Psi|\left(\hat{H}\,|\Psi\rangle - E[\Psi]\,|\Psi\rangle\right) + c.c.\right]\end{aligned} \tag{2.23}$$

Where c.c. stands for complex conjugate and the second (or higher) order terms of $\delta\Psi$ have been neglected. We find that $E[\Psi]$ is stationary, that is $\delta E[\Psi] = 0$, when Ψ is an eigenvalue of $\hat{H}$. It follows from equation (2.23) that the eigenvalues of $\hat{H}$ can be found obtained by finding the stationary values of $E[\Psi]$, subject to $\langle\Psi|\Psi\rangle$ being constant (typically equal to unity).

For most of this thesis DFT will be used, where the electronic ground-state ψ_0 (which is the state of $\hat{H}$ with the lowest eigenvalue) is the main quantity of interest. Assume then that we are searching for the ground state function $|\psi_0\rangle$ and we find a wave function ($|\Psi\rangle$), which we normalize. Given that the set of ϕ_i form a complete representation we can expand the error of our approximation ($\delta\Psi$) w.r.t to the ground-state, in the following way

$$|\Psi\rangle = |\psi_0\rangle + |\delta\Psi\rangle = |\psi_0\rangle + \sum_{i=1}^{\infty} c_i\,|\psi_i\rangle \tag{2.24}$$

in which $i = 0$ is excluded from the sum and we assume that the ground state is non-degenerate. Calculating $E[\Psi]$ we find that:

$$\begin{aligned}E[\Psi] = E_0 + E\Big[\sum c_n\phi_n\Big] &= E_0 + \sum_{i,j} c_i^* c_j\,\langle\psi_i^*|\hat{H}|\psi_j\rangle \\ &= E_0 + \sum_{i,j} c_i^* c_j E_j\,\langle\psi_i^*|\psi_j\rangle\end{aligned} \tag{2.25}$$

Since $E_0 < E_j$, and ψ_i are orthonormal we have:

$$E[\Psi] > E_0 + \sum_{i,j} c_i^* c_j E_0\,\langle\psi_i^*|\psi_j\rangle = E_0\left(1 + \sum_j |c_j|^2\right) \tag{2.26}$$

The variational principle then gives us two important properties:

1. $E[\Psi] > E[\psi_0]$; for any energy calculated from a guess function will always be higher

than $E[\psi_0]$

2. The error in energy depends on the square of the error in the wave function.

2.2.3 The Rayleigh-Ritz method

The variational principle explained in the previous section allows us to employ the Rayleigh-Ritz method to approximate solutions to the time independent Schrödinger equation and end up with a finite dimensional problem. Let us assume that we approximate the ground state with a trial function $|\Psi\rangle$. This function can be expanded in a finite set of *basis functions* ($\phi_i(r)$), which we might take to be any set of normalized functions and not necessarily eigenfunctions of any operator,

$$\Psi(r) = \sum_{i=1}^{n} c_i \phi_i(r) \tag{2.27}$$

The Rayleigh-Ritz method thus allows one to cast the problem of minimizing $E[\Psi]$ into one of finding a set of $(c_1, c_2, .., c_n)$ which minimizes $E[c_1, c_2, .., c_n]$, with our trial function approaching the true ground state as $n \to \infty$. The variational principle ensures that as the quality of our trial function increases the respective energy will tend to the true ground state value.

In this thesis non-orthogonal functions will be used. When using non-orthogonal basis sets the time-independent Schröndinger equation is mapped into a generalized eigenvalue problem (GEP) :

$$\mathbf{H}\,|\Psi\rangle = \epsilon \mathbf{S}\,|\Psi\rangle \tag{2.28}$$

Where $\mathbf{S}$ is know as the *overlap* matrix, with elements given by

$$S_{ij} = \int \phi_i(\mathbf{r})\phi_j(\mathbf{r}) d\mathbf{r} \tag{2.29}$$

The overlap matrix and non-orthogonal basis sets will be discussed in later chapters.

2.3 Angular momentum

Later on in the thesis some methods will be introduced in which the angular momentum of electrons in different states is used to justify a particular choice of functions, therefore a brief overview of the quantum mechanical treatment of angular momentum is presented here.

In classical mechanics the angular momentum of a particle is given by:

$$\hat{L} = \hat{r} \times \hat{p} \tag{2.30}$$

As mentioned previously, any observable has a corresponding linear operator in quantum mechanics. Using the quantum mechanical operator form of momentum $\hat{p} = -i\hbar\bigtriangledown$ (itself given by the canonical substitution) we arrive at a vector representation of the angular momentum operator:

$$\mathbf{L} = -i\hbar\mathbf{r} \times \bigtriangledown \tag{2.31}$$

Using equation 2.31 we can derive the following commutation relations:

$$[\hat{L}_x, \hat{L}_y] = i\hbar\hat{L}_z, \quad [\hat{L}_y, \hat{L}_z] = i\hbar\hat{L}_x, \quad [\hat{L}_z, \hat{L}_x] = i\hbar\hat{L}_y \tag{2.32}$$

Where :

$$[\hat{L}_i, \hat{L}_j] = \hat{L}_i\hat{L}_j - \hat{L}_j\hat{L}_i \tag{2.33}$$

With the intent of finding eigenvectors and eigenvalues of $\hat{L}$ we introduce the following operator,

$$\hat{L}^2 = \hat{L}_x^2 + \hat{L}_y^2 + \hat{L}_z^2 \tag{2.34}$$

which in vector terms is the magnitude of $\mathbf{L}$. In addition let us introduce the *ladder* operators:

$$\hat{L}_\pm = \hat{L}_x \pm i\hat{L}_y \tag{2.35}$$

The $\hat{L}_\pm$ are known as the ladder operators because they either raise or lower the eigenvalue of $\hat{L}_z$ by $\hbar$. That is let f be an eigenstate of $\hat{L_z}$ with eigenvalue β (by construction f is also an eigenvector of $\hat{L}^2$ with eigenvalue α),

$$\hat{L}_z\hat{L}_\pm f = (\beta \pm \hbar)\hat{L}_\pm f \tag{2.36}$$

We can derive the following commutators for the ladder operators,

$$[\hat{L}_z, \hat{L}_\pm] = \pm\hbar\hat{L}_\pm \tag{2.37}$$

and

$$[\hat{L}^2, \hat{L}_\pm] = 0 \tag{2.38}$$

Furthermore $\hat{L}^2$ can be written in terms of the ladder operators in the following way:

$$\hat{L}^2 = \hat{L}_\pm\hat{L}_\mp + \hat{L}_z^2 \mp \hbar\hat{L}_z \tag{2.39}$$

We can now find relations for the eigenvectors of $\hat{L}^2$ and $\hat{l_z}$ by systematic application of the raising and lowering ladder operators to a state (call it f) assumed to be the highest and lowest, respectively, eigenstate of $\hat{L}_z$ and using equation (2.39). A detailed explanation of this is unnecessary and can be found in [8]. From this we find that in

quantum mechanics the angular momentum of f is quantized. Furthermore the angular momentum of a state can be described by 2 quantum numbers m and l (f can therefore be expressed as $|l, m\rangle$ with regards to angular momentum) which are related to eigenvalues of L^2 and L_z,

$$\hat{L}^2 |l, m\rangle = \hbar^2 l(l+1) |l, m\rangle); \quad \hat{L}_z |l, m\rangle = \hbar m |l, m\rangle) \tag{2.40}$$

where $l = 0, 1, 2....$ is the total angular momentum of the state and $m = -l, -l+1, ..., l-1, l$ is the angular momentum projected along the Z-axis (the direction of measurement is arbitrary chosen but conventionally we use Z-axis). These two quantum numbers, allow us to construct a vector model of the atom, in terms of angular momentum which explains the Bohr model of the atom. This momentous result elucidates in large part the atomic nature of electronic structure, and together with the principal quantum number (representing different eigensolution of the Hamiltonian) and the spin quantum number (explained next section) fully describe an electron in an atom (in a non-relativistic treatment).

2.4 Fermions and Bosons

When looking at the macroscopic world one can always, in theory, discern the path of a specific object, however for atomic particles the same is not true. This is a direct consequence of physical observations being eigenvalues of operators. "Observing" a particle requires a measurement of some kind, position for example $\hat{r}$. However before any measurement is performed, i.e. an operator is applied to a state, there is no a priori requirement that the state must be in a specific eigenstate of said operators.

Consider a system of two electrons, and let us measure their position. Let us say that we found the electrons to be at $\mathbf{r}_\mathrm{a}$ and $\mathbf{r}_\mathrm{b}$. At a later time we again measure the positions of the two electrons and we find $\mathbf{r}_\mathrm{c}$ and $\mathbf{r}_\mathrm{d}$. One can not say if the electron which was previously at $\mathbf{r}_a$ is now at $\mathbf{r}_\mathrm{c}$ and similarly if $\mathbf{r}_\mathrm{b}$ is now at $\mathbf{r}_\mathrm{d}$, or vice-versa. As far as quantum mechanics is concerned one electron is indistinguishable from another. The easiest way to accommodate indistinguishable particles when constructing a many electron wave function from single particle states is to not commit a particle to a specific state. For a system of two indistinguishable particles $(\mathbf{x}, \mathbf{y})$ we can write

$$\Psi_\pm(\mathbf{x}, \mathbf{y}) = [\psi_a(\mathbf{x})\psi_b(\mathbf{y}) \pm \psi_a(\mathbf{y})\psi_b(\mathbf{x})] \tag{2.41}$$

where Ψ_- corresponds to *fermions*, like electrons, and Ψ_+ to *bosons*, like photons. The underlying theory of fermions and bosons is derived in relativistic quantum mechanics. In quantum mechanics however, the division of atomic particles into fermions and bosons is axiomatic.

An important consequence of electrons being fermions is the requirement that any

wave function describing a system of interacting electrons be anti-symmetric. Let $\hat{P}_{\mathbf{xy}}$ be the operator that changes the coordinates $\mathbf{x}$ to $\mathbf{y}$ (which amounts to interchanging the particles). Applying $\hat{P}_{\mathbf{xy}}$ to the fermionic wavefunction (Ψ_- from equation (2.41)) we have,

$$\hat{P}_{\mathbf{xy}}\Psi_-(\mathbf{x},\mathbf{y}) = -\Psi_-(\mathbf{x},\mathbf{y}) \tag{2.42}$$

A further consequence of the anti-symmetry is that no two identical particles can occupy the same state:

$$\Psi(\mathbf{x},\mathbf{y}) = [\psi_a(\mathbf{x})\psi_a(\mathbf{y}) - \psi_a(\mathbf{y})\psi_a(\mathbf{x})] = 0 \tag{2.43}$$

Equation (2.43) is the famous Pauli exclusion principle, which states that: two electrons can not occupy the same state, i.e no two electrons can have the same quantum numbers (more on this in the next section). The anti-symmetry requirement of a wave function of electrons adds complications to any electronic calculations as we will see over the next few sections.

2.5 Spin

Before the advent of quantum physics, it was already known that atoms with even numbers of electrons were more stable than those with odd numbers. This order is a manifestation of an underlying theory that, even after the first strides of quantum mechanics, was not fully understood.

Niels Bohr, in an attempt to explain this behaviour, suggested that the perceived stability was a result of the electrons being order in groups 2, 6 and 8 in what he called "closed shell " packing [9].

From the section on angular momentum we know that an eigenstate of the angular momentum operator can be specified by the quantum numbers l and m_l. Similarly eigenstates of a Hamiltonian (2.1) can be specified by the *principal quantum number* n. Using all of the aforementioned quantum numbers and the exclusion principle one still is not able to explain the closed shell packing. To do this Wolfgang Pauli introduced a new quantum number called *Spin*, the electron was assumed to be a particle with *spin quantum number* of magnitude $\frac{1}{2}$. When measured along an axis the spin operator ($\hat{S}_i$) has only two eigenstates, which we label m_s with corresponding eigenvalues of $\frac{1}{2}\hbar$ and $-\frac{1}{2}\hbar$. This new spin quantum number together with Pauli's exclusion principle, which states that no two electrons can have the same set of quantum numbers (n, l, m_l, m_s), explains closed shell packing and a good part of the atomic structure in nature. Relativistic quantum mechanics would later verify Pauli's assumption, Dirac eventually showed that indeed the electron has an immutable spin quantum number of $\frac{1}{2}$.

However Pauli's assignment of a spin quantum number was not just an ad-hoc assump-

tion. The Stern-Gerlach experiment in 1922 [7] demonstrated the need for an "intrinsic" angular momentum of the electron, which would eventually be labelled spin and, the z-component of which, is quantized in units of $\frac{1}{2}\hbar$.

The algebraic treatment of the spin is similar to that for angular momentum. The commutators of the spin operators along the different axis are:

$$[\hat{S}_x, \hat{S}_y] = i\hbar\hat{S}_z, \quad [\hat{S}_y, \hat{S}_z] = i\hbar\hat{S}_x, \quad [\hat{S}_z, \hat{S}_x] = i\hbar\hat{S}_y \tag{2.44}$$

Constructing the $\hat{S}^2$ operator as before:

$$\hat{S}^2 = \hat{S}_x^2 + \hat{S}_y^2 + \hat{S}_z^2 \tag{2.45}$$

And introducing ladder operators:

$$\hat{S}_\pm = \hat{S}_x^2 \pm \hat{S}_y^2 \tag{2.46}$$

we find as before:

$$\hat{S}^2 \left|s, m_s\right\rangle = \hbar^2 s(s+1) \left|s, m_s\right\rangle); \hat{S}_z \left|l, m_s\right\rangle = \hbar m_s \left|l, m_s\right\rangle) \tag{2.47}$$

where $s = 0, \frac{1}{2}, 1, \frac{3}{2}, 2....$ and $m_s = -s, -s-1, ..., s-1, s$.

However unlike the case of angular momentum the spin value (s) of a particle is immutable, it is one of their defining characteristics. For this thesis the quantum mechanical treatment of spin presented here suffices.

For most calculations performed in this thesis the systems will be in a *spin unpolarized* state i.e. there will be no net spin. However there will be some systems with ferromagnetic and anti-ferromagnetic properties, this requires a slightly different approach which will be explained in the next chapter.

2.6 The Many-Body Hamiltonian.

Expanding on the previous sections one must now construct the Hamiltonian for a system of N electrons in a potential field generated by K nuclei with charge Z_n. This is the typical Hamiltonian for electronic structure studies often called the *many-body interacting Hamiltonian*, which can be written in the following form:

$$\begin{aligned}\hat{H}(\mathbf{r}_n, \mathbf{R}_k) = &\sum_{i=1}^{N} \frac{\mathbf{p}_i^2}{2m_e} + \sum_{n=1}^{K} \frac{\mathbf{p}_n^2}{2M_n} + \frac{1}{4\pi\epsilon_0}\frac{1}{2} \sum_{i,j=1;i\neq j}^{N} \frac{e^2}{|\mathbf{r}_i - \mathbf{r}_j|} \\ &- \frac{1}{4\pi\epsilon_0} \sum_{n=1}^{K}\sum_{i=1}^{N} \frac{Z_n e^2}{|\mathbf{r}_i - \mathbf{R}_n|} + \frac{1}{4\pi\epsilon_0}\frac{1}{2} \sum_{n,n'=1;n\neq n'}^{K} \frac{Z_n Z_{n'} e^2}{|\mathbf{R}_n - \mathbf{R}_{n'}|}\end{aligned} \tag{2.48}$$

where the indexes i and n label sums over the electrons and the nuclei respectively, M_n are the masses of different nuclei and m is the electron mass. The first two terms of the Hamiltonian (2.51) represent the kinetic energy of the electrons and nuclei respectively. The remaining terms are, the electron-electron, nuclear-electron and nuclear-nuclear Coulomb interactions.
Once we have this Hamiltonian we must solve the time-independent Schrödinger equation given by,

$$\hat{H}(\mathbf{r}_n, \mathbf{R}_k)\Psi(\mathbf{r}_n, \mathbf{R}_k) = E\Psi(\mathbf{r}_n, \mathbf{R}_k) \tag{2.49}$$

where now, $\Psi(\mathbf{r}_n, \mathbf{R}_k)$ depends on both electronic and nuclear coordinates.

Equation (2.48) is best written in atomic units where,

$$e = m_e = \hbar = \frac{e^2}{4\pi\epsilon_0} = 1 \tag{2.50}$$

Energy is then expressed in terms of the Hartree (27.2 eV) and distance in terms of the Bohr radius a_0. Rewriting equation (2.48) in atomic units we have,

$$\begin{aligned}\hat{H} = &\sum_{i=1}^{N} \frac{\mathbf{p}_i^2}{2} + \sum_{n=1}^{K} \frac{\mathbf{p}_n^2}{2M_n} + \frac{1}{2} \sum_{i,j=1;i\neq j}^{N} \frac{1}{|\mathbf{r}_i - \mathbf{r}_j|} \\ &- \sum_{n=1}^{K}\sum_{i=1}^{N} \frac{Z_n}{|\mathbf{r}_i - \mathbf{R}_n|} + \frac{1}{2} \sum_{n,n'=1;n\neq n'}^{K} \frac{Z_n Z_{n'}}{|\mathbf{R}_n - \mathbf{R}_{n'}|}\end{aligned} \tag{2.51}$$

It is clear that any eigenfunction of this Hamiltonian will be a function of both the electronic and nuclear coordinates. However it is widely understood, particularly in chemistry, that most electronic properties of matter result from interaction of electrons, with the valence electrons playing a greater part than core ones. Thus it would seem wasteful to consider the nuclear coordinates in the same footing as electronic ones. It would be ideal if one could separate the wave function as

$$\Psi(\text{electrons}, \text{nucleus}) = \Psi(\text{electrons}) \times \Phi(\text{nucleus}) \tag{2.52}$$

Studying electronic structure then would in principle be greatly simplified because we would have a much simpler Hamiltonian, or at least concern ourselves with only the wave functions of the electrons. Even if Ψ(electrons) had some parametrical dependence on the nuclear positions one could, in principle, calculate it separately from Φ(nucleus).

In fact the previous assumption is physically realistic when one considers the nature of the electron-nuclear interaction. The Coulomb force acting on both the electron and the nucleus due to their charges has the same order of magnitude. Thus one could propose that any change in momenta to both the nucleus and the electron must also be

similar. The proton being massive when compared to the electron would have a much smaller velocity and move very little. Therefore in the time-scale of an electronic structure calculation one could assume that the protons remain stationary and the electrons quickly adapt to any ground-state nuclear distribution. This is known as the Born-Oppenheimer approximation.

2.6.1 The Born-Oppenheimer approximation

Proceeding as described in the previous section we wish to separate the eigenfunctions of the many-body Hamiltonian in the following manner:

$$\Psi'(\mathbf{r}_n, \mathbf{R}_k) = \Psi(\mathbf{r}_n; \mathbf{R}_k)\Phi_{\text{nucleus}}(\mathbf{R}_k) \tag{2.53}$$

where $\Psi(\mathbf{r}_n; \mathbf{R}_k)$ depends only parametrically in the nuclear coordinates $\mathbf{R}_k$ and is a solution to:

$$\hat{H}_e\Psi(\mathbf{r}_n; \mathbf{R}_k) = \epsilon_e\Psi(\mathbf{r}_n; \mathbf{R}_k) \tag{2.54}$$

where ϵ_e is known as the adiabatic contribution of the electrons to the system's energy, and

$$\hat{H}_{\text{e}} = \sum_{i=1}^{N} \frac{\mathbf{p_i}^2}{2m} + \frac{1}{2}\sum_{i,j=1;i\neq j}^{N} \frac{1}{|\mathbf{r}_i - \mathbf{r}_j|} - \sum_{n=1}^{K}\sum_{i=1}^{N} \frac{Z_n}{|\mathbf{r}_i - \mathbf{R}_n|} \tag{2.55}$$

is the electronic part of the many-body Hamiltonian (2.51).

Applying the full Hamiltonian (2.51) to the eigenfunction (2.53) we have:

$$\begin{aligned}
\hat{H}\Psi'(\mathbf{r}_n, \mathbf{R}_k) &= \left(\hat{H}_e + \sum_{n=1}^{K} \frac{\bigtriangledown^2_{\mathbf{R}_k}}{2M_n} + \frac{1}{2}\sum_{n,n'=1;n\neq n'}^{K} \frac{Z_n Z_{n'}}{|\mathbf{R}_n - \mathbf{R}_{n'}|}\right)\Psi'(\mathbf{r}_n, \mathbf{R}_k) \\
&= \Psi(\mathbf{r}_n; \mathbf{R}_k)\left(\epsilon_e + \sum_{n=1}^{K} \frac{\bigtriangledown^2_{\mathbf{R}_k}}{2M_n} + \frac{1}{2}\sum_{n,n'=1\neq n'}^{K} \frac{Z_n Z_{n'}}{|\mathbf{R}_n - \mathbf{R}_{n'}|}\right)\Phi(\mathbf{R}_k) \\
&- \sum_{K} 2 \bigtriangledown_{\mathbf{R}_k} \Phi(\mathbf{R}_k) \bigtriangledown_{\mathbf{r}_n} \Psi(\mathbf{r}_n; \mathbf{R}_k) + \Phi(\mathbf{R}_k) \bigtriangledown^2_{\mathbf{r}_n} \Psi(\mathbf{r}_n; \mathbf{R}_k)
\end{aligned} \tag{2.56}$$

The non-adiabatic terms involving derivatives with respect to the nuclear position contribute very little to the energy and therefore can be neglected. To a first approximation eq. (2.56) can be recast:

$$\hat{H}\Psi' = \Psi\left(\epsilon_e + \frac{1}{2}\sum_{n,n'=1\neq n'}^{K} \frac{Z_n Z_{n'}}{|\mathbf{R}_n - \mathbf{R}_{n'}|}\right)\Phi \tag{2.57}$$

The total energy of the system is then:

$$E_{total} = \epsilon_e + \sum_{n,n'=1;n\neq n'}^{K} \frac{Z_n Z_{n'}}{|\mathbf{R}_n - \mathbf{R}_{n'}|} \tag{2.58}$$

with the second term being the nuclear-nuclear electrostatic energy.

For the rest of this thesis the adiabatic approximation is used. The nuclear distribution is assumed to be fixed for any systems treated in the next chapters. In addition the nuclear wave function $\Phi(\mathbf{R}_k)$ is dropped and the nuclear-nuclear electrostatic energy is ignored unless stated.

2.7 Independent electron approximations

Although not directly related to the topics of this thesis, we must briefly expand on a particular independent electron approximation (Hartree-Fock), which will be mentioned in later chapters.

2.7.1 Hartree approximation

Despite the adiabatic approximation solving equation 2.55 is still very complicated. One could envisage, for the purposes of simplicity, a gross approximation to the many-electron Hamiltonian (2.55), where one would construct it from single electron Hamiltonians:

$$\hat{H}_{\text{ind}} = \sum_i H_{1\text{el}}(i) = \sum_i \hat{H}_{1el}(\mathbf{r}_i) = \sum_i \Big[-\frac{1}{2} \bigtriangledown_i^2 - V_{\text{eff}}(\mathbf{r}_i) \Big] \tag{2.59}$$

where V_{eff} would be an effective potential. The Schrödinger could then be solved by separation of variables. Let us then form the time-independent problem,

$$H_{\text{ind}} \left|\Psi\right\rangle = \epsilon \left|\Psi\right\rangle \tag{2.60}$$

and

$$\Psi(\mathbf{r}_1, \mathbf{r}_2, ..., \mathbf{r}_n) = \psi_1(\mathbf{r}_1)\psi_2(\mathbf{r}_2).....\psi_n(\mathbf{r}_n) \tag{2.61}$$

Where Ψ is the system's electronic wave function and $\psi_i(\mathbf{r}_i)$ are the wave functions of individual electrons (solutions of $\hat{H}_{1\text{el}}$) and $\langle\psi_i|\psi_j\rangle = \delta_{ij}$.

The product of functions in equation 2.61 is known as the *Hartree product*. This is one of the most basic of approximations for the electronic wave function Ψ. For such approximations to yield any valuable insight into the physics of a system the potential felt by each electron $\hat{V}_{\text{eff}}(\mathbf{r}_i)$ must contain not only the nuclear coulomb potential but also the average potential (mean-field) due to the interaction with other electrons. This term will also include exchange-correlation.

Given the presence of terms in $V_{\text{eff}}(\mathbf{r}_i)$ which depend upon the electric coordinates, one must have knowledge of individual electronic wave functions to construct it. Such wave functions, obtained from one electron calculations in which they must be used to

define the potential, are know as *self consistent*.

2.8 Hartree-Fock theory

Given that the electrons are fermions one would expect that any wave function describing a system of electron should be anti-symmetric with respect to the interchange of two electrons which the Hartree product is not. The Hartree-Fock method improves on the Hartree approximation by constructing an anti-symmetric wave function thereby treating the exchange interaction exactly.

2.8.1 Exchange interaction

The appearance of the exchange interaction is a consequence of the anti-symmetry requirement. Let's assume we have a system of two identical particles and we have two different states ϕ_a and ϕ_b. Let these two states be orthogonal and normalised. We construct the anti-symmetric wave function for the system as :

$$\Psi(\mathbf{x},\mathbf{y}) = \frac{1}{\sqrt{2}}[\phi_a(\mathbf{x})\phi_b(\mathbf{y}) - \phi_a(\mathbf{y})\phi_b(\mathbf{x})] \tag{2.62}$$

To find out the effect of anti-symmetry on the electronic distribution the expectation value of the squared distance between the particles can be calculated :

$$\Delta = (\mathbf{x}-\mathbf{y})^2 = \mathbf{x}^2 + \mathbf{y}^2 + 2\mathbf{x}\mathbf{y} \tag{2.63}$$

The details of the calculation can be found in [8], the expectation value of Δ is:

$$\langle\Delta\rangle = \langle x^2\rangle_a + \langle x^2\rangle_b - 2\langle x\rangle_a \langle x\rangle_b + 2\left|\langle x\rangle_{ab}\right|^2 \tag{2.64}$$

Where $\langle x^2\rangle_a$ and $\langle x\rangle_a$ are the expectation values of x and x^2 in state ϕ_a and:

$$\langle x\rangle_{ab} = \int x\phi_a(x)\phi_b(x)dx \tag{2.65}$$

As we can see from the positive last term in equation (2.64), anti-symmetric particles are further kept apart even in the absence of any Coulomb forces. We now explore the construction of anti-symmetric wave functions for many-electron systems.

2.8.2 Hartree-Fock approximation

As mentioned above, the Hartree wave function is not anti-symmetric, however combinations of Hartree products can be made which do have anti-symmetry. From linear algebra we know that the determinant of a matrix is always anti-symmetric with respect to an exchange of columns (or rows). It follows that constructing a wave function by means of a determinant will ensure the correct behaviour. In electronic structure theory this is know as a Slater determinant,

$$\Psi(\mathbf{r}_1, \mathbf{r}_2, ..., \mathbf{r}_n) = \frac{1}{\sqrt{N!}} \begin{vmatrix} \psi_1(\mathbf{r}_1) & \psi_1(\mathbf{r}_2) & \dots & \psi_1(\mathbf{r}_n) \\ \psi_2(\mathbf{r}_1) & \psi_2(\mathbf{r}_2) & \dots & \psi_2(\mathbf{r}_n) \\ . & . & \dots & . \\ . & . & \dots & . \\ \psi_n(\mathbf{r}_1) & \psi_n(\mathbf{r}_2) & \dots & \psi_n(\mathbf{r}_n) \end{vmatrix}$$

where the individual ψ_i will also be a function of the spin coordinates, however for simplicity in this discussion spin is taken into account by multiplying the last two terms of equation (2.66) by a factor of four.

The expectation value of a wave function constructed from a Slater determinant will be stated here without derivation (a thorough derivation can be found in [10]) :

$$\begin{aligned} \langle \Psi | \hat{H} | \Psi \rangle = & \sum_i \int \psi_i^*(\mathbf{r}_i)^* \Big[-\frac{1}{2} \bigtriangledown + V_{ext} \Big] \ \psi_i(\mathbf{r}_i) d\mathbf{r} \\ & + 2 \sum_{i,j} \int \int d\mathbf{r}_1 d\mathbf{r}_2 \psi_i^*(\mathbf{r}_1) \psi_j^*(\mathbf{r}_2) \frac{1}{|\mathbf{r}_1 - \mathbf{r}_2|} \psi_i(\mathbf{r}_1) \psi_j(\mathbf{r}_2) \\ & - \sum_{i,j} \int \int d\mathbf{r}_1 \mathbf{r}_2 \psi_i^*(\mathbf{r}_1) \psi_j^*(\mathbf{r}_2) \frac{1}{|\mathbf{r}_1 - \mathbf{r}_2|} \psi_j(\mathbf{r}_1) \psi_i(\mathbf{r}_2) \end{aligned} \tag{2.66}$$

Where the two terms, which involve only integration of one-electron terms, are the kinetic energy and electron-nuclear Coulomb energy. The remaining terms, which involve two-electrons, are respectively the electron-electron Hartree energy and the exact exchange energy, which arises directly from the anti-symmetric form of the wave function.

The Hartree-Fock wave function is also an approximation of course. The true wave function for a two electron wave function will also depend on $|\mathbf{r}_1 - \mathbf{r}_2|$, ie. the separation of the two electrons, and this is not the case in a wave function constructed in a Slater determinant. The result is that the Hartree-Fock energy (equation 2.66), E_{HF}, is therefore higher than the true energy, E_{TE}, as according to the variational principle, any restriction in the wave function increases the energy. The difference is known as the *correlation energy*:

$$E_{\mathrm{TE}} = E_{\mathrm{HF}} + E_{\mathrm{corr}} \tag{2.67}$$

where E_{corr} is negative. This is ignored in HF theory, but included approximately in DFT

as will be discussed shortly.

2.9 Summary

A brief introduction to quantum mechanics has been presented, inclunding the time-independent Schrödinger equation which is used to treat quantum mechanical problems. The many-body Hamiltonian, that of a system of electrons in a field of nuclei, which is the basis for any electronic structure calculation was constructed and the Born-Oppenheimer approximation which greatly simplifies the aforementioned Hamiltonian (and any Hamiltonian derived from it) was introduced.

The independent electron approximation was discussed, and one particular methodology, the Hartree-Fock approximation, which is used to find solution for the many-body Hamiltonian (after the Born-Oppenheimer approximation) was discussed briefly.

Some theoretical considerations were stated which will be important, in the next chapter, where the theoretical formulation of DFT is presented, the theory upon which the main results of this work will depend.

Chapter 3

Density Functional Theory

3.1 Density Functional Theory

The complexity of the Hamiltonian equations involved in the study of electronic structure, even after the approximations discussed in the previous chapter, curtail their usefulness. As summarized previously, the main obstacles when solving the time-independent Schrödinger equation for a group of electrons and nuclei, were the many-body interactions between electrons.

In the latter part of the previous chapter independent electron methods were introduced where an approximate ground state of the system is constructed from solutions of a non-interacting Hamiltonian, particularly the Hartree-Fock method which self-consistently finds the best approximation for the true ground state wave function as an anti-symmetric Slater determinant and calculates its energy. These *wavefunctional* methods, where the wave function for a system of n independent electrons is used to calculate the energy of the system, scale in complexity as $\mathcal{O}(n^{(3-4)})$, which can limit the scope of possible calculations.

DFT attempts to overcome the biggest drawbacks of wavefunctional methodology by expressing the energy as a functional of the electronic density $n(\mathbf{r})$.

3.1.0.1 The Hohenberg-Kohn Theorems

In 1964 Hohenberg and Kohn [11] published a set of remarkable statements in a seminal paper, known as the Hohenberk-Kohn (HK) theorems, that laid the foundation of DFT. At its most basic the HK theorems assert that one can deal, without any loss of generality, with the ground state density $n_0(\mathbf{r})$ as one would deal with the ground state wave function $\Psi_0(\mathbf{r})$ and essentially express the energy as a function of density $E[n(\mathbf{r})]$ instead of $E[\Psi_0(\mathbf{r})]$.

As detailed in chapter 2, after performing the Born-Oppenheimer approximation one is left with the following Hamiltonian for a system of electrons in a potential generated by a group of nuclei (call it $V_{\text{ext}}(\mathbf{r})$):

$$\hat{H} = \hat{T} + \hat{U} + \hat{V}_{\text{ext}} \tag{3.1}$$

where

$$\hat{T} = \sum_i \frac{1}{2} \bigtriangledown_i^2 \quad \text{and} \quad \hat{U} = \sum_i \sum_{j \neq i} \frac{1}{|\mathbf{r}_i - \mathbf{r}_j|} \tag{3.2}$$

By solving the Hamiltonian equation, $\hat{H} |\Psi_0\rangle = \epsilon_0 |\Psi_0\rangle$ one obtains the ground state $|\Psi_0\rangle$ and simultaneously the ground-density $n_0(\mathbf{r})$. It follows then, that both the ground state $|\Psi_0\rangle$ and ground state density $n_0(\mathbf{r})$ are uniquely determined by $\hat{V}_{\text{ext}}$ since both $\hat{T}$ and $\hat{U}$ remain the same for any system of electrons. However one of the HK theorems asserts that the reverse statement is also true :

- *The ground state electronic density $n_0(\mathbf{r})$ of a system uniquely determines $\hat{V}_{\text{ext}}$.*

Let us assume that the ground state $|\Psi_0\rangle$ is non-degenerate, and has an associate energy E_0. We proceed to prove the theorem above, i.e. that the potential is a functional of the ground state density $V_{\text{ext}}[n_0(\mathbf{r})]$, by *reductio ad absurdum.* As stated beforehand the ground state density $n_0(\mathbf{r})$ is clearly a functional of $\hat{V}_{\text{ext}}$ since it is constructed from a solution of $\hat{H}$ ($|\Psi_0\rangle$). Let us assume that there exists another potential $\hat{V}'_{ext}$ with a respective ground state $|\Psi'\rangle$ and an energy E'_0, that yields the same density $n_0(\mathbf{r})$ (obtained from $\hat{V}_{\text{ext}}$). Clearly $|\Psi'\rangle \neq |\Psi_0\rangle$ since they are the ground state solutions of two different Hamiltonians $\hat{H}' \neq \hat{H}$ (different potentials $\hat{V}'_{\text{ext}} \neq \hat{V}_{\text{ext}}$).

Let $\hat{\delta} = \hat{V}'_{\text{ext}} - \hat{V}_{\text{ext}}$, by construction it follows that the expectation value $\langle\hat{\delta}\rangle \neq 0$ with respect to both $|\Psi\rangle$ and $|\Psi'\rangle$. Using the variational principle introduced in the previous chapter we find:

$$E_0 = \langle\Psi_0| \hat{H} |\Psi_0\rangle < \langle\Psi'|\hat{H}|\Psi'\rangle = \langle\Psi'|\hat{H}' - \hat{V}' + \hat{V}|\Psi'\rangle = E'_0 + \langle\Psi'| - \hat{\delta}|\Psi'\rangle \tag{3.3}$$

We can construct a similar relation for E'_0,

$$E'_0 < E_0 + \langle\Psi_0|\hat{\delta}|\Psi_0\rangle \tag{3.4}$$

Calculating the expectation value of δ and find:

$$\langle\Psi| \hat{\delta} |\Psi\rangle = \int \Psi^*(\mathbf{r})\delta(\mathbf{r})\Psi(\mathbf{r})d\mathbf{r} = \int n_0(\mathbf{r})\delta(\mathbf{r})d\mathbf{r} \tag{3.5}$$

And similarly for $|\Psi'\rangle$,

$$\langle\Psi'|\,\hat{\delta}\,|\Psi'\rangle = \int n_0(\mathbf{r})\delta(\mathbf{r})d\mathbf{r} \tag{3.6}$$

where equation(3.6) is derived from our initial assumption that both $\hat{H}$ and H' yield the same ground state density $n_0(\mathbf{r})$. Therefore we have,

$$\langle\Psi_0|\,\hat{\delta}_0\,|\Psi\rangle = -\langle\Psi'| - \hat{\delta}\,|\Psi'\rangle \tag{3.7}$$

Summing equation (3.3) with (3.4) and using the equality (3.7) we find the following inequality:

$$E_0 + E_0' < E_0' + E_0 \tag{3.8}$$

Equation (3.8) is a clear contradiction thus our initial assumption is incorrect. If $\hat{V}_{\text{ext}} \neq \hat{V}'_{ext}$ then $n_0(\mathbf{r}) \neq n_0'(\mathbf{r})$ and more importantly the converse of that statement, i.e. if $n_0(\mathbf{r}) \neq n_0'(\mathbf{r})$ then both densities must have been constructed from solutions of Hamiltonians with a different external potential $\hat{V}_{\text{ext}}$. Therefore the external potential $\hat{V}_{\text{ext}}$ is uniquely determined by the ground state density so that one may write the latter as a functional of the former $V_{\text{ext}}[n_0(\mathbf{r})]$. Having proven this we proceed to show that indeed one can write the energy of the system as a functional of the density and that $E_0 = E[n_0(\mathbf{r})]$.

3.1.0.2 Density Functional

The second theorem, which lays out the meaning of Density Functional in DFT, can be stated as follows:

• *There exists a universal functional for the ground state energy in terms of density* $E[n(\mathbf{r})]$ *valid for any external potential. For a particular* $\hat{V}_{\text{ext}}$ *the ground state density minimises said energy functional i.e.* $\min\left[E[n(\mathbf{r})]\right] = E_0 = E[n_0(\mathbf{r})]$.

In the previous chapter it was proven that the ground state density $n_0(\mathbf{r})$ is enough to determine $\hat{V}_{\text{ext}}$, and in turn also $|\Psi_0\rangle$. Therefore both the kinetic energy $\langle\Psi_0|\hat{T}|\Psi_0\rangle$ and the electronic Coulomb energy $\langle\Psi_0|\hat{U}|\Psi_0\rangle$ are functionals of $n_0(\mathbf{r})$. Let us now define the *universal functional*:

$$\hat{F}[n(\mathbf{r})] = \langle\Psi|\,\hat{T} + \hat{U}\,|\Psi\rangle \tag{3.9}$$

according to the previous chapter and using (3.9), for a given $\hat{V}_{\text{ext}}$ we can define the *energy functional* as:

$$E_{\text{HK}}[n(\mathbf{r})] = \int V_{\text{ext}}(\mathbf{r})n(\mathbf{r})d\mathbf{r} + F[n(\mathbf{r})] \tag{3.10}$$

All that remains now is to show that $n_0(\mathbf{r})$ minimizes $E[n(\mathbf{r})]$ at the ground state energy. Let us consider a system with ground state density $n_0(\mathbf{r})$ and the corresponding $V_{\text{ext}}(\mathbf{r})$.

The ground state energy of this system is:

$$E_0 = E_{\mathrm{HK}}[n_0(\mathbf{r})] = \int V_{\mathrm{ext}}(\mathbf{r}) n_0(\mathbf{r}) d\mathbf{r} + F[n_0(\mathbf{r})] = \langle \Psi_0 | \hat{H} | \Psi_0 \rangle \tag{3.11}$$

Now let us consider a different density $n_1(\mathbf{r})$ and corresponding wave function $|\Psi_1\rangle$, using the $E_{\mathrm{HK}}[n(\mathbf{r})]$ in equation (3.11) we find,

$$E_0 = E_{\mathrm{HK}}[n_0(\mathbf{r})] = \langle \Psi_0 | \hat{H} | \Psi_0 \rangle < \langle \Psi_1 | \hat{H} | \Psi_1 \rangle = E_{\mathrm{HK}}[n_1(\mathbf{r})] \tag{3.12}$$

Thus any guess density $n_1(\mathbf{r})$ will always have an higher energy than the ground state $n_0(r)$, i.e. $E_{\mathrm{HK}}[n_0(\mathbf{r})] < E_{\mathrm{HK}}[n_1(\mathbf{r})]$. In addition the ground state $n_0(r)$ minimizes the energy functional $E_{\mathrm{HK}}[n(\mathbf{r})]$. This is known as the *variational principle*.

In principle if one knew the exact form of $F[n(\mathbf{r})]$, it follows that one could find the ground state energy of a system by minimizing $E_{\mathrm{HK}}[n(\mathbf{r})]$, a procedure which would scale linearly with respect to system size.

As powerful as the HK theorems are, they are not without caveats. The HK theorems implicitly restrict the densities $n(\mathbf{r})$, that one can use to minimise $E_{\mathrm{HK}}[n(\mathbf{r})]$, to the subset of functions which are themselves the ground state density of an Hamiltonian with a particular $\hat{V}_{\mathrm{ext}}$. Such densities are known as *V-representable*. This severely hampers any implementation of HK theorems as the subset of V-representable densities is not know *a priori*.

3.1.0.3 The constrained search formalism

Although the ground work for DFT had been laid in the seminal Hohenberg-Kohn paper [11] the difficult task of finding V-representable densities limited its application, in addition there was no indication on how useful approximations to the universal functional $F[n(\mathbf{r})]$ could be generated. To remedy these shortcomings Levy [12] suggested an alternative procedure to minimize the energy functional, which essentially introduces a second minimization step.

Consider the subset of many-body wave functions $|\Psi\rangle$ which have the same density $n(\mathbf{r})$. The total energy for a wave function in this subset can be written as:

$$E = \langle \Psi | \hat{T} | \Psi \rangle + \langle \Psi | \hat{U} | \Psi \rangle + \int V_{\mathrm{ext}}(\mathbf{r}) n(\mathbf{r}) d\mathbf{r} \tag{3.13}$$

One can then minimize the total energy over the subset of wave functions $|\Psi\rangle$ with the same density $n(\mathbf{r})$, for which we can define a unique lowest energy:

$$E_{\mathrm{LL}}[n(\mathbf{r})] = \min_{\Psi \to n(\mathbf{r})} \left[\langle \Psi | \, \hat{T} \, | \Psi \rangle + \langle \Psi | \, \hat{U} \, | \Psi \rangle \right] + \int V_{\mathrm{ext}}(\mathbf{r}) n(\mathbf{r}) d\mathbf{r} \tag{3.14}$$

one can rewrite the previous expression as

$$E_{\mathrm{LL}}[n(\mathbf{r})] = F_{\mathrm{LL}}[n(\mathbf{r})] + \int n(\mathbf{r}) V_{\mathrm{ext}}(\mathbf{r}) d\mathbf{r} \tag{3.15}$$

where $F_{\mathrm{LL}}[n(\mathbf{r})]$

$$F_{\mathrm{LL}}[n(\mathbf{r})] = \min_{\Psi \to n(\mathbf{r})} \left[\langle \Psi | \, \hat{T} + \hat{U} \, | \Psi \rangle \right] \tag{3.16}$$

known as the Levy-Lieb functional, is the minimum kinetic and internal interactions energy with respect to all the wave functions which yield the same density. $E_{\mathrm{LL}}[n(\mathbf{r})]$ is then a function of the density and we can find the ground state density $n_0(\mathbf{r})$ by minimizing $E_{\mathrm{LL}}[n(\mathbf{r})]$.

Although this result may, at a first glance, seem similar to the formulation derived from the HK theorems in the previous section, there are several noteworthy differences. The meaning of the universal functional is now clarified and the minimization is defined for any density $n(\mathbf{r})$ which is constructed from a many-body wave function $\Psi_N(\mathbf{r})$ for N electrons, this is know as "n-representability". It has been shown [13] that any non-negative function (such as density) is n-representable, that is any density can be written in terms of an asymmetric many-body wave function and can therefore be considered in the minimization procedure. In addition the minimization can be extend to sets of degenerate ground states (as long as they generate a density $n(\mathbf{r})$).

Although the V-representabilty restriction as now been removed, no method to generate $F_{\mathrm{LL}}[n(\mathbf{r})]$ is given other than its definition. This as we will see shortly is one of the main results of Kohn-Sham formalism.

3.2 Kohn-Sham equations

The Hohenberg-Kohn theorems allow the problem of finding the ground state energy E_0 and wave function $|\Psi\rangle$ to be mapped into one of minimizing a functional $E[n(\mathbf{r})]$. However, this minimization relies upon an unknown universal functional $F[n(\mathbf{r})]$, of which we only know that it exists. Thus any benefit one could gain from an implementation of the HK theorems, such as the linear scaling with respect to system size and exactness of the method, is overshadowed by the unknown nature of the universal function $F[n(\mathbf{r})]$.

Kohn-Sham [11] devised a method to circumvent the problems mentioned in the paragraph above, however single particle wave functions, such as the ones described at the end of last chapter, are reintroduced resulting in cubic scaling, $\mathcal{O}(n^3)$, with respect to system size, due to the orthonormality condition. However the exactness of the HK method is maintained in the KS reformulation.

Fundamentally the Kohn-Sham formulation of Density Functional Theory (KSDFT) rests on the assumption that:

• *The ground state density of a system of interacting electrons can be represented by the ground state density of an auxiliary system of non-interacting electrons.*

Thus one can deal with independent electrons but the density of an interacting system. Let us start by recasting the HK universal functional,

$$F[n(\mathbf{r})] = \frac{1}{2}\int \frac{n(\mathbf{r})n(\mathbf{r}')}{|\mathbf{r}'-\mathbf{r}|}d\mathbf{r}d\mathbf{r}' + G[n(\mathbf{r})] \tag{3.17}$$

where the first term is the energy which arises out of the long range Hartree potential, i.e. the electron-electron Coulomb potential,

$$V_{\text{Hartree}} = \int \frac{n(\mathbf{r}')}{|\mathbf{r}'-\mathbf{r}|}d\mathbf{r}' \tag{3.18}$$

and $G[n]$, is a new universal functional. Furthermore, Kohn-Sham in a stroke of genius, more on this on a later section, further separated $G[n]$,

$$G[n] = T_{\text{s}}[n] + E_{\text{xc}}[n] \tag{3.19}$$

where $T_{\text{s}}[n]$ is the kinetic energy for a system of non-interacting electrons and $E_{\text{xc}}[n(\mathbf{r})]$, the exchange-correlation energy, contains the complex many-body electron interactions.

In the Kohn-Sham scheme the energy functional (3.10) can then be recast, as:

$$E_{\text{KS}}[n(\mathbf{r})] = T_{\text{s}}[n(\mathbf{r})] + \int V_{\text{ext}}(\mathbf{r})n(\mathbf{r})d\mathbf{r} + \frac{1}{2}\int \frac{n(\mathbf{r})n(\mathbf{r}')}{|\mathbf{r}'-\mathbf{r}|}d\mathbf{r}d\mathbf{r}' + E_{xc}[n(\mathbf{r})] \tag{3.20}$$

we now proceed to find the Hamiltonians from which we will generate the densities so that we might minimize (3.20).

3.2.1 The auxiliary system

Let H_{non} be the Hamiltonian for a system of N non-interacting electrons,

$$\hat{H}_{\text{non}} = -\frac{1}{2}\bigtriangledown^2 + V_{\text{aux}}(\mathbf{r}) \tag{3.21}$$

where at this stage $V_{\text{aux}}(\mathbf{r})$ need not be specified. Let the set of $\psi_i(\mathbf{r})$ be the eigenstates of $\hat{H}_{\text{non}}$ with associated eigenenergies ϵ_i. The N non-interacting electrons must occupy the lowest N states as per Pauli's exclusion principle. The electronic density of this system $n(\mathbf{r})$ is given by :

$$n(\mathbf{r}) = \sum_{i=1}^{N} |\psi_i(\mathbf{r})|^2 \tag{3.22}$$

and the independent electron kinetic energy can be written as:

$$T_{\rm s} = -\frac{1}{2}\sum_{i=1}^{N} \langle \psi_i | \bigtriangledown^2 | \psi_i \rangle \tag{3.23}$$

Following the methodology set forth from the HK theorems, we wish to minimize (3.10) to find the ground state $n_0(\mathbf{r})$ for our system of non-interacting electrons, subject to the condition:

$$\int n_0(\mathbf{r}) d\mathbf{r} = N \tag{3.24}$$

Given our formulation we know that the ground state $n_0(\mathbf{r})$ is a minimum of (3.20),

$$\frac{\delta E_{\rm KS}[n]}{\delta n(\mathbf{r})}\Big|_{n=n_0(\mathbf{r})} = 0 \tag{3.25}$$

in addition:

$$\frac{\delta E_{\rm KS}}{\delta \psi_i} = \frac{\delta E_{\rm KS}}{\delta n_0(\mathbf{r})}\frac{\delta n_0(\mathbf{r})}{\delta \psi_i} = 0 \tag{3.26}$$

the one-to-one correspondence between the ground state density and its corresponding wave function in the HK theorems is further exemplified by the equation above.

Varying $E_{\rm KS}[n(\mathbf{r})]$ with respect to $\psi_i(\mathbf{r})$ we find:

$$\frac{\delta E_{\rm KS}}{\delta \psi_i} = \frac{\delta T_{\rm s}}{\delta \psi_i} + \left[\frac{\delta E_{\rm ext}}{\delta n} + \frac{\delta E_{\rm Hartree}}{\delta n} + \frac{\delta E_{\rm xc}}{\delta n}\right]\frac{\delta n(\mathbf{r})}{\delta \psi_i} = 0 \tag{3.27}$$

Using expressions (3.23) and (3.22) we can recast the following terms from the previous equation,

$$\frac{\delta T_{\rm s}}{\delta \psi_i} = -\frac{1}{2}\bigtriangledown^2 \psi_i(\mathbf{r}) \quad \text{and} \quad \frac{\delta n(\mathbf{r})}{\delta \psi_i} = \psi_i(\mathbf{r}) \tag{3.28}$$

Given the expressions above, equation (3.27) can then be reformulated using the method of Lagrangian multipliers (to handle constraint (3.24)) as:

$$-\frac{1}{2}\bigtriangledown^2 \psi_i(\mathbf{r}) + \left[\frac{\delta E_{\rm ext}}{\delta n} + \frac{\delta E_{\rm Hartree}}{\delta n} + \frac{\delta E_{\rm xc}}{\delta n} - \epsilon_i\right]\psi_i = 0 \tag{3.29}$$

where ϵ_i are the Lagrangian multipliers. But this is simply:

$$(\hat{H}_{\rm KS} - \epsilon_i)\psi_i = 0 \tag{3.30}$$

Here ϵ_i are the eigenenergies of each state ϕ_i and $\hat{H}_{Ks}$ is:

$$\begin{aligned}\hat{H}_{\mathrm{KS}} &= -\frac{1}{2}\bigtriangledown^2 + \frac{\delta E_{\mathrm{ext}}}{\delta n} + \frac{\delta E_{\mathrm{Hartree}}}{\delta n} + \frac{\delta E_{\mathrm{xc}}}{\delta n} \\ &= -\frac{1}{2}\bigtriangledown^2 + V_{\mathrm{ext}}(\mathbf{r}) + V_{\mathrm{Hartree}}(\mathbf{r}) + V_{\mathrm{xc}}(\mathbf{r})\end{aligned} \tag{3.31}$$

Thus we have found the exact formulation for V_{aux} term in equation (3.21). V_{aux} is often written as V_{KS} within the KS formalism.

The total energy of the non-interacting system is given by,

$$\sum_{i=1}^{N} \epsilon_i = T_{\mathrm{s}}[n] + \int (V_{\mathrm{ext}}(\mathbf{r}) + V_{\mathrm{Hatree}}(\mathbf{r}) + V_{\mathrm{xc}}(\mathbf{r}))n(\mathbf{r})d\mathbf{r} \tag{3.32}$$

Comparing this result with the equation (3.20), we can rewrite the energy for the interacting system in terms of these eigenenergies,

$$E_{\mathrm{KS}}[n(\mathbf{r})] = \sum_{i=1}^{N} \epsilon_i - \frac{1}{2}\int \frac{n(\mathbf{r})n(\mathbf{r}')}{|\mathbf{r}' - \mathbf{r}|} d\mathbf{r}'d\mathbf{r} + E_{\mathrm{xc}}[n(\mathbf{r})] - \int V_{\mathrm{xc}}(\mathbf{r})n(\mathbf{r})d\mathbf{r} \tag{3.33}$$

Equation (3.30), (3.31) and (3.33) are known as the Kohn-Sham equations. If one knew the exact exchange-correlation functional, E_{xc}, then the Kohn-Sham scheme presented here would calculate the exact ground state. However, the exact form of E_{xc} is not known and one must employ approximations.

It must be stressed, that the reintroduction of orbitals in KS methodology has resulted in the reintroduction of cubic scaling. For large systems, we will see in later sections, the main culprit responsible for the overall scaling of the method is the Hamiltonian diagonalization (where the KS orbitals are obtained). However, methods have been developed which minimize the required computer effort in this step resulting in a more appealing computational time [14, 15]. Our method, filtration [5, 16], will be presented in chapter 6.

3.2.2 Solving the Kohn-Sham Equations

We will keep the discussion here general, specific details on how different Kohn-Sham schemes are implemented will be presented in the next chapter. The Kohn-Sham equations must be solved within a self-consistent scheme, particularly since the auxiliary potential $V_{\mathrm{KS}}[n](\mathbf{r})$ is a functional of the density, itself constructed from the single-state wave functions, which are solutions of the Kohn-Sham Hamiltonian.

Figure 3.1 presents a schematic representation of the overall kernel of many KSDFT codes using localised orbitals which can, algorithmically, be summarized as:

1. An initial guess $n_{\mathrm{in}}(\mathbf{r})$ is chosen which specifies an initial guess for the Kohn-Sham

potential $V_{\mathrm{KS}}[n_{\mathrm{in}}(\mathbf{r})]$, using this the Kohn-Sham Hamiltonian H_{KS} is built. This should be done efficiently, ideally with linear scaling, if a particular implementation is intended to be used for large scale calculations.

2. The Kohn-Sham equations are solved, i.e. $H_{\mathrm{KS}}\psi_i = \epsilon_i\psi_i$. This step is computationally expensive particularly so for large systems, since it might involve the direct diagonalization of a large matrix. The filtration [5] methodology implemented in `AIMPRO` [16] has been shown to be a reliable method to reduce computational expenditure of this step. This has lead to a considerable speed up of calculations when compared with regular `AIMPRO`. However, in this thesis we will demonstrate that filtration can also be used to perform calculations with the accuracy of a plane wave calculation.

3. A new density $n_{\mathrm{out}}(\mathbf{r})$ is calculated using the Kohn-Sham orbitals obtained from the previous step.

4. The difference $|n_{\mathrm{out}}(\mathbf{r}) - n_{\mathrm{in}}(\mathbf{r})|$ is compared against a chosen tolerance. If the difference is acceptable then the ground state properties of interest are calculated, otherwise both $n_{\mathrm{out}(\mathbf{r})}$ and $n_{\mathrm{in}}(\mathbf{r})$ are used to form a new density $n_{\mathrm{in}}(\mathbf{r})$ and the process reverts back to step 2.

The steps 2-4 are commonly known in literature as a *self-consistent cycle* or a *self-consistent loop*. The density obtained from solving the Kohn-Sham equations in the method described above must eventually converge as the procedure used to generate the new input density $n_{\mathrm{in}}(\mathbf{r})$ is typically modified steepest descent method therefore $|n_{\mathrm{out}}(\mathbf{r}) - n_{\mathrm{in}}(\mathbf{r})|$ will tend to zero as more iterations are performed.

3.2.3 Local Density Approximation

Due to its historical placement, and given that it follows on the tracks of our discussion the Local Density Approximation (LDA) will be discussed here briefly.

The exchange-correlation energy E_{xc}, unlike the HK universal functional, can be sufficiently approximated due to the work of Kohn-Sham. Having separated out the independent particle kinetic energy and the long range Hartee terms Kohn and Sham proposed that the exchange-correlation energy could be approximated locally as

$$E_{\mathrm{xc}}[n(\mathbf{r})] = \int n(\mathbf{r})\epsilon_{\mathrm{xc}}^{\mathrm{hom}}[n(\mathbf{r})]d\mathbf{r} \tag{3.34}$$

where $\epsilon_{\mathrm{xc}}^{\mathrm{hom}}[n(\mathbf{r})]$ is the exchange-correlation energy per electron of an homogeneous electron gas and $n(\mathbf{r})$ is the density obtained from the Kohn-Sham orbitals.

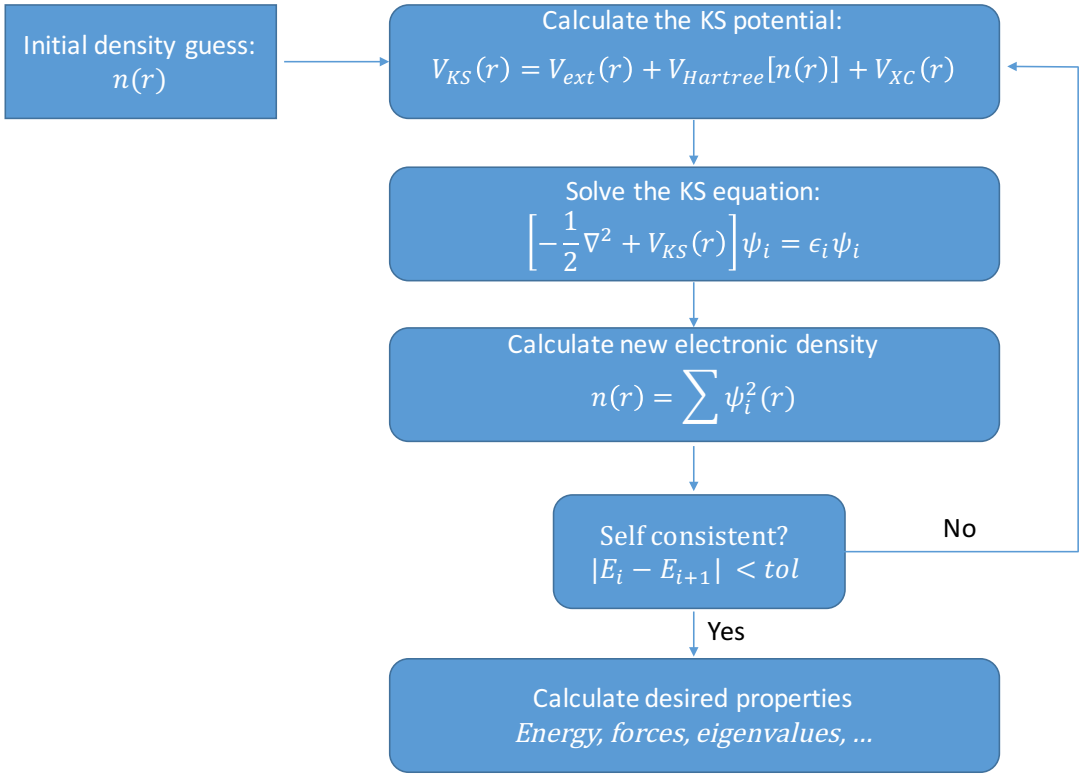

Figure 3.1: *Graphical representation of the different steps in a KSDFT calculation, the four main steps are know as a self-consistence loop.*

Typically the energy exchange-correlation is separated into two different terms,

$$\epsilon_{\mathrm{xc}}^{\mathrm{hom}}[n(\mathbf{r})] = \epsilon_{\mathrm{x}}^{\mathrm{hom}}[n(\mathbf{r})] + \epsilon_{\mathrm{c}}^{\mathrm{hom}}[n(\mathbf{r})] \tag{3.35}$$

Where the exchange term $\epsilon_{\mathrm{x}}^{\mathrm{hom}}[n(\mathbf{r})]$ can be obtained analytically using Hartree-Fock method and the correlation term $\epsilon_{\mathrm{c}}^{\mathrm{hom}}[n(\mathbf{r})]$ must be obtained using a mixture of analytic and numerical Quantum Monte-Carlo methods [17]. Two common parametrizations of $\epsilon_{\mathrm{c}}^{\mathrm{hom}}[n(\mathbf{r})]$ are the Perdew-Zunger (PZ81) [18] and Perdew-Wang (PW92) [19] results.

3.3 Spin Polarization

So far it has been assumed that the Kohn-Sham orbitals are equivalently occupied, by spin-up and spin-down electrons so that there is no overall net spin. However, some systems, such as ferromagnetic materials, owe their ground state properties (like magnetism) to a system wide alignment of the net spin. Thus if such systems are to be studied in a KSDFT calculation we must treat the spin-up and spin-down electrons carefully and separately.

The extension of spin polarization to DFT is due to Von Barth and Hedin [20], a

thorough introduction and review of spin polarized calculations can be found in [21]. Here a brief overview is presented given that spin polarized calculations are performed later in this thesis.

The density of spin polarized system can be expressed as,

$$n(\mathbf{r}) = n_{\downarrow}(\mathbf{r}) + n_{\uparrow}(\mathbf{r}) = \sum_{\sigma} n(\mathbf{r}, \sigma) = \sum_{\sigma} \sum_{i} |\psi_i^{\sigma}(\mathbf{r})|^2 \tag{3.36}$$

where σ is the variable used to keep track of spin in summations, and is typically written as $\sigma =\uparrow$ or $\sigma =\downarrow$ for electrons.
The spin dependent orbitals $\psi_i^{\sigma}(\mathbf{r})$ are solutions of,

$$(\hat{H}_{\mathrm{KS}}^{\sigma} - \epsilon_i^{\sigma})\psi_i^{\sigma} = 0 \tag{3.37}$$

the previous equation seems at first glance to simply be equation (3.30) with a spin label, however expanding the spin dependent Kohn-Sham Hamiltonian we have,

$$\hat{H}_{\mathrm{KS}}^{\sigma} = -\frac{1}{2} \bigtriangledown^2 + V_{\mathrm{Hartree}}[n(\mathbf{r})] + V_{\mathrm{ext}}^{\sigma}[n(\mathbf{r}, \sigma)] + V_{\mathrm{xc}}^{\sigma}[n(\mathbf{r}, \sigma)] \tag{3.38}$$

where we might have $V_{\mathrm{xc}}^{\downarrow}[n_{\uparrow}, n_{\downarrow}] \neq V_{\mathrm{xc}}^{\uparrow}[n_{\uparrow}, n_{\downarrow}]$ if $n_{\uparrow} \neq n_{\downarrow}$ and $V_{\mathrm{ext}}^{\downarrow}[n_{\uparrow}, n_{\downarrow}] \neq V_{\mathrm{ext}}^{\uparrow}[n_{\uparrow}, n_{\downarrow}]$ if there is an external magnetic field. Essentially, the effective potential experienced by the two spins is not necessarily the same. It follows that the two sets of Kohn-Sham orbitals must be obtained separately and simultaneously (within the same iterative loop) given that both densities ($n_{\downarrow}(\mathbf{r})$ and $n_{\uparrow}(\mathbf{r})$) are used to generate the Hamiltonians for the next iteration.

The total energy for the spin polarized system can be written as,

$$E_{\mathrm{KS}} = T_{\mathrm{s}}[n_{\downarrow}(\mathbf{r})] + T_{\mathrm{s}}[n_{\uparrow}(\mathbf{r})] + E_{\mathrm{Hartree}}[n(\mathbf{r})] + E_{\mathrm{ext}}[n(\mathbf{r})] + E_{\mathrm{xc}}[n_{\downarrow}(\mathbf{r}), n_{\uparrow}(\mathbf{r})] \tag{3.39}$$

where the terms are constructed similarly to (3.27).

A LDA formulation for spin polarized calculations is given in [20], known as Local Spin Density Approximation LSDA.

3.4 Fractional Occupation

All of the KSDFT formalism discussed thus far has assumed that the calculations are performed at zero temperature. For metallic systems where the Fermi energy lies in the conducting band, or systems with small or vanishing band gaps, self-consistency calculations can fail to produced a converged density (and therefore a ground state energy) [22]. This can be a result of an attempted crossing of an unoccupied to a occupied energy

level from which follows a discontinuous change in the output $n_{\text{out}}(\mathbf{r})$ for infinitesimal changes in input $n_{\text{in}}(\mathbf{r})$ density.

Such problems can be averted by implementing fractional occupations of the Kohn-Sham orbitals [22, 23], whereupon the density can be expressed as,

$$n(\mathbf{r}) = \sum f_i |\psi_i(\mathbf{r})|^2 \tag{3.40}$$

and f_i is given by a *smearing* function. For the work presented in this thesis this is a Fermi-Dirac distribution,

$$f_i = \frac{1}{e^{\frac{\epsilon_i - \mu}{k_b T}} + 1} \tag{3.41}$$

where $0 < f_i < 1$ and μ is the chemical potential. The energy of the system E_{KS} (given by equation (3.20)) involved in the minimization routine must be substituted by the free energy,

$$F[n(\mathbf{r})] = E_{\text{KS}}[n(\mathbf{r})] - T \cdot S[n(\mathbf{r})] \tag{3.42}$$

where T is the temperature and $S[n(\mathbf{r})]$ is given by,

$$S[n(\mathbf{r})] = -k_b \sum_i [f_i \ln(f_i) + (1 - f_i) \ln(1 - f_i)] \tag{3.43}$$

The value for the electronic temperature used in this work, and the reasoning behind its choice, will be explained in the results chapter.

3.5 Boundary Conditions

In keeping with universality of the discussion thus far we will discuss boundary conditions at this stage. From multi-variable calculus we know that boundary conditions must be specified when solving any differential equation, such as the Kohn-Sham Hamiltonian, if an unique solution is to be obtained. Typically in KSDFT there are two kinds of boundary conditions: periodic and homogeneous (non-periodic). We will now explain the reasoning behind our choice of periodic boundary conditions and how it affects KSDFT implementation.

3.5.1 Crystal structure

Most systems studied in this thesis are crystals: an ordered state of matter where the positions for a set of atoms are repeated periodically over space. It follows that in order to study such systems we don't need to construct our KS Hamiltonian for an almost infinitely large set of atoms, instead we can construct a small cell with a few atoms the

positions of which are repeated periodically. The set of atomic positions in the cell are often called a *basis*. To specify the crystal structure of a system one needs a basis and a set of vectors, which define the lattice. The position of an atom $\mathbf{R}_\alpha$ can then be defined by,

$$\mathbf{R}_\alpha = n_1^\alpha \mathbf{a}_1 + n_2^\alpha \mathbf{a}_2 + n_3^\alpha \mathbf{a}_3 \tag{3.44}$$

in which the set of different $(n_1^\alpha\, n_2^\alpha, n_3^\alpha)$, are the basis and the three vectors $\mathbf{a}_1, \mathbf{a}_2, \mathbf{a}_3$ define the lattice. Given the periodic representation of a basis it seems natural then to choose periodic boundary conditions.

3.5.2 Periodic boundary conditions

As mentioned above the periodicity of a system is given by the set of lattice vectors $\mathbf{a}_i$. This periodicity, in the position of atoms (and therefore nuclei), implies a periodicity of the external potential $V_{\text{ext}}(\mathbf{r})$,

$$V_{\text{ext}}(\mathbf{r}) = V_{\text{ext}}(\mathbf{r} + \mathbf{a}_i) \tag{3.45}$$

From the HK theorems, discussed in a previous section, it is easy to see that,

$$n_0(\mathbf{r}) = n_0(\mathbf{r} + \mathbf{R}) \tag{3.46}$$

It follows then that specifying the atomic positions $\mathbf{R}_\alpha$ and the lattice vectors $\mathbf{a}_i$ specifies the system's ground state.

Periodicity of $n_0(\mathbf{r})$, however, does not imply a periodicity of the Kohn-Sham orbitals ψ_i, in fact they can change by a phase factor in different cells. Such functions, commonly referred to as Bloch functions, can be expressed as,

$$\psi_{\mathbf{k}} = e^{i\mathbf{k}\cdot\mathbf{r}} u_{\mathbf{k}}(\mathbf{r}) \tag{3.47}$$

where $u_{\mathbf{k}}(\mathbf{r})$ is a periodic function ($u_{\mathbf{k}}(\mathbf{r} + \mathbf{R}_\alpha) = u_{\mathbf{k}}(\mathbf{r})$) and $e^{i\mathbf{k}\cdot\mathbf{r}}$ is the phase factor.
If we use the periodic form of KS orbitals in equation (3.30) we find that,

$$\hat{H}_{\text{KS}}(e^{i\mathbf{k}\cdot\mathbf{r}} u_{\mathbf{k}}(\mathbf{r})) = \epsilon(e^{i\mathbf{k}\cdot\mathbf{r}} u_{\mathbf{k}}(\mathbf{r})) \tag{3.48}$$

rearranging the previous equation,

$$\hat{H}_{KS}^{\mathbf{k}} u_{\mathbf{k}}(\mathbf{r}) = \epsilon^{\mathbf{k}} u_{\mathbf{k}}(\mathbf{r}) \tag{3.49}$$

where $\hat{H}_{KS}^{\mathbf{k}} = e^{-i\mathbf{k}\cdot\mathbf{r}} \hat{H}_{KS} e^{i\mathbf{k}\cdot\mathbf{r}}$, and $\epsilon^{\mathbf{k}}$ depends on the choice of $\mathbf{k}$-vector. Specifying boundary conditions has therefore introduced a $\mathbf{k}$ dependence in the KSDFT formalism, where

$\mathbf{k}$ is a vector in the reciprocal space constructed from the reciprocal lattice vectors $\mathbf{b}_i$,

$$\mathbf{b}_1 = 2\pi \frac{\mathbf{a}_2 \times \mathbf{a}_3}{\mathbf{a}_1 \cdot \mathbf{a}_2 \times \mathbf{a}_3} \tag{3.50}$$

and $\mathbf{b}_2$, $\mathbf{b}_3$ are given by cyclical permutations of the previous equation.

It follows that the ground state energy E_{KS}, and many other system properties (let us label them f), must be averaged over states with different $\mathbf{k}$,

$$\bar{f} = \frac{1}{N_{\mathbf{k}}} \sum_{\mathbf{k}} f(\mathbf{k}) \tag{3.51}$$

where $N_{\mathbf{k}}$ is the number of $\mathbf{k}$-vectors used. The details on how the previous summation is performed are left to later chapters as it pertains to specific code nuances.

3.6 Summary

We now have an exact recipe to calculate the ground state energy, or any other ground state property, of a system. The key points behind a KSDFT implementation are:

1. The total energy of an interacting system of electrons can be expressed in terms of a density calculated from an auxiliary system of non-interacting electrons.

2. This density must be calculated from solutions of the Kohn-Sham equations, which results in a cubic scaling in the computational effort with respect to system size. However under certain conditions this can be reduced, as it will be shown later.

3. Periodic boundary conditions introduce a $\mathbf{k}$ dependence in a KSDFT calculation, this, however does not affect the overall scaling.

Having now a solid theory and methodology to calculate the total energy, all that remains is to code it according to the pseudo-algorithm given in section 3.2.2.

Chapter 4

Kohn-Sham DFT implementation

Having established, broadly, the theoretical framework behind KSDFT we are left with its implementation and code specific nuances. As it was noted in the previous chapter the Kohn-Sham equations must be solved numerically and therefore the theory discussed thus far must be expressed in a form which favours a computational implementation. A KSDFT code must then be able to obtain the solution of the Kohn-Sham equations (the heart of any KSDFT implementation) in a reasonable time with a controllable computational accuracy. Advances in functionality of one such code (`AIMPRO`) in both of these aspects are the main topics of this thesis.

The advantages and disadvantages of different KSDFT implementations are discussed in this chapter. We will built upon this discussion later when presenting the results. Particularly how regular ($\mathcal{O}(n^3)$ or scaling) KSDFT codes constructed using plane waves (PW) are taken to be the most accurate and have systematic convergence, whilst regular KSDFT codes which use Gaussian Type Orbitals, GTOs, are usually presented as not as accurate and do not offer systematic convergence. However, we will show that with filtration we can attain plane wave accuracy, at a cost of a GTO calculation.

In the latter parts of this chapter the details pertaining to an efficient matrix construction for in `AIMPRO` are discussed, this is an important step in reducing the overall time of a calculation.

4.1 Basis sets

One of the most important characteristics of a KSDFT code is the choice of basis set. Often the choice of basis sets even determines the fields in which a code is used. For example in quantum chemistry it is customary to use Gaussian basis sets, for reasons which will be presented shortly, whilst in solid state physics PW codes are more commonly used.

Essentially, a basis set is a group of functions chosen to expand the electronic wave functions (solutions of the Hamiltonian) in either Hartree-Fock methods or DFT. In KS-

DFT a Kohn-Sham orbital can be expanded as,

$$\psi_i \approx \sum_j^N c_{ij}\phi_j(\mathbf{r}) \tag{4.1}$$

where the set of N functions (ϕ_j) is known as the basis set. The expansion in equation (4.1) will undoubtedly introduce some error in the calculation, however it follows from the variational principle discussed in chapter 2 that increasing the accuracy of expansion (4.1), using better basis functions (ϕ_j) or increasing the basis set size (N), should result in a more accurate prediction of the ground-state energy i.e. smaller basis set error.

There is no a priori requirement for what constitutes a good basis set, the choice of which depends on the problem at hand. In this thesis we are concerned with KSDFT calculations which can be accurate and efficient so that they can be used for a large number of systems, thus the choice of basis sets should enable the rapid construction of both the Hamiltonian and overlap matrices. In addition they should have properties which would help with their transferability. These aspects will be a major topic of discussion in chapter 5 where we introduce our own basis set generation.

For now let us summarize some of the different kinds of basis sets which will be mentioned more prominently in this thesis. This is not an exhaustive summary, codes which use wavelets [24] or augemented plane waves [25] are used as comparisons in chapter 7 and such basis sets are not summarized over the following sections since their only feature of interest (with regards to the discussion in this thesis) is the ability to provide well converged results. However in this regard, the ability to produce converged results is explored when plane waves are discussed, in section 4.1.2, and the relevance of this with regards to the results presented in this thesis is discussed in section 4.5 and chapter 7.

4.1.1 Slater-Type orbitals

One of the first types of functions to be employed as a basis set were Slater-type orbitals (STOs) [26], which are solutions of Schrödinger time-independent equations for Hydrogen-like atoms (one electron and positive $Z > 1$ nuclear charge). Such functions are considered to be the best physically motivated candidates for localized basis sets, since they behave has one would expect for a function representing electrons. A STO centred on an atom at $\mathbf{R}_\alpha$ with an angular momentum value $l = n_1 + n_2 + n_3$ can be written as:

$$\phi(\mathbf{r}) = (x - R_{\alpha,x})^{n_1}(y - R_{\alpha,y})^{n_2}(z - R_{\alpha,z})^{n_3}e^{-\alpha|\mathbf{r}-\mathbf{R}_\alpha|} \tag{4.2}$$

The main attractive features of STOs are their locality (i.e. they are centred around an atom) and correct physical description of the true wave function behaviour around $\mathbf{r} = \mathbf{R}_\alpha$,

which is referred to in literature as *Kato's cusp condition* [27]. However constructing the Hamiltonian elements for STOs is difficult, and in addition Gaussian type orbitals (GTOs, introduced below) share some similarities in behaviour but decay much faster making for a sparser Hamiltonian and overlap matrices, which is more desirable for efficient implementations.

4.1.2 Plane Waves

ABINIT [28] a PW KSDFT code will be used as a reference in the result section of this thesis therefore a brief discussion of PW implementations is warranted and will be presented in this section.

A periodic function $f(x)$ with period P, that is $f(x) = f(x+P)$, can be expanded in terms of plane waves (e^{ikx}) by performing a Fourier expansion:

$$f(x) = \sum_{n=-\infty}^{\infty} c_n e^{i\frac{2\pi nx}{P}} \tag{4.3}$$

where the Fourier coefficients c_n are,

$$c_n = \frac{1}{P}\int_{x_0}^{x_0+P} f(x)e^{i\frac{2\pi nx}{P}}dx \tag{4.4}$$

In the discussion at the end of last chapter it was shown that a single-state KS orbital ψ_{ϵ_i} can be written as a Bloch function when periodic boundary conditions are employed. It seems natural then to expand the periodic part of the Bloch function, $u_{\mathbf{k}}(\mathbf{r})$, using PW,

$$u_k(\mathbf{r}) = \sum_{m=1}^{N} c_m \frac{1}{\sqrt{\Omega}} e^{i\mathbf{G_m}\cdot\mathbf{r}} = \sum_{m=1}^{N} c_m \left|G_m\right\rangle \tag{4.5}$$

where Ω is the volume of the Brillouin zone, c_m is the expansion coefficient, $|G_m\rangle = \frac{1}{\sqrt{\Omega}}e^{i\mathbf{G_m}}$ is a reciprocal vector and N controls the number of plane waves used. In the limit that $N \to \infty$ the expansion (4.5) becomes exact, however for practical purposes, i.e. numerical implementation, the expansion (4.5) must always be truncated at some chosen N. The simplicity of controlling the accuracy of the expansion (equation (4.5)) with increasing N, is one of the great strengths, and a hallmark, of PW calculations.

Another benefit of PW is their mutual orthogonality,

$$\frac{1}{\Omega}\int_{\Omega} e^{-i\mathbf{G}_m\cdot\mathbf{r}} e^{i\mathbf{G}_n\cdot\mathbf{r}} d\mathbf{r} = \delta_{m,n} \tag{4.6}$$

as discussed in chapter 2 if orthonormal basis are used the KS equations can be mapped into a ordinary eigenvalue problem, as opposed to the more complicated case of non-orthogonal basis which forms a generalized eigenvalue problem.

Let us now form the KS eigenvalue problem using PW. For simplicity assume we are dealing the Γ-point in the Brillouin zone (i.e. $\mathbf{k} = 0$) so that the KS wavefunction is simply with the periodic part of the Bloch function. Using equation (4.5) we can express the KS equation as,

$$\sum_m H_{\mathrm{KS}} \left|G_m\right\rangle c_{i,m} = \epsilon_i \sum_m c_{i,m} \left|G_m\right\rangle \tag{4.7}$$

where the index i indicates an expansion of the KS wavefunction (ψ_i) with eigenvalue ϵ_i. Multiplying on the right by $\langle G_n|$ we have

$$\sum_m \left\langle G_n\right| H_{\mathrm{KS}} \left|G_m\right\rangle c_{i,m} = \epsilon_i \sum_m c_{i,m} \left\langle G_n|G_m\right\rangle = \epsilon_i c_{i,m} \tag{4.8}$$

which can be written in matrix notation as,

$$\sum_m H_{nm} c_{i,m} = \epsilon_i c_{i,m} \tag{4.9}$$

Most modern PW implementations do not solve the previous eigenvalue problem directly, instead they use iterative methods [29, 30] which dramatically reduce the cost of calculations. For large-scale calculations, which employ iterative solving methods, the orthogonalisation of KS orbitals becomes the leading time consuming step. Due to the delocalized nature of PW there is little prospect that the computational effort involved in this step can be reduced making PW less attractive for calculations involving large systems. Despite this drawback, the popularity of PW implementations stems from the easiness to converge the result with respect to the basis sets. This is accomplished by performing different calculations on the same system whilst increasing the number of plane waves (N).

To demonstrate how plane wave KSDFT calculations should converge with increasing N let us calculate the kinetic energy term in equation (4.8):

$$\sum_m c_{i,m} \left\langle G_n\right| -\frac{1}{2} \bigtriangledown^2 \left|G_m\right\rangle = c_{i,m} G_m^2 \tag{4.10}$$

It is reasonable to assume, from equation (4.10), that after a certain m the kinetic energy G_m^2, of the respective $|G_m\rangle$, becomes unphysically high, it follows that the coefficients of expansion corresponding to that reciprocal vector $c_{i,m}$ must approach zero. It is therefore safe to assume that the coefficients $c_{i,n}$ for plane waves with smaller kinetic energy, i.e. $n < m$, must be more important than ones with a very high kinetic energy. From this line of reasoning we can define a quantity $e_{\mathrm{cut}} = \frac{1}{2} G_{\mathrm{max}}^2$ and truncate the expansion (4.5) to PW with kinetic energy lower than e_{cut}, i.e. $|G_m\rangle$ is used in the expansion if

$\frac{G_m^2}{2} < E_{cut}$. Equation (4.5) can then be rewritten as,

$$u_k(\mathbf{r}) = \sum_{m}^{G_{\max}} c_{i,m} \, |G_m\rangle \tag{4.11}$$

where $G_{\max} < \sqrt{4e_{\text{cut}}}$. The e_{cut} value will typically vary depending on the type of *psedudopotential* used, i.e. the approximation to the true nuclear potential (explained in section 4.2).

The truncation in equation 4.11 introduces some error in the KSDFT calculation. However this error can be quantified by systematically increasing e_{cut} for different calculations on the same system, which are commonly known as "runs", until the difference in total energy of the present and previous run (with smaller e_{cut}) is less than a chosen tolerance:

$$E_{\text{KS}}^{i} - E_{\text{KS}}^{i-1} \leq tol \tag{4.12}$$

When condition (4.12) is met, the resulting energy is said to be converged with respect to the basis set. This is regarded as one of the greatest strengths of PW implementations since one can confidently state that whatever error is found when attempting to explain a physical observation must be due to the other approximations used in the KSDFT code (exchange-correlation, pseudopotential). Thus as far as KSDFT is concerned for a chosen exchange-correlation and pseudopotential a well converged PW result is correct and any other implementation (such as ones which use localised basis sets) that attempts to solve the same Hamiltonian (like-to-like calculation) will most likely produce a higher energy than the respective PW one. This has led to the widespread use of plane wave codes in fields such as solid state physics. It should be noted though that in practice, calculations are usually performed with fewer plane waves than needed to reasonably converge the energy.

A drawback of the plane wave basis set, which is not shared by GTOs, deals with the unadaptiveness of a plane wave basis set. That is the e_{cut} value must be increased for the whole system even if only one of the atoms requires it. The prototypical example of this is an oxygen atom embedded in a unit cell of many Silicon atoms, here the Oxygen atom dictates the high value of e_{cut} to be used in the calculation even though Silicon can be ran with a far small value of e_{cut}.

For a modern discussion in PW implementation consult [31], and particularly [28] which presents the plane wave code ABINIT, used later in this thesis. For the purposes of our discussion however the benefits and drawbacks presented here and summarized at the end of this chapter are enough.

4.1.3 Discrete variable representation

In pseudo spectral methods such as the Discrete variable representation (DVR) one uses both a finite basis over a set of grid points, i.e.

$$\phi_i(\mathbf{r}) = \sum_i^N \psi_i(\mathbf{r}) \tag{4.13}$$

and a set of grid points $\mathbf{r}_1, \mathbf{r}_2, ..., \mathbf{r}_n$. For a given set of basis functions, one chooses a quadrature to convert scalar products into sums over the quadrature points $\mathbf{r}_i$,

$$\int_a^b \psi_m(\mathbf{r})\psi_n(\mathbf{r})d\mathbf{r} = \sum_k \psi_m(\mathbf{r})\psi_n(\mathbf{r}_k)w_k \tag{4.14}$$

where the w_k are the weights. In DVR an operator which is a function of position, i.e. $V(\mathbf{r})$ can be applied to a state, say $\phi(\mathbf{r})$ by multypling it at the quadrature points,

$$V(\mathbf{r})\psi(\mathbf{r}) = \sum_k V(\mathbf{r}_k)\psi(\mathbf{r}_k) \tag{4.15}$$

For the purpose of this thesis the systematic convergence of a DVR code will be important. In Chapter 5 some results will be presented which will be compared against an atomic DFT DVR code where the convergence of the DVR results is shown by performing calculations with increasing number of points (and as a result of that functions). A more detailed explanation of the DVR code used in this thesis can be found in [32].

4.1.4 Gaussian Basis sets

GTOs, like STOs, are local functions $X_\alpha(\mathbf{r} - \mathbf{R_I})$ associated with an atom at a specific point ($\mathbf{R_I}$). A Cartesian Gaussian function can be written as:

$$\phi(\mathbf{r} - \mathbf{R_I}) = (x - R_{I_x})^{n_x}(y - R_{I_y})^{n_y}(z - R_{I_z})^{n_z}e^{\alpha|\mathbf{r}-\mathbf{R_I}|^2} \tag{4.16}$$

where $n_x + n_y + n_z = l$ the angular momentum and α is the exponent responsible for the spatial resolution of the function. Unlike STOs, GTOs do not fulfil Kato's cusp condition [27] however, this isn't a serious problem as pseudopotentials are used for all the calculations in this thesis and the nuclear cusps are removed. The implementation of GTOSs in a KSDFT code is simpler and more efficient than with STOs, due to some favourable mathematical properties of Gaussian functions. One such property being: The product of two Gaussian functions is another Gaussian function,

$$e^{-\alpha|\mathbf{r}-\mathbf{R}_A|^2}e^{-\beta|\mathbf{r}-\mathbf{R}_B|^2} = K_{AB}e^{-\gamma|\mathbf{r}-\mathbf{R}_C|^2} \tag{4.17}$$

where K_{AB}, R_C and γ are given in section 4.4.0.1. Further useful analytic properties regarding the integrals of functions constructed from the product of a polynomial and a Gaussian can be derived from repeat applications of the following identity,

$$\frac{d}{dx}e^{-\alpha x^2} = -2x\alpha e^{\alpha x^2} \tag{4.18}$$

The properties described above in conjunction with other tabulated formulas for Gaussian integrals [33], allow for most integrals involving GTOs in the matrix building stage to be performed analytically. Particular details pertaining to the use of GTOs in `AIMPRO` are left for later sections. The analytical evaluation of integrals not only eliminates the error associated with numerical integration, but it also speeds up calculations considerably.

4.2 Pseudopotentials

Describing the core electrons of an atom can be problematic and inefficient, since we must account for the singularity in the potential as $r \to 0$, which would require plane waves with high kinetic energy, or similarly, if one is dealing with finite difference, a very fine mesh.

However in most electronic calculations, be it in solid state physics or in quantum chemistry, the core electrons contribution to the total energy of a system is mostly unchanged from its counterpart in isolated atom calculations. The differences in energies of valence electrons involved in binding are of much larger importance, as these differences are pertinent to the physics and chemistry of the system. It is conceivable then that the energy associated with an atom's core electrons could be removed from a KSDFT calculation involving many different atoms, considerably lowering the total binding energy, with little loss to the physical prediction of the calculation.

Furthermore wave functions of core electrons add to the complexity of valence wave functions, given that a valence electron wave function must oscillate rapidly as $r \to 0$, to preserve orthogonality with core states. This translates to a higher computational effort as more PW are needed.

A new effective potential called the *pseudopotential* is therefore constructed which replaces the combined potential of the core electrons and the nucleus. This pseudopotential is "weaker" than the nuclear potential (includes core electrons). Furthermore the valence wave function is replaced with a pseudo-wave-function which has a smooth behaviour in the core region.

The method of pseudopotentials was, historically, developed to help with plane wave calculations. The fast oscillations in the core region of regular KSDFT calculations

severely restricts the range of possible systems that one could study because of the system wide high e_{cut} requirements. GTOs however do not suffer from this uniform spacial resolution, they are adaptive bases and one can increase the number of functions for specific atoms. Therefore if one required increased accuracy for a particular atom in a system, to study defects for example, a stronger pseudopotential with its corresponding larger basis set could be used just for that atom. Nevertheless pseudopotentials can be used with GTOs, as is done in this thesis. This allows us to compare AIMPRO results with well converged ("correct") PW calculations.

There are two main approaches used to justify and introduce pseudopotentials: The operator approach and the scattering approach in which a weaker pseudopotential is generated with the constraint that it has similar scattering properties to the full potential. We will introduce pseudopotentials using the operator approach given that it highlights the introduction of non-locality to the KSDFT scheme.

4.2.1 Operator approach (Non-locality)

This discussion follows the pseudopotential transformation of Philips and Kleinman [34] and Antonick [35]. Consider an Hamiltonian $\hat{H}$ for an atom, let $|\psi^v\rangle$ be a valence state with energy E_v and let the set of $|\psi_n^c\rangle$ be the core states with corresponding energies E_n, all of the previous states are eigenstates of $\hat{H}$. Based on the previous section's discussion we attempt to construct a pseudo wave function $|\Psi\rangle$:

$$|\psi^v\rangle = |\Psi\rangle + \sum_n^{\text{core}} a_n |\psi_n^c\rangle \tag{4.19}$$

The expansion coefficients a_n are fixed by the requirement that $|\psi^v\rangle$ must be orthogonal to $|\psi_n^c\rangle$,

$$|\psi^v\rangle = |\Psi\rangle + \sum_n^{\text{core}} |\psi_n^c\rangle \langle\psi_n^c|\Psi\rangle \tag{4.20}$$

Now we can substitute this into $\hat{H}|\psi^v\rangle = E_v|\psi^v\rangle$:

$$\hat{H}|\Psi\rangle - \sum_n^{core} E_n |\psi_n^c\rangle \langle\psi_n^c|\Psi\rangle = E|\Psi\rangle - E\sum_n^{core} |\psi_n^c\rangle \langle\psi_n^c|\Psi\rangle \tag{4.21}$$

This can be simplified to:

$$\begin{aligned} \hat{H}|\Psi\rangle + \sum_n^{\text{core}} (E - E_n) |\psi_n^c\rangle \langle\psi_n|\Psi\rangle &= E|\Psi\rangle \\ [\hat{H} + \hat{V}_{nl}]|\Psi\rangle &= E|\Psi\rangle \end{aligned} \tag{4.22}$$

Where we define,

$$\hat{V}_{\text{nl}} = \sum_{n}^{\text{core}} (E - E_n) \left|\psi_n^c\right\rangle \left\langle\psi_n^c\right| \tag{4.23}$$

to be an extra non-local potential. The smoother pseudo wave function Ψ has the same energy as the valence state $|\psi_v\rangle$, but it is now a solution of $\hat{H}$ with an extra energy dependent non-local contribution $\hat{V}_{\text{nl}}(\mathbf{r}, \mathbf{r}')$. The repulsive non-local potential is concentrated on the core which results in a weaker overall pseudopotential around this region.

4.2.2 Norm-conserving pseudopotentials (NCPPS)

It was shown in the section above that in order to construct a pseudo wave function one introduces a degree of non-locality in the KSDFT implementation. However, besides the introduction of non-locality, no requirements were made on how to construct an accurate and transferable *ab-initio* pseudopotential (without any empirical input). That is a pseudopotential that can be used on a multitude of different environments, despite being constructed on an isolated atom.
A list of requirements for such a construction was given by Hammann, Schluter and Chiang[36]:

1. Pseudo and all-electron valence eigenvalues agree for a referenced atomic electronic configuration.

2. (Norm-conservation) The integral of the real and pseudo charge density agree, from 0 to r for $r > r_c$, for valence states. That is $\int_0^r |\psi^v(\mathbf{r})|^2 d\mathbf{r}$ and $\int_0^r |\Psi_{ps}(\mathbf{r})|^2 d\mathbf{r}$ agree for $r > r_c$ for valence states.

3. The logarithmic derivatives of the all-electron and pseudo wave functions agree at $r = r_c$

Point 3, the most unintuitive out of all the points, and point 2 are taken as steps to give better transferability of the constructed pseudopotential and to ensure the scattering characteristics of the pseudopotential mimic that of the all-electron potential. Point 1 follows intuitively from the expectations of the pseudopotential wave function presented in the previous section.

The choice of r_c is a crucial one. Choosing a smaller r_c increases the accuracy of the pseudopotential and its transferability but leads to a "harder" pseudopotential which for PW implementation results in high e_{cut} values. This drawback, however, is not shared by GTOs.

Based on the work of HSC Bachlet, Hamman and Schluter (BHS) [37] constructed pseudopotentials which satisfy all the properties stipulated above and are expressed in a

Gaussian expansion with tabulated coefficients. These potentials are still popular today a testament to the title of the paper "Pseudopotentials that work" [37].

4.2.3 Goedecker-Tetter-Hutter (GTH) potentials

Goedecker, Tetter and Hutter presented a construction of pseudopotentials which is separable, local and non-local calculated separately, and can be efficiently implemented in plane wave sets due favourable reciprocal space form (similarly for GTOs) [38]. A GGA optimization of these potentials [39] is used in this thesis thus their form will be described below.

The local part of a GTH pseudopotential is given by:

$$V_{\text{loc}}(r) = \frac{-Z_{\text{ion}}}{r}\text{erf}(\frac{r}{\sqrt{2}r_{loc}}) + \exp\left[-\frac{1}{2}\left(\frac{r}{r_{loc}}\right)^2\right] \times \left[C_1 + C_2\left(\frac{r}{r_{loc}}\right)^2 + C_3\left(\frac{r}{r_{loc}}\right)^4 + C_4\left(\frac{r}{r_{loc}}\right)^6\right] \tag{4.24}$$

where Z_{ion} is the charge of the nucleus minus that of the core electrons, r_{loc} is a chosen core radius set by the parameter list in GTH. The coefficients C_i are found by minimizing the difference between the eigenvalues of an all electron atomic calculation and those of the pseudo atom. This is done using a downhill simplex, chapter 5.4.3. The non-local part is given by:

$$\begin{aligned} V_{\text{nl}}(\mathbf{r},\mathbf{r}') = &\sum_{i}^{3}\sum_{j}^{3}\sum_{m=-l}^{m=+l} Y_{lm}(\theta,\phi)p_i^l(r)h_{i,j}^l p_i^l(r')Y_{lm}(\theta,\phi)^* \\ &+ \sum_{i}^{3}\sum_{j}^{3}\sum_{m=-l}^{m=+l} Y_{lm}(\theta,\phi)p_i^l(r)h_{i,j}^l p_i^l(r')Y_{lm}(\theta,\phi)^* \end{aligned} \tag{4.25}$$

The projectors p_i^l are:

$$p_i^l(r) = \frac{\sqrt{2}r^{l+2(i-1)}exp(\frac{-r^2}{2r_l})}{r^{l+(4i-1)/2}\sqrt{\Gamma(l+\frac{4i-1}{2})}} \tag{4.26}$$

where the r_l and $h_{i,j}^l$ are parameters given in [38]. The total pseudopotential is then:

$$V(\mathbf{r},\mathbf{r}') = V_{loc}(r)\delta(\mathbf{r}-\mathbf{r}') + \sum_l V_{\text{nl}}(\mathbf{r},\mathbf{r}') \tag{4.27}$$

V_{loc} and V_{nl} both have an analytical form in reciprocal space. Even though this pseudopotential was primarily developed for plane waves it is easily extended to GTOs. Furthermore the analytical dual-space character of these pseudopotentials make them computational efficient to implement.

4.3 The Hartree potential

The Hartree potential $V_{\mathrm{H}}(\mathbf{r})$ can be found from Poisson's equation for an electron charge density $n(\mathbf{r})$:

$$\nabla^2 V_{\mathrm{H}}(\mathbf{r}) = 4\pi n(\mathbf{r}) \tag{4.28}$$

For reasons which will become clearer shortly, It is beneficial to expand both $n(\mathbf{r})$ and $V_{\mathrm{H}}(\mathbf{r})$ in PW,

$$n(\mathbf{r}) = \sum_{\mathbf{G}} n(\mathbf{G}) e^{i\mathbf{G}\cdot\mathbf{r}} \quad \text{and} \quad V_{\mathrm{H}}(\mathbf{r}) = \sum_{\mathbf{G}} n(\mathbf{G}) e^{i\mathbf{G}\cdot\mathbf{r}} \tag{4.29}$$

we can the substitute these into (4.28), and apply the Laplacian to obtain:

$$\sum_{\mathbf{G}} \mathbf{G}^2 V_{\mathrm{H}}(\mathbf{G}) e^{i\mathbf{G}\cdot\mathbf{r}} = -4\pi \sum_{\mathbf{G}} n(\mathbf{G}) e^{i\mathbf{G}\cdot\mathbf{r}} \tag{4.30}$$

Comparing the terms, and omitting $\mathbf{G} = 0$ we find:

$$V_{\mathrm{H}}(\mathbf{G}) = \frac{-4\pi}{\mathbf{G}^2} n(\mathbf{G}) \tag{4.31}$$

The $\mathbf{G} = 0$ term needs to be treated separately. From the expansion in PW of $n(\mathbf{r})$, the $n(\mathbf{G})$ term for $\mathbf{G} = 0$:

$$n(\mathbf{G} = \mathbf{0}) = \frac{1}{\Omega} \int n(\mathbf{r}) d\mathbf{r} \tag{4.32}$$

This is just the average of the charge density. The energy arising from this term is included in a separate term E_{Ewald} which contains the energy due to a static infinite distribution of charges. Thus the calculations for V_{ij}^{H} (and E_{H}) can proceed without the $\mathbf{G} = 0$ term.

The Hartree energy can be found from:

$$E_H = 2\pi \sum_{\mathbf{G}} \frac{|n(\mathbf{G})|^2}{|\mathbf{G}|^2} \tag{4.33}$$

4.3.1 The Generalized Eigenvalue Problem

At the heart of any KSDFT code lies an eigenvalue problem. It was noted in chapter 2 that for non-orthogonal basis sets, such as GTOs, instead of an OEP one must solve a GEP. We will now summarize how a GEP is formed in a KSDFT implementation from a choice of non-orthogonal basis sets.

A KS state (ψ_λ) (associated eigenvalue λ) can be expanded in terms of non-orthogonal functions (such as GTOs) as follows:

$$\psi_\lambda = \sum_{i=1}^{N} c_i^\lambda \phi_i(\mathbf{r}) \tag{4.34}$$

The density can be expressed as:

$$n(\mathbf{r}) = \sum_{\lambda}^{n_{\text{occ}}} |\psi_\lambda|^2 = \sum_{i,j} \sum_{\lambda}^{n_{occ}} f_\lambda c_i^\lambda \phi_i c_j^\lambda \phi_j = \sum_{i,j} \sum_{\lambda}^{n_{\text{occ}}} b_{ij} \phi_i \phi_j \tag{4.35}$$

where n_{occ} is the number of occupied states and

$$b_{ij} = \sum_{\lambda} f_\lambda c_i^\lambda c_j^\lambda \tag{4.36}$$

contains all the information pertaining to the expansion, where f_λ can be given by a Fermi-Drirac distribution eqn. (3.41). It follows from our discussion thus far, that finding the ground-state density of the system amounts to find b_{ij} which minimizes $E[b_{ij}]$. Therefore, we require that the expansion (4.35) be a minimum at the ground-state with respect to changes in the coefficients c_i^λ with the constraint

$$\int n(\mathbf{r}) d\mathbf{r} = 1 \text{ or } \sum_{i,j} \sum_{\lambda} S_{ij} c_i^\lambda c_j^\lambda = 1 \tag{4.37}$$

where we have defined the overlap matrix $\mathbf{S}$ with terms given by

$$S_{ij} = \int \phi_i^*(\mathbf{r}) \phi_j(\mathbf{r}) d\mathbf{r} \tag{4.38}$$

Doing this we find,

$$\frac{\delta}{\delta c_i^\lambda} \left[E[b_{ij}] - \sum_{\lambda} \epsilon_\lambda \left(\sum_{i,j} S_{ij} c_i^\lambda c_j^\lambda - 1 \right) \right] = 0 \tag{4.39}$$

The differentiation $\frac{\delta E[b_{ij}]}{\delta c_i^\lambda}$ can be found using chain rule:

$$\frac{\delta E[b_{ij}]}{\delta c_i^\lambda} = \frac{\delta E[b_{ij}]}{\delta b_{ij}} \frac{\delta b_{ij}}{\delta c_i^\lambda} \tag{4.40}$$

Where $\dfrac{\delta E[b_{ij}]}{\delta b_{ij}}$ is the Hamiltonian matrix H_{ij}. The resulting equation is :

$$\sum_{j} H_{ij} c_j^\lambda = \epsilon_\lambda \sum_{j} S_{ij} c_j^\lambda \tag{4.41}$$

This is the Generalized Eigenvalue Problem (GEP) which must be solved in a non-orthogonal KSDFT implementation. The Hamiltonian matrix in the primitive space (the space generated by the primitive basis) can be formed as follows,

$$H_{ij} = T_{ij} + V_{ij}^{\text{ps}} + V_{ij}^{\text{H}} + V_{ij}^{\text{xc}} \tag{4.42}$$

where the O_{ij} terms corresponding to local operators $O(\mathbf{r})$ are given as,

$$O_{ij} = \int \phi_i^*(\mathbf{r}) O(\mathbf{r}) \phi_j(\mathbf{r}) d\mathbf{r} \tag{4.43}$$

whilst for non-local operators O_{ij}^{nl} is given by,

$$O_{ij}^{\mathrm{nl}} = \int \phi_i^*(\mathbf{r}') O(\mathbf{r}', \mathbf{r}) \phi_j(\mathbf{r}) d\mathbf{r} d\mathbf{r}' \tag{4.44}$$

a more detail discussion on the construction of the terms in (4.42) performed in `AIMPRO` will be discussed in the next section.

It must be noted that for GTOs the overlap matrix $\mathbf{S}$ is particularly sensitive to the basis set choice. A poorly constructed expansion (4.35) will lead to an ill-conditioned overlap matrix which typically either prevents diagonalization, rows in $\mathbf{S}$ become linear dependent, or yields inaccurate results. Care must be taken when generating a primitive basis sets and using it to minimize such errors, this too will be discussed in the next chapter.

4.4 AIMPRO code

`AIMPRO` [5, 40, 16] is a KSDFT code which uses GTOs as a basis set, i.e. as a set of ϕ_i to be used as described in the previous section. In this section the periodic version of `AIMPRO` is discussed, we will focus our discussion on the efficient Hamiltonian and overlap matrix construction present in the version of `AIMPRO` used in this thesis, which takes advantage of the short ranged nature of Gaussian functions for efficient evaluation of the integrals required during the matrix building (4.42). This is an essential requirement for large-scale calculations and, if large basis sets are used, allows us to build the Hamiltonian and overlap matrices efficiently. The construction of the elements in equation (4.41) will be summarized here.

4.4.0.1 The overlap matrix

It follows from the properties describe in section 4.1.4 that the overlap matrix can be constructed analytically. Let us consider two distinct s-type Gaussian, the overlap between them is given,

$$\begin{aligned} S_{ij}^{ss} &= \int \phi_i^s(\mathbf{r}) \phi_j^s(\mathbf{r}) d\mathbf{r} = \int e^{-\alpha_i (\mathbf{r}-\mathbf{R}_i)^2} e^{-\alpha_j (\mathbf{r}-\mathbf{R}_j)^2} d\mathbf{r} \\ &= \int e^{-\frac{\alpha_i \alpha_j}{\alpha_{ij}} (\mathbf{R_i}-\mathbf{R}_j)^2} e^{-\alpha_{ij} (\mathbf{r}-\tilde{\mathbf{R}}_{ij})^2} d\mathbf{r} \end{aligned} \tag{4.45}$$

where

$$\alpha_{ij} = \alpha_i + \alpha_j \quad \text{and} \quad \tilde{\mathbf{R}}_{ij} = \frac{\alpha_i \mathbf{R}_i + \alpha_j \mathbf{R}_j}{\alpha_{ij}} \tag{4.46}$$

By performing a change of variables, $\mathbf{r}' = \mathbf{r} - \tilde{\mathbf{R}}_{ij}$, and using the well know identity $\int_{-\infty}^{\infty} e^{-x^2} dx = \sqrt{\pi}$, we find:

$$S_{ij}^{ss} = \left(\frac{\pi}{\alpha_i + \alpha_j}\right)^{\frac{3}{2}} e^{-\frac{\alpha_i \alpha_j}{\alpha_i + \alpha_j}(\mathbf{R_i} - \mathbf{R}_j)^2} \tag{4.47}$$

Similarly, analytic relations can be found for two-centre integrals involving higher angular momentum type Gaussians. For a p-type Gaussian, $\phi_i^p(\mathbf{r})$ we have the following identity,

$$\phi_i^p(\mathbf{r}) = (\mathbf{r} - \mathbf{R})_u e^{-\alpha_i(\mathbf{r}-\mathbf{R}_i)^2} = \frac{1}{2\alpha_i} \frac{d}{d\mathbf{R}_{i,u}} e^{-\alpha_i(\mathbf{r}-\mathbf{R}_i)^2} \tag{4.48}$$

where u represents x, y or z. To capitalize on this property let us now differentiate equation (4.47), we find,

$$S_{ij}^{ps} = \frac{1}{2\alpha_i} \frac{d}{d\mathbf{R}_{i,u}} S_{ij}^{ss} = (\mathbf{R}_i - \mathbf{R}_j)_u S_{ij}^{ss} \tag{4.49}$$

Similarly for S_{ij}^{sp} we have:

$$S_{ij}^{sp} = (\mathbf{R}_i - \mathbf{R}_j)_u S_{ij}^{ss} \tag{4.50}$$

Equation (4.49) can be generalized for higher orbital type Gaussians, however the usefulness of such relations is quickly overshadowed by it's cumbersomeness. Instead overlap terms involving high orbital momentums such as S_{ij}^{dp} are written in terms of simpler results, these relations are given in [33].

From equation (4.47) it follows that for two distinct Gaussians (in this case s-type), satisfying certain conditions, their overlap is small if they are located far from each other, i.e. $S_{ij} << 1$. Furthermore we can approximate the V_{ij} matrix element involving these Gaussians as,

$$V_{ij} = \int \phi_j^*(\mathbf{r}) V(\mathbf{r}) \phi_i(\mathbf{r}) d\mathbf{r} \leq S_{ij} V_{\max} \tag{4.51}$$

Where $V_{\max} = \max[V(\mathbf{r})]$. It follows that, constructing the Hamiltonian matrix H_{ij} can be sped up if we allow some of the V_{ij} terms to be set to zero without them being formally evaluated, as long as $S_{ij} V_{\max}$ falls below a certain threshold. This is called *integral screening*, and can be controlled by a tolerance chosen at the beginning of a KSDFT calculation. As system size increases the inter-atom distances $|\mathbf{R}_i - \mathbf{R}_j|$ increases, and more elements of the Hamiltonian can be set to zero without being properly evaluated, reinforcing the usefulness of the screening relation (4.51).

4.4.1 The kinetic energy

The kinetic energy for a system of independent-electrons $T_s[n(\mathbf{r})]$, where the density $n(\mathbf{r})$ is given by equation (4.35), can be written as:

$$T_{\mathrm{s}}[n(\mathbf{r})] = -\frac{1}{2}\sum_{\lambda}^{n_{\mathrm{occ}}} \int f_\lambda \psi_\lambda(\mathbf{r}) \nabla^2 \psi_\lambda(\mathbf{r}) d\mathbf{r} = \sum_{ij} b_{ij} T_{ij} \tag{4.52}$$

where b_{ij} is given in equation (4.35) and T_{ij} is given by:

$$T_{ij} = -\frac{1}{2}\int \phi_i^*(\mathbf{r}) \nabla^2 \phi_j(\mathbf{r}) d\mathbf{r} \tag{4.53}$$

From the previous section's discussion, particularly equation (4.49), it follows that the T_{ij} terms can be calculated analytically, recurrence relations to do so are given in [33]

4.4.2 External potential

In `AIMPRO` the external potential $V_{\mathrm{ext}}(\mathbf{r})$, due to charge of the nucleus, is given by a pseudopotential. The non-local term of the pseudopotential is given by,

$$V_{ij}^{nl} = \int\int \phi_i(\mathbf{r}) V_{\mathrm{nl}}(\mathbf{r}, \mathbf{r}') \phi_j(\mathbf{r}') d\mathbf{r} d\mathbf{r}' \tag{4.54}$$

where $V_{\mathrm{nl}}(\mathbf{r}, \mathbf{r}')$ is short ranged, V_{ij}^{nl} can be evaluated analytically using the recuring relations in [33]. The energy corresponding to the non-local part of the pseudopotential is given by,

$$E_{\mathrm{nl}} = b_{ij} V_{ij}^{\mathrm{nl}} \tag{4.55}$$

The local part of the pseudopotential is given by:

$$V_{ij}^{\mathrm{loc}} = \int \phi_i(\mathbf{r}) V_{\mathrm{loc}}(\mathbf{r}) \phi_j(\mathbf{r}) d\mathbf{r} \tag{4.56}$$

where $V_{\mathrm{loc}}(\mathbf{r})$ is long-ranged. Given the periodic boundary conditions of our implementation this term V_{ij}^{loc} can be calculated more efficiently in reciprocal space.

$V_{\mathrm{loc}}(\mathbf{r})$ can be expressed in reciprocal space as:

$$V_{\mathrm{loc}}(\mathbf{r}) = \sum_{G} V_{\mathrm{loc}}(\mathbf{G}) e^{i\mathbf{G}\cdot\mathbf{r}} \tag{4.57}$$

Therefore equation (4.56) can be rewritten as:

$$\begin{aligned} V_{ij}^{loc} &= \int \phi_i(\mathbf{r}) \sum_{G} V_{\mathrm{loc}}(\mathbf{G}) e^{i\mathbf{G}\cdot\mathbf{r}} \phi_j(\mathbf{r}) d\mathbf{r} \\ &= \sum_{G} V_{\mathrm{loc}}(\mathbf{G}) \int \phi_i(\mathbf{r}) \phi_j(\mathbf{r}) e^{i\mathbf{G}\cdot\mathbf{r}} d\mathbf{r} \end{aligned} \tag{4.58}$$

where an efficient method to evaluate the previous integral is presented in [5], in which the fast decay, over the reciprocal space, of the fourier transformation of the overlap terms $\phi_i\phi_j$, is used to then recast the sum in equation (4.58) over a real space grid. This method allows the same number of real space grid points to be used for all $\phi_i\phi_j$, which leads to a large increase in speed.

The energy associated with this term $E_{\rm loc}$, can similarly, be obtained efficiently in reciprocal space,

$$E_{\rm loc}[n(\mathbf{r})] = \int n(\mathbf{r})V_{\rm loc}(\mathbf{r})d\mathbf{r} \tag{4.59}$$

expanding both $V_{\rm loc}(\mathbf{r})$ and $n(\mathbf{r})$ in reciprocal space we find,

$$\begin{aligned} E_{\rm loc}[n(\mathbf{r})] &= \sum_G \sum_{G'} \int n(\mathbf{G})e^{i\mathbf{G}\cdot\mathbf{r}}V_{\rm loc}(\mathbf{G'})e^{i\mathbf{G'}\cdot\mathbf{r}}d\mathbf{r} \\ &= \sum_G \sum_{G'} n(\mathbf{G})V_{\rm loc}(\mathbf{G'}) \int e^{i\mathbf{G}\cdot\mathbf{r}}e^{i\mathbf{G'}\cdot\mathbf{r}}d\mathbf{r} \\ &= \Omega \sum_G n(\mathbf{G})V_{\rm loc}(-\mathbf{G}) \end{aligned} \tag{4.60}$$

where in the last equation we took advantage of the orthonormality of PW. In these calculations the real to reciprocal space transformation, like in the case of PW implementations, uses FFT to reduce the computational effort.

4.4.3 Exchange-Correlation

The calculations presented in this thesis use the Perdew-Burke-Erzenrhof (PBE) [41] parametrization of the General Gradient Approximation (GGA) to the exchange-correlation [42, 43]. In the GGA scheme the energy due to the exchange-correlation is given by:

$$E_{\rm XC}^{\rm GGA}[n(\mathbf{r})] = \int f_{\rm xc}(n(\mathbf{r}), \mid \bigtriangledown n(\mathbf{r})\mid)d\mathbf{r} \tag{4.61}$$

and the exchange-correlation potential $V_{xc}(\mathbf{r})$ given by,

$$V_{xc}^{GGA}(\mathbf{r}) = \frac{\delta E_{XC}[n(\mathbf{r})]}{\delta n(\mathbf{r})} \tag{4.62}$$

The $V_{ij}^{\rm xc}$ can be constructed efficiently using the method described above to obtain the local pseudopotential term. More details of this construction can be found in [44].

4.4.4 Hartree terms

The Hartree energy and potential terms are found using the plane wave expansion of the density described in section 4.3. A detailed explanation of this can be found in [5].

4.4.5 Brillouin sampling

Periodic boundary conditions are used in all calculations presented in this thesis. From chapter 3 we found that in a periodic calculation the eigenvalues obtained from solving the KS Hamiltonian, $\lambda(\mathbf{k})$, depend on the chosen reciprocal vector $\mathbf{k}$. Thus any properties which are calculated from the eigenvalues have an associated $\mathbf{k}$ dependence. It is essential, then, to integrate any such properties over the reciprocal space.
The reciprocal vector $\mathbf{k}$ can be expressed as,

$$\mathbf{k} = \sum_{i=1}^{3} \frac{l_i}{N_i} \mathbf{b}_i \tag{4.63}$$

where $\mathbf{b}_i$ are the reciprocal vectors introduced in chapter 2, l_i and N_i are integers. Although initially it could appear as if the integrals in reciprocal space should be done over an infinite number of k-vectors, it follows from the properties of Bloch functions that k-points which differ by a reciprocal vector are equivalent, therefore one can restrict our sum to vectors which lie in the Brillouin zone (BZ). Although the number of k-vectors in the Brillouin zone is still infinite it is far easier to integrate properties over this smaller zone accurately.

Let $f_i(\mathbf{k})$ be a function which varies over BZ, the average value $\bar{f}$ can be found by:

$$\bar{f} = \frac{1}{\Omega_{BZ}} \int f_i(\mathbf{k}) d\mathbf{k} \rightarrow \frac{1}{N_k} \sum_{\mathbf{k}} f_i(\mathbf{k}) \tag{4.64}$$

where Ω_{BZ} is the volume of reciprocal space and N_k is the number of k-points. The calculations in this thesis involve finding the total energy, and thus a summation over the BZ is required. To find the averaged total energy the Kohn-Sham equations must be solved at each of the k-points included in the sum (in equation (4.64)), this often severely increases the computational time of a calculation. However this has no impact in the regular scaling of the code.

For very large systems the BZ becomes very small since,

$$\Omega_{BZ} = \frac{2\Pi^3}{\Omega_{cell}} \tag{4.65}$$

It follows then that for large systems typically the $\mathbf{k} = 0$ point suffices for the sum in equation (4.64).

Several different methods have been developed to efficiently span the BZ [45, 46, 47]. Most methods try to reduce the number of k-points necessary by using the symmetry to eliminate any equivalent k-points inside the BZ zone, thereby reducing the number of different calculations greatly. This new zone, without equivalent k-points, is known as the Irreducible Brillouin Zone (IBZ).The calculations in this thesis use the Monkhorst-pack

method [48] to generate a grid of special k-points inside the IBZ.

When spanning the Brillouin Zone there is no *a priori* method of choosing the correct grid. Several calculations must be performed with increasing grids. The total energy must be converged with respect to grid size. For all the calculations presented here, when a summation over the Brillouin Zone was necessary, the results were converged with respect to number of k-points chosen.

4.5 Summary

An overview of the different algorithms involved in implementing a KSDFT scheme, including basis sets, have been discussed.

Concerning the choice of basis sets, I must stress a few salient points, which will highlight the novelty and usefulness of the method presented in this thesis:

- Any ground-state properties calculated using (PW) implementations are, up to a choice of pseudopotential and exchange-correlation functional, the correct KSDFT answer. Whether PW KSDFT codes accurately replicate physical observations is a question of the quality of pseudopotential and exchange-correlation approximations, not basis set quality. For a theory-to-theory comparison it follows that any other implementation which uses different basis sets should, in a like-to-like calculation, strive to obtain the well converged PW result.

- GTOs have localization properties which allow for an efficient matrix build.

- GTOs do not have systematic basis set convergence, therefore in regular $\mathcal{O}(n^3)$ calculations the accuracy of GTOs lag behind that of plane waves.

Point 2 and 3 will be expanded in some detail in the next chapter, where a thorough overview of the benefits and drawbacks of GTOs is given in addition to our method of choosing a primitive basis.

Chapter 5

New method for generating Gaussian Basis Sets for filtration.

5.1 Introduction

Basis sets of Gaussian type orbitals are almost always associated with an atom, given that they are optimized for that particular atom in an separate atomic calculation (although often extra functions can be added, which might be optimized for test molecules [49]). This implicitly assumes that molecule or solid formation is a relatively small perturbation on the atoms of the system (at least energetically) [50]. The atomic calculation used to generate the basis sets can be performed with any of the independent-electron approximations discussed previously. In our generation the atomic energy is calculated using KSDFT, elsewhere Hartree-Fock is often used and we will briefly review two such basis sets.

Accurately optimizing GTOs to properly describe the ground state of an atom (and often some unfilled orbitals too) should in principle produce a basis set which can be used in a variety of environments, such basis sets are deemed to be *transferable*. It is often the case that attaining high accuracy and good transferability requires a large number of primitives which would undoubtedly be very inefficient. It can be beneficial with regards to computational expense if the primitives are contracted into a smaller set of functions (explained in section 5.2.2). However the basis sets then loses transferability given that the functions contracted during the atomic calculation lose some flexibility, as each primitive can no longer be individual adjusted to better represent the atom in a different environment. Thus, for most calculations requiring high accuracy, extra Gaussian functions can be added to contracted basis sets to adequately describe bonding environments [51]. This leads to yet more basis sets, the number of which grows considerably larger when one takes into account that the electronic properties of different atoms may require the addition of characteristic Gaussians. It follows that to properly use GTOs in KSDFT

requires a degree of knowledge into the current state of the GTO field and, often, how the specific GTOs behave for systems with similar properties to the one we wish to study [51]. In addition different system properties (energy, structure, vibrational frequency) converge differently with respect to basis set. Unlike the case for plane waves where convergence is obtained systematically, with GTOs different basis sets must be used each with increasing accuracy (and typically size) to demonstrate that one is approaching the complete basis limit (CBS). However there is no *a priori* basis set progression roadmap which makes converging results far from trivial [50].

In the novel method of generating GTO basis sets presented in this thesis the uncontracted even-tempered basis sets is constructed by minimizing the difference in energy calculated using said basis set and an atomic DVR calculation, unlike other basis sets [52] where often convergence of the energy is demonstrated with increasing number of Gaussian functions. This methodology avoids having the routine pick an local minima which could lead to erroneous results. Furthermore the routine presented here produces the basis set with the highest first exponent for which a choosen tolerance is met, which reduces the likelihood of calculation failure due to linear dependence. This new basis set when used in a KSDFT calculation with filtration methodology will substantially decrease many of the requirements/difficulties stated above. Only one basis set composed of uncontracted primitives is generated per atom, with the same routine, for all atoms in the periodic table. This primitive basis set is generated in a KSDFT calculation (for a given choice of pseudopotential and exchange correlation) to an error of less than 1 meV. This yields a very large set of primitives that is both tailored for the specific atom and has a good degree of flexibility by virtue of being large and uncontracted [53, 54]. Such large primitive sets (typically more than 100 functions) would be useless in conventional KSDFT were it not for filtration [5, 40]. By contracting the large primitive basis sets on site (for the system at hand) using filtration, one is able to adapt it to better represent the atom in its surrounding electronic environment than one would using atomic contracted GTOs. This should translate into good transferability and adaptability of the basis set, whilst maintaining the computational benefits enjoyed by smaller contracted basis sets. Furthermore, as we will demonstrate, this methodology allows us to attain PW accuracy at a cost of an efficient GTO implementation.

Given that ultimately in this work the basis set that is to be used in the KSDFT calculation is generated during the filtration stage of the calculation, the requirements on the underlying primitive basis are not as strict as they would be otherwise that is, the basis set can be very large. Regarding the primitive basis set we must ensure that it accurately describes the atom (in order that atomisation energies are accurate) and it contains the appropriate angular momentum primitives that might be required when the atom is used in any polyatomic system. In addition it could prove beneficial with regards

to efficiency and stability if the parameters used to construct the basis set follow certain conditions. All these points will be explored here.

The present chapter is divided in two parts: In the first part we will provide a brief overview of the GTO field, particularly different methods to generate basis sets. At this point two widely used Gaussian basis sets will also be briefly mentioned. In the second part of this chapter the basis set generation routine that I developed is introduced.

When we discuss Pople and Dunning basis sets in the first part of this section any mention of accuracy refers to the calculations provided in the respective papers. These are used solely in the discussion therein to reinforce or discard some conclusions regarding the said basis sets. The accuracy of our implementation is measured by using a recently developed benchmark [6], wherein our data is compared directly with well converged plane wave results. This will be presented in chapter 7.

5.2 Preamble

Before reviewing some common basis sets let us briefly summarize the basic recipe to optimize primitives for the atom, introduce contracted functions and even-tempered exponents.

5.2.1 Atomic energy minimization with respect to primitives

The majority of Gaussian basis sets are generated by systematically modifying the primitives - for example, by changing the exponents - to find which set of primitives minimises the energy of an isolated atom [55, 52]. The energy of an isolated atom can be expressed as a functional of the set of single-electron orbitals ψ_i in both Hartree-Fock, DFT and KSDFT:

$$E^{\gamma}_{\text{atom}} = E_{\text{atom}}[\{\psi^{\gamma}_i\}] \tag{5.1}$$

where $i \in [0, 1, 2, ..., N]$ represents the number of electronic states considered in the atomic calculation. The γ index indicates the energy and single-electron orbital dependence on a particular choice of the parameters which are used to generate the basis set:

$$|\psi^{\gamma}_i\rangle = \sum_j c^{\gamma}_{ij} |\phi^{\gamma}_j\rangle \tag{5.2}$$

The set of ψ^{γ}_i are solutions of an independent-particle atomic Hamiltonian:

$$\mathbf{H}^{\gamma}_{\text{atom}} |\psi^{\gamma}_i\rangle = \lambda_i \mathbf{S}^{\gamma}_{\text{atom}} |\psi^{\gamma}_i\rangle \tag{5.3}$$

where $\mathbf{S}^{\gamma}_{\text{atom}}$ is the overlap matrix.

What constitutes a choice of parameters γ and how they are modified iteratively is characteristic of a basis generation routine. Typically each angular momentum channel has a predetermined number of primitives, for example for the $1s$ orbital we have 6 exponents, for $2p_x$ we have 4 etc... A minimal basis set has one basis function per core state and valence state [52].

Broadly speaking, a basis set generating routine consists of specifying how the energy $E_{\text{atom}}[\psi_i^{\gamma}]$ minimization is performed with respect to the choice of parameters γ used to construct our basis, and what kind of independent electron approximation we use. In the next section we will briefly summarize two methods, one which uses Hatree-Fock and another which uses post-Hartree–Fock methods to calculate the atomic energy involved in generating the basis sets, equation (5.1).

In addition to the Gaussian primitives generated during the atomic calculations, often extra Gaussian primitives are added to better describe the atom in a bonding environment. The two main ones of particular importance are:

1. **Polarization functions** are higher angular momentum functions (than those of the occupied states) that are added to a basis set to better describe charge polarization and correlation effects, thus often in literature they are also referred to as *correlation functions*. Given that primitives with higher angular momentum than that present in the atom will not have an effect on the ground state atomic energy polarization functions must be optimized in either molecular [49] or atomic calculations which include correlation effects.

2. **Diffuse functions** are Gaussian primitives with exponents lower than that of the basis set generated for the isolated atom. There are several ways of adding them to the existent basis set, for instance the minimal augmentation, labeled by affixing "ma-" to the basis set name, adds a primitive, for each angular momentum shell present in the basis set, with the exponent set by dividing the lowest exponent of said shell by 3. A good summary of diffuse functions can be found in [56].

5.2.2 Contracted GTOs

A single Cartesian Gaussian function, often referred to as a *primitive*, for an atom centred at the origin, can be expressed as:

$$\phi_i(\mathbf{r}) = x^{n_x} y^{n_y} z^{n_z} e^{-\eta_i r^2} \tag{5.4}$$

where η_i is a chosen exponent, $n_x + n_y + n_z = l$ and l is the angular momentum of the primitive.

For Gaussian bases, the choice of parameters that govern the quality of a basis set, the most important of which are the number of different primitives and their exponents, is neither clear nor straightforward. Using a large number of primitives or using high angular momentum should correspond to a better result according to the variational principle. However, this quickly becomes counter-productive as the increase in accuracy is defeated by instability either in basis sets generation procedure (as we will see shortly) or during its usage in a KSDFT calculation. To benefit from the accuracy that large primitive sets offer but still keep the computational benefits of using a relative small number of GTOs, a basis function can be constructed by contracting different primitives together:

$$\phi_i^c = \sum_{j=i}^{n} c_{ij}\phi_j \ , \quad i = 1, n_c \tag{5.5}$$

where the ϕ_j are Gaussian primitives, c_{ij} are the contraction coefficients, n the number of primitives being contracted. The construction of a contracted GTO basis set (CGTO) is often done in two stages: first the minimization of an atomic energy calculation with respect to the primitives is performed, then the contraction coefficients are taken from the atomic orbitals obtained during this minimization.

The contraction of primitives can be separated into two different schemes: *Segmented contraction* where each primitive is constrained to contribute only to one contracted function and *General contraction* where primitives may contribute to any contracted function. An efficient method to implement general contraction can be found in [57].

5.2.3 Even-tempered Gaussians.

It is clear, from the discussion in section 5.2.1, that unconstrained minimization of primitives is very demanding for even small numbers of primitives. Minimising any function of n variables $f(x_1, x_2, x_3, ..., x_n)$ is not trivial, especially given that $f(\mathbf{x})$ in our case involves an atomic energy calculation.

Let us assume for now that l and n have been chosen and we wish to minimize $E_{atom}(\eta_1, ..., \eta_n)$. Unconstrained minimization of the previous function is still difficult [58]. In addition, calculating atomic energies with ill constructed primitives, particularly with high l value, can lead to variational collapse [59]: a failure in solving the GEP, equation (5.3).

For basis sets with large numbers of primitives and high angular momentum the GEP in equation (5.3) can fail due to the overlap matrix becoming singular. Let $\phi_1(\mathbf{r})$ and $\phi_2(\mathbf{r})$ be two normalized primitives with high angular momenta if the overlap between them,

$$S_{12} = \int \phi_1(\mathbf{r})\phi_2(\mathbf{r})d\mathbf{r} \approx 1 \tag{5.6}$$

then **S**, is singular and not invertible, since $\phi_1(\mathbf{r})$ completely describes $\phi_2(\mathbf{r})$ or vice-versa. Therefore the GEP in (5.3) can't be solved. The topic of numerical failures will be discussed in more detail in section 5.6.5.

The problem of variational collapse was recognized early on [55], and a simple solution was proposed to circumvent it. Instead of using unconstrained exponents, where each exponent is optimized separately, they are constrained to form a geometric series:

$$\eta_i = \alpha_0 \beta^{i-1} \tag{5.7}$$

With $\alpha_0 > 0$ and $\beta > 1$. Basis sets which use this geometric constraint are known as *even-tempered* basis sets. The geometric constraint reduces the search space radically, for any choice of n and l one must only span $\mathbb{R}^2$ to generate different primitives as opposed to $\mathbb{R}^n$ for unconstrained optimization. It follows that higher values of n can be chosen without the large overhead that comes with minimizing a n-variable function. However, the atomic energy with n different exponents ($E_{atom}(\alpha, ..., \alpha * \beta^{(n-1)})$) will still need to be calculated and this is often time consuming.

The possibility of variational collapse present in unconstrained optimization is also reduced by the geometric constraint. The overlap of two consecutive even-tempered and normalized Gaussian primitives is given by [58]:

$$S_{i,i+1} = \Big[\frac{2\sqrt{\beta}}{1+\beta}\Big]^{(2l+3)/2} \tag{5.8}$$

variational collapse can then be avoided with a suitable choice of β.

Constraining Gaussians functions to have even-tempered parametrization allows for basis sets to be constructed which converge to the basis set limit as the basis set size is increased. This was used to develop "universal" basis sets [54, 60] (and similarly using STO's as a basis set [61, 62]), where successive sets of large Gaussians functions are generated. A mathematical analysis on the behaviour of the even-tempered parameters (α, β) as the number of exponents increases is given by [53].

It is important to note that even-tempered basis sets are often larger than individually optimized basis sets of similar quality [63]. For conventional calculations this is not ideal since diagonalization would be more expensive. However, this is not a drawback when the filtration algorithm is used to choose contractions from very large pools of primitive functions, where this overhead is absent.

5.3 History of Gaussian basis sets

Due to the immense amount of work and knowledge developed in the generation of Gaussian basis sets, attempting any sort of field wide summary is no trivial matter. For our purposes a brief historical survey concerning the usage of GTOs in electronic calculations basis followed by an overview of two commonly used basis sets are enough to extract some principles to compare and contrast during the discussion of our own basis set generation.

As we have summarized in previous chapters, most *ab initio* methods used in electronic structure calculations invoke the independent-particle approximation. In the early stages of quantum mechanical electronic calculations (before the advent of DFT) most electronic structural calculations were performed using Hartree-Fock methods (chapter 2), where the wave function is expressed as a Slater-determinant of single electron orbitals. Since the exact form of single-electron orbitals is unknown they are expanded in a basis set.

During the first strides of molecular HF calculations, STOs were used as a basis sets given that they are solutions to Hydrogen-like atomic Hamiltonians and have the correct cusp behaviour ([27]). However for molecule calculations, constructing and solving the GEP which arises in Self-Consitent Hartree-Fock calculations (often referred to in literature as *self-consistent field* equations, SCF) quickly became complicated and inefficient for any accurate application due to the complexity of integrating STOs [64].

It so happens that a simpler type of function that could be used as a basis sets had already been introduced for electronic calculations before SCF was developed: Boys [65] had suggested that due to its favourable integration properties Gaussian functions could be useful in electronic structure calculations, especially in regard to computational efficacy.

A first approach to implementing GTOs in SCF calculations aimed to keep the natural qualities of STOs whilst simultaneously foregoing the difficulties involved with integrating them. This was accomplished by representing STOs ($\chi(\mathbf{r})$) in terms of GTOs($\phi(\mathbf{r})$),

$$\chi(\mathbf{r}) = \sum_i c_i \phi_i(\mathbf{r}) \tag{5.9}$$

where the contraction coefficients are given by least square fittings. Basis sets generated in this way are named, for example, STO-3G. The other approach is to introduce GTOs directly in SCF (or DFT). This is the approach taken in this thesis and for most of the basis sets discussed in the current literature, including the two basis set which we will now summarize.

5.3.1 Pople and Dunning basis sets

Continuing with the historical motif of the current section one must introduce the Pople basis sets, which were one of the first basis sets to be widely accepted into the quantum chemistry community, and even to this day are referenced in research [66] as a standard.

Pople basis sets are generated from an all-electron Hartree-Fock calculation, they are often called *split valence* because they use two or more contracted sets of Gaussian primitives to represent each valence electron, this provides much better flexibility and transferability than a minimal basis set. The wave functions of core electrons are represented by one set of contracted Gaussians primitives, although different Pople basis sets may use different numbers of primitives to form that contraction function [52, 67].

The notation used to describe Pople basis sets is $X - YZG$ where X represents the number of primitives in the contracted function used to describe each core state and Y, Z represent the number of primitives in each of the two functions used to represent each valence state. The angular momentum of each CTGO is set by the orbital which it represents. The method of optimizing the primitives using Hartree-Fock employed by Pople is both lengthy and outdated. Details can be found in [52].

Historically, the most commonly mentioned Pople basis sets is the 6-31G [67, 68]. In addition the accuracy of the 6-31G basis set is typically increased by augmenting it with other Gaussian functions:

$$\text{6-31m++G**} \tag{5.10}$$

where m indicates triple valence split, $*$ indicates polarization functions on heavy atoms, $**$ indicates polarization functions on heavy atoms and hydrogen, $+$ indicates diffuse functions on heavy atoms and $++$ indicates diffusion functions on heavy atoms and hydrogen.

When to use which basis and how to show convergence is not clear with Pople basis sets. An early good review concerning these facts can be found in [50]. Pople basis sets tend be used when some accuracy can be sacrificed at the behest of speed.

It is important to notice that the Pople basis sets were developed over time for different chunks of the periodic table (i.e. first-row, second-row, etc...) [67, 68]. This is a common feature shared by some other basis sets, due to the range of requirements necessary to maintain similar accuracy for different sections of the periodic table [69].

A drawback of generating basis set using solely Hartree-Fock was found to be that such basis sets were not optimal when applied to post HF calculations [51]. Dunning therefore introduced "correlation consistent" basis set [70, 71], designed to converged these more sophisticated calculations. They feature successively greater number of polarization functions (d, f, g, etc...), which increase systematically as the description of the valence shell is improved. More recently Karlsrhue basis sets [72] have extended this and are published for elements H-Rn of the periodic table. The Dunning basis set [70] uses post-Hartree–Fock

methods, configuration interaction (CI), to calculate polarization orbitals (correlation orbitals) for the atomic basis set. Configuration interactions improve on Hartree-Fock by including a treatment of electron correlation [70].

Dunning basis sets, often called *correlation consistent* basis sets, have the following nomenclature:

$$\text{cc-pVNZ} \tag{5.11}$$

where cc-p stands for correlation-consistent polarized, V indicates that the basis sets have correlation treatment for valence states only and NZ where $N \in [1, 2, 3, ...]$ indicates the split of the valence basis (Z stands for zeta which during the heydays of STOs was the nomenclature used when referring to the exponents of valence orbitals). The polarization functions are generated by minimizing a CI calculation and the exponents for the primitives of each function (d, f, g, etc.) are given by an even-tempered distribution.

Dunning basis sets are designed to allow for pseudo-systematic convergence of energy and other ground state properties in post-Hartree–Fock calculations. Dunnning suggested that polarization functions should be added in well-defined sequences, such as 2d1f, 3d2f1g, 4d3fg1h for double, triple and quadruple zeta for example, so that each includes successively larger shells and higher polarization functions. In addition with each increase in the description of the valence states the number of function in the core states is also increased, so as to evenly distribute the basis set error amongst the different basis functions. It follows that with each step in quality Dunning basis sets consistently reduce errors at both HF and correlated levels, however the number of basis functions nearly doubles with each step in quality.

5.3.2 Summary

Just from the brief overview presented above of two commonly used basis sets we are left with a large and specific lexicon which must be understood before one can apply any of the basis sets accurately and efficiently. A recent paper reviewing basis sets [63] list 8 popular basis sets (6 additional ones to the two mentioned above) each with individual nuances and taxonomy. Furthermore some basis sets are accompanied by a cornucopia of unrelated, and often confusing, nomenclature.

The myriad of different basis sets and the specificity of their applications can be a drawback when Gaussian basis sets are discussed. Not only would a potential user of a Gaussian DFT code need to be familiar with the language and scope of the different basis sets, he should be able to converge results with respect to them which is not always clear. With these drawbacks in mind and the discussion above I would like to highlight the following points:

1. Larger basis sets are more flexible and therefore offer greater transferability.

2. Large basis sets are expensive to run and thus most basis sets are contracted during the isolated atomic calculation and this will to some extent at least limit transferability.

3. Different sections of the periodic table have been tackled separately when generating many traditional basis sets.

4. There is no systematic recipe to show convergence with respect to basis sets for GTOs.

5. For certain calculations extra exponents are added to basis sets depending on the system at hand, which often are optimized separately, and in some cases there is no agreed prescription to this.

6. For large-scale calculations using large basis sets can lead to ill conditioned overlap matrices, thus the the accuracy demanded of the basis set must be weighted against stability reassurance.

In this work a new approach is presented. A single large uncontracted primitive set is generated for each atom which is then contracted *on-site* during the KSDFT calculation using filtration. This allows us to have only one basis set per atom, and by contracting it during the KSDFT calculation we can control its accuracy as needed. Figure 5.1 highlights the main characteristics of the primitive basis sets and the filtered (contracted) basis set.

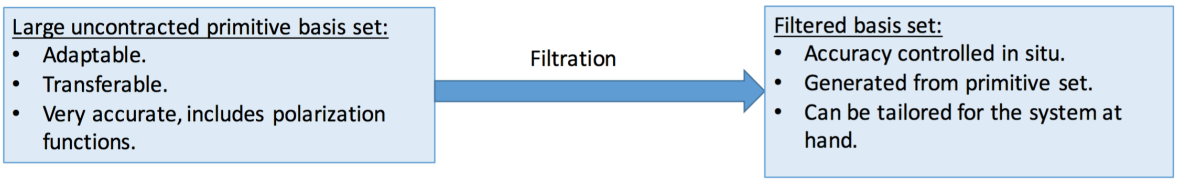

Figure 5.1: *Figure highlighting the main characteristic of both our primitive and filtered basis sets.*

Now we will introduce our primitive basis set generation.

5.4 Theoretical preamble

Before proceeding to explain our basis set generation method we must present some well known theorems and principles which ground our method on a sound theoretical foundation.

5.4.1 The intermediate value theorem

The intermediate value theorem will be stated here without proof, which can be found in any calculus book.

Theorem 5.4.1 *Let f be a continuous function defined on an interval $I = [a, b]$, $f : I \to \mathbb{R}$. Let u be a number between $f(a)$ and $f(b)$, i.e* $\min[f(a), f(b)] < u < \max[f(a), f(b)]$, *then,*

$$\textit{there exists } c \in I, \textit{ such that } f(c) = u.$$

Theorem 5.4.1 is related to the completeness property of the real numbers. For the purposes of this thesis a corollary of theorem 5.4.1 is more relevant. This corollary, sometimes referred to as the Bolzano theorem, can be stated as:

Theorem 5.4.2 *Let f be a continuous function defined on an interval $I = [a, b]$, $f : I \to \mathbb{R}$ and let $f(a) < 0$ and $f(b) > 0$ then,*

$$\textit{there exists } c \in (a, b), \textit{ such that } f(c) = 0$$

The Bolzano theorem is particularly important for applied mathematics, and physics, since it forms the theoretical basis for many root finding algorithms. Most root finding algorithms do so by systematically reducing an interval $I_0 = [a_0, b_0]$, $f(a_0) < 0$ and $f(b_0) > 0$ to smaller intervals $I_i = [a_i, b_i]$ such that $0 > f(a_{i-1}) > f(a_i)$ and $0 < f(b_{i-1}) < f(b_i)$. Eventually the size of I_i will be approximately zero and we can form a linear combination of a_i and b_i as the numerical approximation of the root i.e. $f(c) = 0$ where $c = c_a a_i + c_b b_i$.

In the basis generating procedure, introduced in a later section, the bisection method for root finding is used. This method is introduced in the section below.

5.4.2 The bisection method

The bisection method is, perhaps, one of the simplest root finding algorithms available, both to code and understand. This easiness stands in stark contrast with its usefulness and reliability. For most applications the bisection method is accurate enough to find the root of a well behaved function in circumstances where the number of iterations is not critical.

Let f be a continuous function, and assume we have a interval $[a, b]$ such that $f(a) < 0$ and $f(b) > 0$, to find $f(x) = 0$ according to the bisection method we proceed in the following manner:

1. Generate $c = \frac{a+b}{2}$
2. Find $f(c)$
3. If $|f(c)| < \epsilon$, where ϵ is a tolerance chosen at the beginning, then c is taken as the root, otherwise proceed to step 4.
4. If $f(c) > 0$, let $b = c$ else if $f(c) < 0$ let $a = c$ and go to step 1.

Figure 5.2 illustrates the bisection method, applied to the function $f(x) = x^2 - 1$. In this example $f(c) > 0$ thus we will form a new interval $I = [a, c]$, generate $c_2 = \frac{a+c}{2}$ and proceed according to the algorithm presented above.

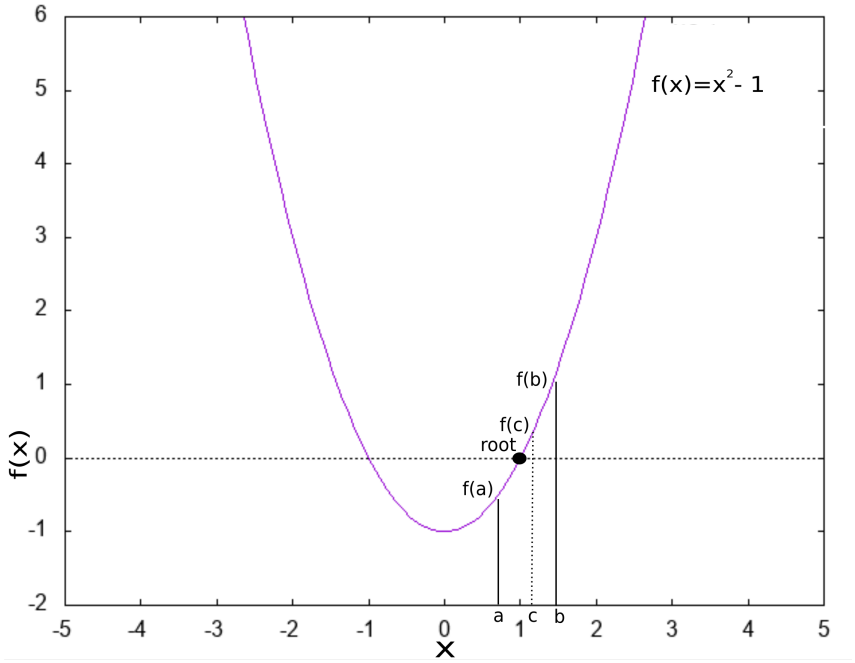

Figure 5.2: *One iteration of the bisection method algorithm applied to* $f(x) = x^2 - 1$. *The black dot indicates the root. The points a and b are taken as starting points for the bisection routine, yielding point c with* $f(c) > 0$.

The bisection method, in theory, must converge since the size of interval is always halved at each cycle, it follows that after several iterations of the bisection method the size of the interval must be smaller than our chosen tolerance, $|I_n| < \epsilon$, therefore any point $x \in I_n$ can be considered a root. The error after n iterations is bounded by:

$$|c_n - c| \leq \frac{|a - b|}{2^n} \tag{5.12}$$

5.4.3 The downhill simplex method

The downhill simplex method, often called the Nelder-Mead method after its developers [73], is a method for the minimization of a function of n-variables $f(x_1, x_2...x_n)$. Unlike other methods, such as steepest descent, it is "direct" i.e. it uses only function's evaluation and not derivatives, which removes some complications that could result from ill conditioned derivatives but often results in a large number of iterations.

A simplex is a polytope of n+1 vertices in n-dimensions. In this thesis the downhill simplex method will be used to minimize a function of two variables $f(x, y)$ the corresponding simplex is a triangle.

The basic idea behind the downhill simplex method is to systematically move the simplex to the minimum of $f(\mathbf{x}) = f(x_1, x_2...x_n)$ by a series of reflections, expansions and contractions.

Let $f(\mathbf{x})$ be the function we wish to minimize and let $(\mathbf{x_1}, \mathbf{x_2}, ..., \mathbf{x_3})$ be our starting trial points. To find the global minimum of $f(\mathbf{x})$, using the downhill simplex method, we perform the following steps:

1. Order the points according to their values at the vertices; $f(\mathbf{x}_1) \leq f(\mathbf{x}_2) \leq \dots f(\mathbf{x}_{n+1})$. Where $f(\mathbf{x}_1)$ is a "better" value, i.e. a better approximation to $f(\mathbf{x}_{min})$, than $f(\mathbf{x}_2)$.

2. Calculate the centroid $\bar{\mathbf{x}}$ of all points except $\mathbf{x}_{n+1}$; $\bar{\mathbf{x}} = \frac{\sum_i^n \mathbf{x}_i}{N}$

3. Generate a new point $\mathbf{x}_r$ by reflection, $\mathbf{x}_r = \bar{\mathbf{x}} + \alpha(\bar{\mathbf{x}} - \mathbf{x}_{n+1})$ with $\alpha > 0$. After this step there are three possible outcomes:

   (a) $f(\mathbf{x}_r)$ is neither the best value or the worst, i.e. $f(\mathbf{x}_1) < f(\mathbf{x}_r) < f(\mathbf{x}_n)$, replace $f(\mathbf{x}_{n+1})$ by $f(\mathbf{x}_r)$ and go to point 1.

   (b) $f(\mathbf{x}_r)$ is better than the best value i.e. $f(\mathbf{x}_r) < f(\mathbf{x}_1)$. If this is the case we are moving in the "right" direction, $\mathbf{x}_r$. Given this we move further in the $\mathbf{x}_r$ direction, this is done by computing the extended point $\mathbf{x}_e = \bar{\mathbf{x}} + \gamma(\mathbf{x}_r - \bar{\mathbf{x}})$, with $\gamma > 1$. This step is commonly referred to as **expansion** in the literature. After the expansion there are two outcomes, depending on the value of $\mathbf{x}_e$,

      i. We are still moving in the "right" direction i.e. $f(\mathbf{x}_e) < f(\mathbf{x}_r)$. Replace $\mathbf{x}_{n+1}$ with $\mathbf{x}_e$ and go to step 1.

      ii. Else, $f(\mathbf{x}_e) < f(\mathbf{x}_r)$, replace $f(\mathbf{x}_{n+1})$ by $f(\mathbf{x}_r)$ and proceed to step one.

   (c) The last outcome, concerning the value of $f(\mathbf{x}_r)$, is $f(\mathbf{x}_r) > f(\mathbf{x}_n)$ i.e. the simplex has stretched too far, therefore it must be contracted. A new point $\mathbf{x}_c$ is generated, $\mathbf{x}_c = \bar{\mathbf{x}} + \beta(\mathbf{x}_{n+1} - \bar{\mathbf{x}})$ where $0 < \beta < 1$. After generating $\mathbf{x}_c$, a step commonly referred to as **contraction**, we are left with two possible outcomes,

i. $f(\mathbf{x}_c) < f(\mathbf{x}_{n+1})$, the contraction has been successful, replace $\mathbf{x}_{n+1}$ buy $\mathbf{x}_c$ and go to step 1

ii. $f(\mathbf{x}_{n+1}) < f(\mathbf{x}_c)$, the contraction step has not been successful. All points $\mathbf{x}_i$, with the exception of $\mathbf{x}_1$, are replaced with $\mathbf{x}_i = \mathbf{x}_1 + \rho(\mathbf{x}_i - \mathbf{x}_1)$ with $0 < \rho < 1$. This step is often referred to as **shrink**. After all $\mathbf{x}_i \neq \mathbf{x}_1$ have been recalculated proceed to step 1

4. The termination of the downhill simplex method is controlled by the standard deviation:

$$\sigma = \sqrt{\frac{1}{N}\sum_{i=1}^{n}(f(\mathbf{x}_i) - f(\bar{\mathbf{x}}))^2} \tag{5.13}$$

Once σ is smaller than a chosen tolerance the method terminates, otherwise it returns to set one.

For a function of two variables, such as the one present in the basis generation routine, the downhill simplex can be illustratively explained as a series of triangles generated by: reflection, expansion and contraction. The triangles get progressively smaller as they reach the region where the minimum of the function is located.

It has been noted [74] that for some functions the simplex downhill could get stuck in a cyclic motion, or even a local minimum. These criticisms are overcome, in our basis generation method, by a careful choice of starting points after an exhaustive search of the underlying variable space. The application of the downhill method to our basis set generation will be discussed in the following sections.

The details and FORTRAN implementation of the downhill simplex method, can be found in [75]. The routine AMOEBA is used in this thesis.

5.5 Basis generation procedure

In contrast with the basis sets discussed beforehand our basis sets are optimized by solving an atomic Gaussian KSDFT calculation which uses pseudopotentials. It follows that this basis set must only be used in calculations with the same exchange correlation and pseudopotential that was used to generate the basis. In this thesis PBE exchange correlation [43] and Mathias Krack's GTH pseudopotentials [39] are used.

The procedure presented here produces an uncontracted basis sets for any element of the periodic table, pending the existence of a pseudopotential for the particular atom.

Our basis sets use even-tempered Cartesian Gaussian functions which can be written as:

$$\phi_i(\mathbf{r}) = x^{n_x} y^{n_y} z^{n_z} e^{-\alpha\beta^i \mathbf{r}^2} \tag{5.14}$$

where

$$n_x + n_y + n_z = l_{\alpha\beta^i} \tag{5.15}$$

and $l_{\alpha\beta^i}$ it the angular momentum value of this Gaussian function (with exponent $\alpha\beta^i$). Given that we are dealing with uncontracted basis sets it follows that the basis sets, of a particular atom, is entirely defined the following set of parameters:

$$n, \alpha, \beta, l_\alpha, l_{\alpha\beta}, .., l_{\alpha\beta^{n-1}} \tag{5.16}$$

where, as before, n is the number of exponents, (α, β) the even-tempered constraints and l_i the angular momentum value of each exponent.

In our basis set the number of different primitives with the same exponent $\alpha\beta^{i-1}$ is set by its corresponding angular momentum value in the following manner: All primitives, with the same exponent, generated by the different permutations of equation (5.15) are included for $n_x + n_y + n_z \leq l$. That is, let $\phi^i_{l_\alpha}$ be Gaussian primitives with exponent α generated from an angular momentum value l_α. If we have $l_\alpha = 0$ then our basis sets has only one primitive with α exponent:

$$\phi^s_{l_\alpha=s}(\mathbf{r}) = e^{-\alpha\beta^i\mathbf{r}^2} \tag{5.17}$$

if instead $l_\alpha = 1$ the basis sets will have three different Gaussian primitives:

$$\phi^{p_1}_{l_\alpha=p}(\mathbf{r}) = xe^{-\alpha\mathbf{r}^2}$$
$$\phi^{p_2}_{l_\alpha=p}(\mathbf{r}) = ye^{-\alpha\mathbf{r}^2}$$
$$\phi^{p_3}_{l_\alpha=p}(\mathbf{r}) = ze^{-\alpha\mathbf{r}^2}$$

and an extra s-state

$$\phi^s_{l_\alpha=p}(\mathbf{r}) = e^{-\alpha\mathbf{r}^2} \tag{5.18}$$

for a total of four primitives. If instead we have $l_\alpha = 2$ then the basis set contains six primitives with $l = 2$, three primitives with $l = 1$ and one primitive with $l = 0$ for a total of ten primitives with the same exponent. Table 5.1 list the number of primitives included in the basis set according to the choice of angular momentum for the range of angular momentum values considered in this work.

For illustrative purposes let us now construct a hypothetical uncontracted even tempered basis sets for hydrogen. Let us say that the hydrogen basis set has 3 exponents, $n = 3$, with $\alpha = 0.1$ and $\beta = 2.0$. As is customary with common `AIMPRO` notation, the angular momentum of the basis set is typically expressed as a set of values $(l_1, l_2, .., l_n)$ where l_1 is the angular momentum value for the lowest exponent, l_2 for the second lowest, and so forth. Let us say that the angular momentum value for this basis set is (s, p, p),

l-value	number of primitives
$l = 0$	1
$l = 1$	4
$l = 2$	10
$l = 3$	20
$l = 4$	35

Table 5.1: *The number of primitives with the same exponent included in the basis set, as a function of its respective angular momentum.*

i.e. $(0, 1, 1)$. From what was discussed above the basis set for Hydrogen contains nine primitives:

$$\begin{aligned}\{&e^{-0.1\mathbf{r}^2}, e^{-0.2\mathbf{r}^2},\ xe^{-0.2\mathbf{r}^2},\ ye^{-0.2\mathbf{r}^2},\\ &ze^{-0.2\mathbf{r}^2},\ e^{-0.4\mathbf{r}^2}, xe^{-0.4\mathbf{r}^2},\ ye^{-0.4\mathbf{r}^2},\ ze^{-0.4\mathbf{r}^2}\}\end{aligned} \tag{5.19}$$

In an atomic calculation, such as the ones performed in this section to generate the basis sets, the different KS orbitals - in the current case hydrogen ones are expressed as linear combinations of the functions in eq. (5.19).

Having established the necessary parameters used to construct a basis set, equation (5.16), and how the basis set is constructed, equation (5.19) we are left with finding the optimal set of parameters that will specify our basis. This will be presented in the next sections

5.5.1 Assignment of angular momentum l.

In this section we will discuss how the angular momentum of each exponent in a basis set is assigned.

In our construction each exponent in an element's basis sets shares the same value of l so that, $l_{\alpha\beta^i} = l$ for $i = 1, ..., n$. For each atomic basis set this l value is picked to be one above the atom's highest occupied orbital l_{occ}. Elsewhere in this thesis this is referred to as the "$l + 1$" policy.

As an example consider hydrogen which has only one electron in a s-state ($l_{\text{occ}} = s$) will have $l = 1$ for all the exponents in it's basis set. For carbon with electrons in a p-state each exponent in it's basis set has $l = 2$. Note that for basis set with $l > 3$ primitives with smaller l are included for each exponent, as detailed in the previous section.

From the parameter set (5.16), having assigned l, we are left with finding n, α and β to generate our basis set. This is all done inside our basis generation routine.

5.5.2 Assignment of n, α and β

The first step in our basis set generation is to calculate a converged energy for the pseudo-atom. Here, too, the exchange correlation and pseudopotential choice must be consistent with the one referenced at the beginning of this section. This energy is obtained using a Discrete Variable Representation (DVR) atomic KSDFT code [32], therefore we label this energy E_{DVR}. The main motive for using the DVR atomic code rests on its ability to provide a well converged pseudo-atomic energy comparatively quickly and simply. Convergence can be shown by calculating several energies with increasing number of functions. Evidence of this is presented in figure 5.3 where the convergence of the atomic energy with respect to the number of basis function is shown for the elements considered here. Each point in the graph is the average (for 70 elements) of the following quantity:

$$\Delta(i) = E_{\mathrm{DVR}}(i) - E_{\mathrm{DVR}}(300) \tag{5.20}$$

where the index i represents the number of points (corresponding to the number of functions used in the calculation) with 300 points being the highest value with which calculations were performed. As we can see from figure 5.3 by 150 points we find that our energies are already converged, nevertheless the energy resulting from the run with 300 points is used in the basis set generation routine.

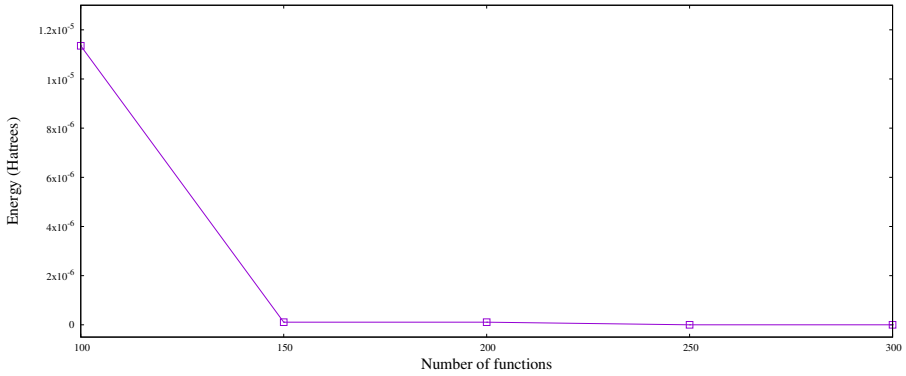

Figure 5.3: *Convergence of the atomic energies for all the elements for which we generate a basis set (70 atoms, averaged) with respect to number of basis functions for the DVR code. Each point represents the difference* $\Delta(i) = E_{\mathrm{DVR}}(i) - E_{\mathrm{DVR}}(300)$.

From a variational standpoint E_{DVR} can be taken to be the "true" pseudo-atom energy so that in a like-to-like calculation any energy obtained using a Gaussian KSDFT code, E_{GAT}, will always be higher. It follows from the variational principle that we can judge the quality of a basis set by minimizing the following positive quantity

$$\delta = E_{\mathrm{GAT}} - E_{\mathrm{DVR}} \tag{5.21}$$

whilst systematically modifying the basis sets. The logic being that as $\delta \to 0$ the basis set increases in quality. This is markedly different if only energies obtained with Gaussian KSDFT codes were to be considered in the minimization routine, as one would first need to converge the energies with respect to Gaussian basis sets i.e.

$$E^{i+1}_{\mathrm{GAT}} - E^{i}_{\mathrm{GAT}} < tol \tag{5.22}$$

which, undoubtedly, requires a large number of exponents given that condition (5.22) must be observed over several changes in the number of exponents n for it to be considered converged. Furthermore, if the parameters that generate the basis sets are not spanned carefully it could lead to erroneous results i.e. the method can be stuck on a local minima and trigger condition (5.22) even over different n without it being the true minimum (which might have a lower energy by several factors of the tolerance). By using E_{DVR} we do not need to worry about such problems, figure 5.4.

Having pre-assigned l, the atomic basis set is constructed using the set of (α,β), for

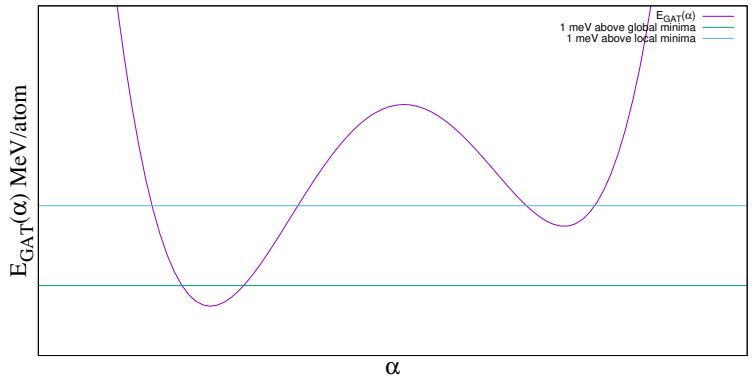

Figure 5.4: *Schematic of a energy convergence curve with respect to a parameter that governs the basis set construction, in this case α. There is both a global and local minimum, using E_{DVR} as a check of convergence ensures the global minimum is choosen. In the example curve above for the chosen olerance convergence could be triggered (blue and green curve) in any of the minima if only E_{GAT} was to be used to check convergence.*

a particular n, that satisfy the following condition,

$$\delta = E_{\mathrm{GAT}}(n, \alpha, \beta) - E_{\mathrm{DVR}} = tol \tag{5.23}$$

where *tol* is a tolerance, chosen to be 1 meV in our case. We choose the smallest n for which this can be achieved. In addition our procedure finds the highest α for which condition (5.23) is satisfied for the chosen "n" (more on this in the next section). Although this is not necessary, it reduces the likelihood of failure due to the ill condition of the overlap matrix in the KSDFT calculation (even after filtration as we will see in the next chapter) and more importantly it increases the efficiency of the Hamiltonian and overlap matrices building stage.

Note that for a chosen value of n equation (5.23) describes a contour line on a 3D surface. Given that δ involves a KSDFT calculation it does not have an analytical form, therefore we must find points on this line numerically (condition (5.24)), so that the point, (α, β) pair, with the highest α can be chosen. The algorithm to do so is introduced in the next section.

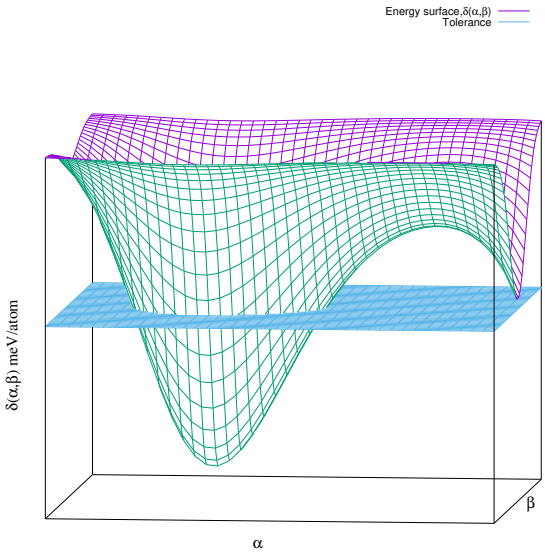

Figure 5.5: *Schematic of a 3D $\delta(\alpha, \beta)$ surface, bisected by the plane which describes the tolerance. The intersection between the plane and the surface can be represented by a curve (or several if several minima exist) in a α vs. β plane.*

5.5.3 Basis set generation; Main loop

This section introduces the main part of the algorithm used to find the (n, α, β) set which will be used to generate the basis sets.

Having obtained E_{DVR} for the pseudo-atom and chosen the angular momentum value, l, we proceed to find a set of (α_b, β_b) such that,

$$\delta(\alpha_b, \beta_b) = E^n_{\mathrm{GAT}}(\alpha_b, \beta_b) - E_{\mathrm{DVR}} = tol \tag{5.24}$$

where the raised index (n) indicates that we are currently searching over energies obtained with constant n (only α and β are changed). Our routine begins with $n = 5$ and spans the $(\alpha, \beta) \in \mathbb{R}^2$ plane. If no (α, β) are found such that $\delta(\alpha, \beta) \leq tol$ then n is increased and the procedure starts again. Once the previous condition is reached we find points which satisfy equation (5.24) and choose the one with highest α

The procedure to span the (α, β) plane and to find the set of $(\alpha_b \beta_b)$ that meet condition (5.23) is the following:

1. Assuming that E_{DVR} has been found and l has been chosen. For a starting value of n, the plane $(\alpha, \beta) \in \mathbb{R}^2$ is spanned with a coarse grid to generate a set of points, (α_i, β_j). These points are used to calculate a set of energies; $E^{n,i,j}_{\mathrm{GAT}} = E^n_{\mathrm{GAT}}(\alpha_i, \beta_j)$.

2. The minimum value from the set of $E^{n,i,j}_{\mathrm{GAT}}$ is used as a starting point for a downhill-simplex run. The downhill-simplex returns $(\alpha_{\min}, \beta_{\min})$ which minimizes $E^n_{\mathrm{GAT}}(\alpha, \beta)$,

$$\min[E^n_{\mathrm{GAT}}(\alpha, \beta)] = E^n_{\mathrm{GAT}}(\alpha_{\min}, \beta_{\min}) \tag{5.25}$$

and, by construction, also minimizes $\delta(\alpha, \beta)$. If $\delta(\alpha_{\min}, \beta_{\min}) > tol$ then the number of exponents is increased, $n_{new} = n + 1$, and the procedure returns to step one. Otherwise proceed to step three.

3. A new function is constructed,

$$\delta'(\alpha, \beta) = \delta(\alpha, \beta) - tol \tag{5.26}$$

by construction $(\alpha_{\min}, \beta_{\min})$ also minimizes $\delta'(\alpha, \beta)$, in addition:

$$\delta'(\alpha_{\min}, \beta_{\min}) < 0 \tag{5.27}$$

The set of (α_b, β_b) such that $\delta'(\alpha_b, \beta_b) = 0$ can be found by performing the following steps:

(a) A small set of points with constant $\alpha = \alpha_{\min}$ but changing β, $(\alpha_{\min}, \beta_i)$, are generated and a new set of energies, $E^n_{\mathrm{GAT}}(\alpha_{\min}, \beta_i)$, are calculated. These points, and respective energies, can be taken to form a line,

$$f(\beta) = \delta'(\alpha_{min}, \beta) \tag{5.28}$$

which lies on the $\delta'(\alpha, \beta)$ surface and crosses $\delta'(\alpha, \beta) = 0$ at two points β_{low} and β_{high}, that is $f(\beta_{\mathrm{high}}) = f(\beta_{\mathrm{low}}) = 0$. These two points are actually $(\alpha_{\min}, \beta_{\mathrm{high}})$

and $(\alpha_{\min}, \beta_{\text{low}})$ respectively. The roots $f(\beta_{\text{high}})$ and $f(\beta_{\text{low}})$ are found using the bisection method.

(b) Using β_{low} and β_{high} as interval limits a new set of points are generated and the respective energies calculated, E_{GAT}. As before these points and respective energies can be taken to form k lines,

$$f_{\beta_j}(\alpha) = \delta'(\alpha, \beta_j) \tag{5.29}$$

with

$$\beta_j = \beta_{\text{low}} + \frac{j}{k+1}(\beta_{\text{high}} - \beta_{\text{low}}) \tag{5.30}$$

where $1 < j < k$. For all these lines the α interval from which they are generated begins at $\alpha_{\min}$, that is for the points which define these lines we have $\alpha \geq \alpha_{\min}$. If at any β_j we have $f_{\beta_j}(\alpha_{\min}) < 0$ then α is increased until $f_{\beta_j}(\alpha) > 0$. We then use the bisection method to find the exact α, call it α_{b}, at which $f_{\beta_j}(\alpha_b) = 0$. It follows then that at $(\alpha_{\text{b}}, \beta_{\text{b}})$, where now $\beta_{\text{b}} = \beta_j$, we have $\delta'(\alpha_b, \beta_b) = 0$. A more rigorous proof that this will indeed produce such points is provided below.

4. Once the resulting set of $(\alpha_{\text{b}}, \beta_{\text{b}})$ points is obtained the one with highest α_b is chosen and the primitives are generated. Let us call this point $(\alpha_{\text{end}}, \beta_{\text{end}})$.

A pictorial representation of the algorithm described above is shown in figure 5.6. In broad terms, the procedure presented here produces the even tempered parameters that minimize the atomic energy $(\alpha_{\min}, \beta_{\min})$, step 1 and 2. Then it produces a set of even tempered parameters $((\alpha_b, \beta_b))$ with $tol = 1$ meV, step 3. Finally, from this set the (α, β) pair with the highest α is chosen $(\alpha_{\text{end}}, \beta_{\text{end}})$, step 4.

Proof Concerning point 3.b We provide a proof below that the procedure will return a set of (α_b, β_b) such that $\delta'(\alpha_b, \beta_b) = 0$.

Let us assume that the chosen tolerance is reasonable i.e. at least smaller than the difference between any two values of E_{GAT}. Consider the surface $\delta'(\alpha, \beta)$ given by

$$\delta'(\alpha, \beta) = |E_{\text{DVR}} - E^n_{\text{GAT}}(\alpha, \beta)| - tol \tag{5.31}$$

Let $(\alpha_{\min}, \beta_{\min})$ be the global minimum of $\delta'(\alpha, \beta)$ and let us assume that for a given n we have $\delta'(\alpha_{\min}, \beta_{\min}) < 0$. Let us construct a set of functions $f(\alpha) = \delta'(\alpha, \beta(\alpha))$ that cross the point $(\alpha_{min}, \beta_{min})$. In fact we could construct infinitely many functions $f(\alpha)$ by

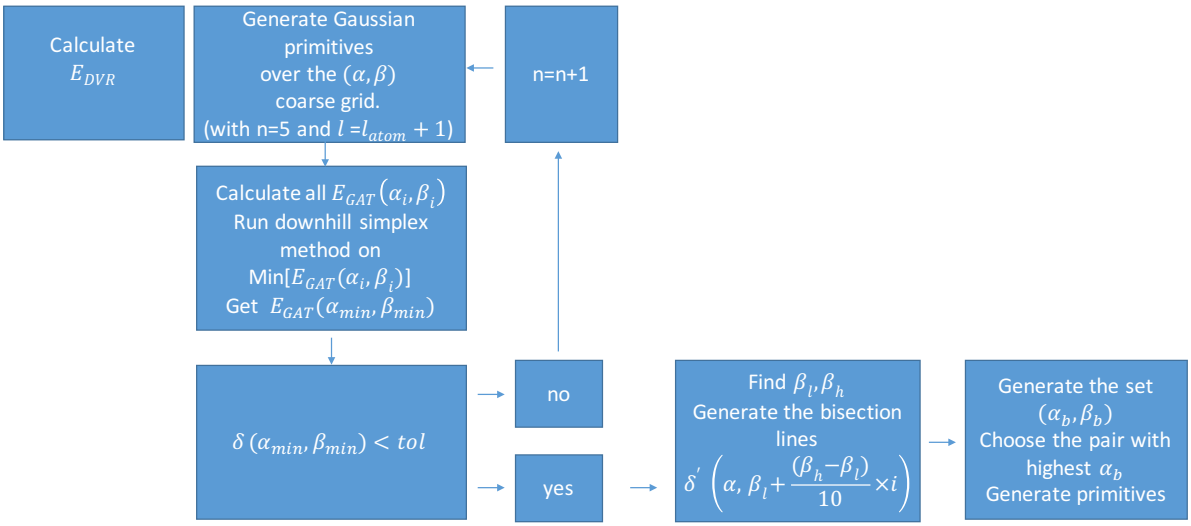

Figure 5.6: *Pictorial representation of the proposed basis set generation routine. These steps are used to find a set of parameters (α, β, n) to generate the uncontracted primitive basis set of a particular atom.*

having $\beta(\alpha) = m\alpha + c$ where m and c are defined by solving

$$\beta_{min} = m\alpha_{min} + c \tag{5.32}$$

for different choices of m (or c). Similarly one could define $f(\beta)$, with the same properties as $f(\alpha)$. The following argument uses $f(\alpha)$ but it could equally use any $f(\beta)$.

Pictorially, the family of functions $f(\alpha)$ are just lines that lie on the surface of $\delta'(\alpha, \beta)$ and cross its minimum. From definition of $f(\alpha)$we have,

$$\min[f(\alpha)] = \min[\delta'(\alpha, \beta(\alpha))] = \delta'(\alpha_{\min}, \beta_{\min}) < 0 \tag{5.33}$$

Now as α increases we must have, bar numerical failures, $|E_{\mathrm{DVR}} - E_{\mathrm{GAT}}(\alpha, \beta(\alpha))| > \epsilon$ for some interval of α with ϵ increasing as α increases (for reasonable intervals) since $E_{\mathrm{GAT}}(\alpha, \beta(\alpha))$ must progressively gets worse as the basis sets will only contain very short ranged Gaussian and thus not be good representation of the Kohn-Sham orbitals. It must be noted that the increase in ϵ is not necessarily monotonic (the surface might have multiple minima). Nevertheless, given our reasonable choice *tol* we can assume that $tol << \epsilon$ for an interval of α, if not let us just redefine *tol*. We can therefore assume that for a big enough α, call it α_{big} we have,

$$
\begin{aligned}
f(\alpha_{\text{big}}) &= \delta'(\alpha_{\text{big}}, \beta(\alpha_{\text{big}})) \\
&= |E_{\text{DVR}} - E^{n}_{\text{GAT}}(\alpha_{\text{big}}, \beta(\alpha_{\text{big}}))| - tol > \epsilon - tol > 0
\end{aligned}
\tag{5.34}
$$

and so $f(\alpha_{\text{big}}) > 0$. Therefore we have $f(\alpha_{\text{min}}) < 0$ and $f(\alpha_{\text{big}}) > 0$ for some α_{big}. By the Bolzano theorem we know that $f(\alpha)$ has a root, which could be found numerically using the bisection method. Thus, in principle, one should be able to find the (α_b, β_b) line, given by $\delta'(\alpha_b, \beta_b) = 0$, by constructing infinitely many $f(\alpha)$ lines.

The basis generation procedure described above, particular step 3.b is, guaranteed to generate at least two points (α_b, β_b) such that $\delta'(\alpha_b, \beta_b) = 0$. It is often the case, however, that all the lines generated in step 3.b will yield the valuable (α_b, β_b) points.

Parameter choice We have found the method above to be robust, with respect to the parameters used to specify the intervals and spanning ranges. A discussion regarding some of these values will be presented in the next section.

In step 1 of our routine we span $\alpha \in [0.01, 0.25]$ in 25 equidistant steps. Similarly for β we generate 25 points in $\beta \in [1.80, b_{end}]$ where

$$
b_{end} = \Big(\frac{e_{fix}10.0}{0.25}\Big)^{\frac{1.0}{n-1}} \tag{5.35}
$$

and e_{fix} is the lowest r_{loc} in the pseudopotential. We have found having b_{beg} less than 1.80 can lead to instability in the atomic calculation for some elements, further justification for this choice will be presented in section 5.6.3. In point 3b we have found that ten lines are enough to yield a valuable (α_b, β_b) set.

5.6 Results

Regarding basis sets their utility and value is measured by application. That is, whether or not a basis set is good depends on how well it performs a particular KSDFT calculation. This is one of the driving factors behind the appearance of many benchmarks, such as the G2-benchmark [76]. Typically a positive result in a benchmark test is taken to imply accuracy and transferability, the two main qualities of any useful GTO basis set. Our own basis set will be tested along with filtration using the recently developed Δ-test [6]. These calculations will be presented in chapter 7. For the present discussion it is important to note that the Δ-test contains 70 different elemental crystals therefore 70 primitive basis sets were generated, one for each atom. Any results presented below were calculated for this particular set of atoms, which we call the Δ-set. However our basis set routine could

be used for any atom provided a suitable pseudopotential exists.

In the remaining sections of this chapter we will analyse the data obtained from the application of the basis generation routine described above to the elements in the Δ-set. Doing this we may verify the proper working of the algorithm and, in addition, investigate some properties regarding the parameters involved in the construction of uncontracted even-tempered basis sets.

5.6.1 Output of the hydrogen run.

The data resulting from step 1 (grid search) and step 3 (search for high α) of our routine during the basis set generation for the hydrogen atom is plotted in Fig. 5.7. The purple surface represents the $\delta(\alpha, \beta)$ surface where as before:

$$\delta(\alpha, \beta) = E_{\mathrm{GAT}}^{n,l=l_{\mathrm{occ}}+1}(\alpha, \beta) - E_{\mathrm{DVR}} \tag{5.36}$$

In the current example the grid energies, $E_{\mathrm{GAT}}^{n,l=l_{\mathrm{occ}}+1}$, were calculated with $n = 6$ (the last iteration of the Hydrogen basis generation). The green points overlaid in this surface are the resulting (α_b, β_b) pairs – recall that any points labelled (α_b, β_b) have $\delta(\alpha_b, \beta_b) = 1$ meV – obtained during the search for the highest α for which $\delta(\alpha, \beta) = 1$ meV. As intended our routine found several points in the $E_{\mathrm{GAT}}(\alpha, \beta)$ surface that satisfy condition (5.24). Note that this surface appears to have several local minima but our routine correctly picked the global one, a consequence of using E_{DVR} as a reference.

For easier visualization the green points in figure 5.7 are replotted in a α vs. β axis in figure 5.8. Bear in mind that all points in this graph have $\delta(\alpha, \beta) = 1meV$.

The (α_b, β_b) pair with the highest α, the rightmost point in figure 5.8, is chosen to construct our primitive basis set (step 4 in section 5.5.3). This point has,

$$\alpha_{high} = 0.0734173 \quad \beta_{high} = 2.8252 \tag{5.37}$$

the uncontracted even-tempered Hydrogen basis set can then be constructed using $l = 1$, $n = 6$, $\alpha = 0.0734173$ and $\beta = 2.8252$. In common `AIMPRO` notation this can be written has:

$$\begin{gathered} \{p, p, p, p, p, p\} \\ 0.0734173 \quad 0.2074241 \quad 0.5860304 \quad 1.6556974 \quad 4.6778019 \quad 13.2160808 \end{gathered} \tag{5.38}$$

The two leftmost points in figure 5.8 are obtained during step 3a in section 5.5.3. Therefore both points have $\alpha = \alpha_{min}$ where α_{min} is obtained from the simplex minimization (step 2 in section 5.5.3). We have $\alpha_{\mathrm{high}} > \alpha_{\mathrm{min}}$ thus, as intended, step 3b has

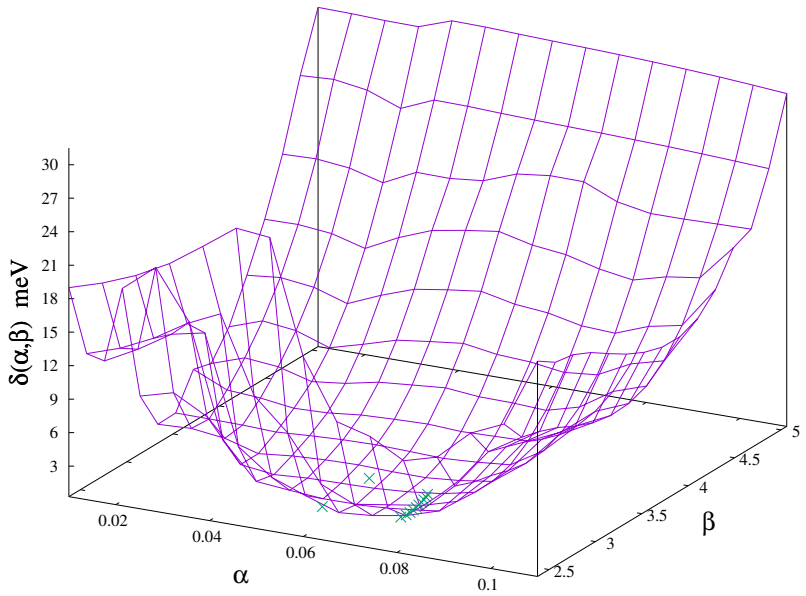

Figure 5.7: *Plot of $\delta(\alpha, \beta)$ surface with $n = 6$, in purple, generated during the Hydrogen basis set generation. The green points correspond to the set of (α_b, β_n) obtained during the search for the highest α.*

produced a higher α than the one obtained from the simplex minimization.

The average difference between the individual atomic α_{min} and corresponding α_{high} is presented in section 5.6.5. In addition the computational savings resulting from using uncontracted primitives with higher α are also discussed therein. Beforehand the convergence of the Gaussian atomic energy, $E_{\text{GAT}}(\alpha, \beta)$, for each element in the set is presented.

The resulting parameter set which define the individual uncontracted even-tempered basis set for the 70 elements considered in this thesis is presented at the end of this chapter in table 5.4.

5.6.2 Convergence of the Gaussian atomic energy

In Figure 5.12, located at the end of this chapter, the minimum $\delta(\alpha, \beta)$ obtained from the different simplex minimizations ($\delta(\alpha_{\text{min}}, \beta_{\text{min}})$) is plotted for all elements. For elements with several data points each point corresponds to the simplex energies obtained using a different number of exponents (n), this is step 2 of our basis generation routine. Each line links all the simplex energies obtained using the same number of exponents.

As expected below the dotted line – 1 meV line – there is one point for each element. This indicates that a converged Gaussian atomic energy (according to our chosen tolerance) has been found for all elements in the Δ-set. This is the necessary condition for the

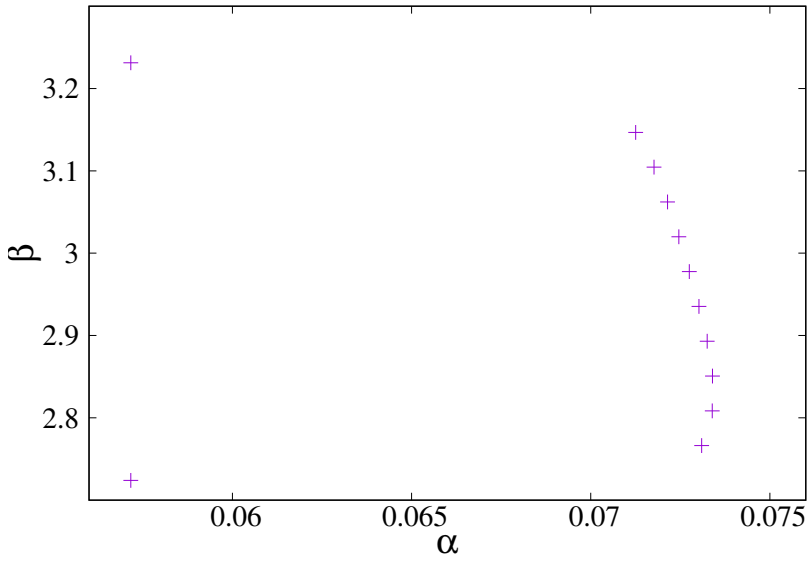

Figure 5.8: *The set of α_b, β_b generated from step 3.b for Hydrogen atom ($n = 6$).*

basis generation routine (section 5.5.3) to proceed to step 3 and eventually finish.

5.6.3 Behaviour of even-tempered parameters

In this section, and the next two, the behaviour of α and β for the different elements is analysed in some detail to reinforce and explain the choice of parameters presented in section 5.5.3. In this section when α and β are mentioned it is assumed that these are the parameters which minimize the Gaussian atomic energy for a specific number of exponents, i.e. in our case these are found at each simplex run $(\alpha_{\min}, \beta_{\min})$.

The mathematical analysis regarding convergence of even-tempered basis sets (for atomic calculations) is due to Schmidt and Ruedenberg [53]. Perhaps the most appealing feature of an even-tempered distribution of Gaussian primitives is that as the number of primitives is increased, i.e. $n \to \infty$, we can expect the basis set to become complete [53, 60]. Furthermore, if the basis set does tend to completeness as n increases then both α and β must be functions of n [60],

$$\alpha = \alpha(n) \qquad \beta = \beta(n) \tag{5.39}$$

In addition, we must have

$$\lim_{n\to\infty} \alpha(n) = 0 \qquad \lim_{n\to\infty} \beta(n) = 1 \qquad \lim_{n\to\infty} [\alpha(n)\beta(n)] = \infty \tag{5.40}$$

Schmidt and Ruedenberg [53] and Wilson and Kryachko [60] use these identities to postulate relations for $\alpha(n)$ and $\beta(n)$ in terms of n. For example Schmidt and Rudenberg

postulate the following,

$$\begin{aligned} ln[ln[\beta]] &= bln[n] + b' \\ ln[\alpha] &= aln[\beta - 1] + a' \end{aligned} \tag{5.41}$$

Where a, a', b, b' can be found by least square fittings of several $\alpha_{\min}(n)$ and $\beta_{\min}(n)$ obtained from regular non-linear multivariable minimization for each angular momentum symmetry, i.e. $\alpha_l(n)$, $\beta_l(n)$. This set of parameters would be derived for each atom. Although such construction should indeed provide systematic convergence for a particular atomic calculation and would most likely do so on polyatomic calculations as well by virtue of its size, it is unlikely that such a basis set would be of use directly due to its predictably large size. In addition calculations on large systems or calculations which use large basis sets predicate some preferable constraints on $\alpha(n)$ and $\beta(n)$, particularly on $\alpha(n)$, which are contrary to their expected behaviour as n increases, this will be expanded upon in section 5.6.5 since it is one of the features of our basis set generation. Nevertheless as we will see in the next section the different $(\alpha_{min}, \beta_{min})$ found during the basis set generation for each atom follow the behaviour dictated by 5.40 with a few caveats.

5.6.4 Behaviour of β

The only constraint placed on β during our basis set generation is that intevarls which span β space start at 1.8. This might appear to be counter intuitive based on the analysis of previous section, Schmidt and Ruedenberg [53], but we found that the isolated atomic calculations (using Cartesian Gaussian functions) can be sensitive to low β, with some calculations failing due to numerical instabilities. However we found the smallest β required to achieve our tolerance was $\beta = 1.83$ for Cu and the atomic calculation was perfectly stable at this value.

To see how numerical instability creeps up as β becomes smaller let us consider as an example two consecutive normalized primitives $\phi_i(\mathbf{r})$ and $\phi_{i+1}(\mathbf{r})$, both with p-symmetry. Their overlap integral is, according to section 5.2.3:

$$S_{i,i+1} = \left[\frac{2\sqrt{\beta}}{1+b}\right]^{5/2} \tag{5.42}$$

If $\beta = 1$ then we have $S_{i,i+1} = 1$, which implies that $\phi_i = \phi_{i+1}$ therefore $\mathbf{S}$ has a linear dependency and the atomic calculation will fail. Given this let us say that we take $S_{i,i+1} = 0.999$ to be the highest overlap integral that the particular atomic calculation can manage. That is, assume that if $S_{i,i+1} > 0.999$ the diagonalization of $\mathbf{S}$ fails. Let

$S_{i,i+1} = k$, we can rearrange equation 5.42,

$$k^{\frac{4}{5}}\beta^2 + (2k^{\frac{2}{5}} - 4)\beta + k^{\frac{2}{5}} = 0 \tag{5.43}$$

from which we find that for $k = 0.999$ we get $\beta = 1.09$. Thus for any β smaller than 1.09 the calculation will fail. From this discussion it follows that care must be taken regarding the choice of β in a basis set given that we don't know a priori if the calculation will fail or not. This is particularly important during a basis set generation routine where several β might be systematically searched, especially as n is increased. Furthermore the limiting β will change for different elements.

To visualize the behaviour of α and β with respect to the number of exponent, let us plot the α and β for copper and galium (two elements whose basis sets contain the largest number of exponents) at the simplex stage (averaged) in figure 5.9. Since at this point in our basis set routine we would expect α and β to follow the behaviour proposed by Schmidt and Rudenberg (equation (5.40)).

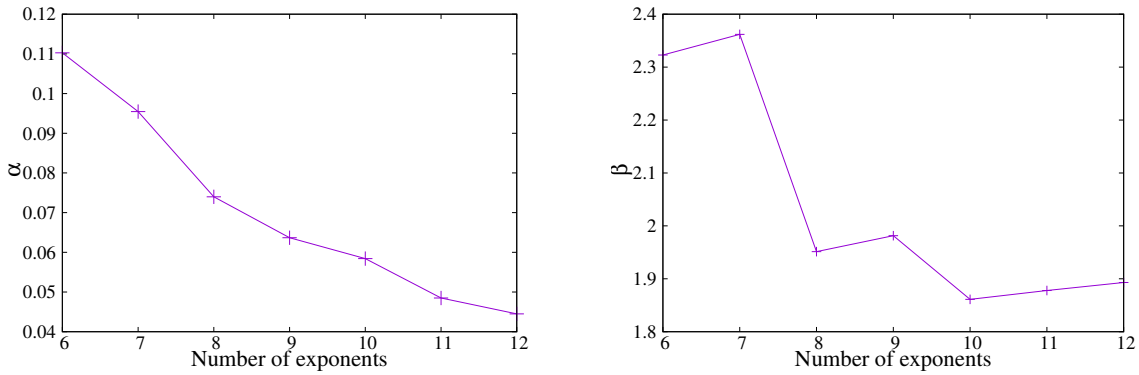

(a) Plot of α versus the number of exponents

(b) Plot of β versus the number of exponents

Figure 5.9: *Plots of the averaged values (for copper and galium) of α_{min} and β_{min} with respect to the number of exponents.*

From figure 5.9 we find that α_{min} does decay towards zero, that is $\lim_{n\to\infty} \alpha(n) = 0$. However as we expected based on our discussion β (in this case β_{min}) does not decrease monotonically to 1. This shows that our energy surface is more complex that that of Schmidt and Rundenberg for two reasons. First we have s, p and d occupied states in our calculation which share the same α and β values whereas Schmidt and Ruedenberg looked at a single angular momentum channel. Also our basis sets for Ga and Cu (semi-core pseudopotential) includes f-type orbitals, meaning we have additional s and p type functions (multiplied by r^2) in our basis sets, something not considered in the above analysis.

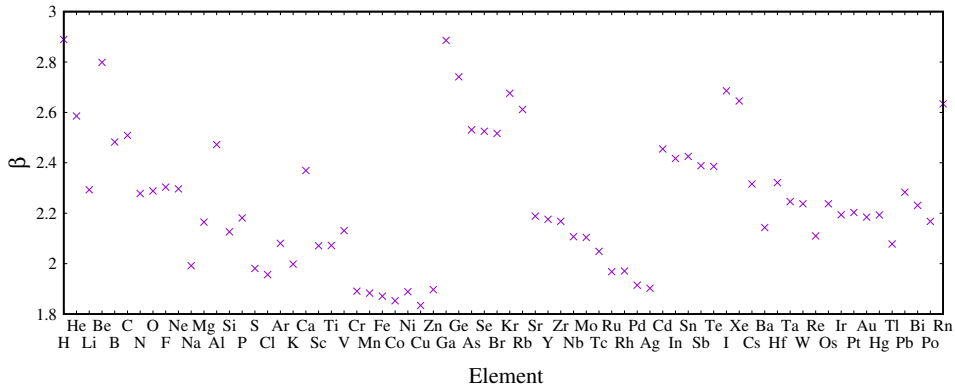

Figure 5.10: *Plot of the individual β used to generate the uncontracted primitive basis set.*

5.6.5 Regarding the choice of high first exponent (α)

When generating the basis sets we implemented steps with the goal of choosing the highest α which satisfies our chosen stopping condition. To verify that this goal has been accomplished we can compare the α obtained during the last simplex minimization with the one that is chosen by the routine to form the basis set. Table 5.2 contains the average (over all atoms) for the first exponent (α) and difference in energy (δ') at those two stages, for the last iteration of each atom's run. The first row contains the averaged values obtained at the simplex stage, the second row contains the resulting values from the basis generation routine.

	average α	average δ' (meV)
Simplex	0.0481406755	0.5845902638
Final	0.0584184143	0.999998068

Table 5.2: *Simplex α vs final α, and the respective average delta$'$ values.*

As intended we obtain a higher α using our routine than one would using regular minimization (simplex) whilst maintaining an error smaller than 1 meV.

To relate α to efficiency recall from chapter 4 the concept of *integral screening*. If for two primitives centred around different atoms their overlap term S_{ij} is less than a certain value we might disregard the corresponding Hamiltonian term (H_{ij}) if $S_{ij}V_{max}$ is smaller than a chosen tolerance. It follows that efficiency increases as the number of *screened* terms increases, firstly because we do not need to compute the integral exactly and in addition both the overlap and Hamiltonian matrices become sparser.

To see the effect that increasing alpha has on integral screening let us consider two Gaussian with different centers $\mathbf{R}_a$ and $\mathbf{R}_b$ but with the same exponent α, i.e. a system with at least two atoms of the same kind. For reasons of simplicity let us consider only

one $s-state$ primitive on each atom, with the following form:

$$\phi_a = e^{-\alpha(\mathbf{r}-\mathbf{R}_a)^2} \qquad \phi_b = e^{-\alpha(\mathbf{r}-\mathbf{R}_b)^2} \tag{5.44}$$

Let $\mathbf{R}_a - \mathbf{R}_b = \mathbf{D}$, from chapter 4.4 we find that the overlap integral between these two primitives is:

$$\begin{aligned} S_{\text{ab}} &= \int \phi_a(\mathbf{r})\phi_b(\mathbf{r})d\mathbf{r} = \int e^{-\alpha(\mathbf{r}-\mathbf{R}_a)^2} e^{-\alpha(\mathbf{r}-\mathbf{R}_b)^2} d\mathbf{r} \\ &= \left(\frac{\pi}{2\alpha}\right)^{\frac{3}{2}} e^{-\frac{\alpha}{2}D^2} \end{aligned} \tag{5.45}$$

where the exponential factor of the previous equation (5.45) is the dominant term, we can therefore approximate the equation as,

$$S_{\text{ab}} \approx e^{-\frac{\alpha}{2}D^2} = e^{-\tau} \tag{5.46}$$

where

$$\frac{\alpha}{2}D^2 = \tau \tag{5.47}$$

rearranging the previous equation we have

$$D = \sqrt{\frac{\tau}{2\alpha}} \tag{5.48}$$

therefore a bigger α is advantageous, since it allows us to discard integrals at a much smaller distance than one would with a smaller α. From this analysis it also follows that increasing α reduces the likelihood of linear dependency.

For calculations on large systems or calculations which use very large basis sets where efficiency and stability are a main concern, it follows that the basis generation routine presented above produces the most efficient and stable basis set (for basis sets constructed from uncontracted even-tempered primitives as we described in section 5.5) in the matrix building stage, within our chosen atomic tolerance. That is, it is unlikely that there exist other primitives which will generate an equally sparse Hamiltonian and overlap matrices and produce atomic results within 1 meV at the basis generation stage, given that we pick the highest α possible. Although the primitive basis set will be contracted on-site during the filtration stage for the calculations present in this thesis, the overlap and Hamiltonian matrices still need to be constructed in primitive space (this will be discussed in the next chapter) therefore the choice of high α does indeed make the overall calculation more efficient and stable.

Atomic radius Keeping our discussion focused on α let us now analyse its relation with atomic radius.

The lowest exponent (α) of our primitive basis should, in principle, correlate with each element's radius since it controls the spatial decay of the KS orbitals. As a first approximation we might expect that has the atomic radius decreases the lowest α increases, since the Gaussian primitive $e^{-\alpha r^2}$ must decay faster. We might approximate the following relation for our data:

$$R_{\text{atomic}} \propto \frac{1}{\sqrt{\alpha_{\text{min}}}} \tag{5.49}$$

where R_{atomic} is the atomic radius and α_{min} is obtained from the last simplex minimization of each run. The actual relation between each individual α_{min} and the atomic radius is not important for the current discussion and this approximation suffices.

In figure 5.11 we have plotted $\frac{1}{\sqrt{R_{\text{atomic}}}}$ (where R_{atomic} is taken to be the atomic covalent radius) against α_{min} of the respective atomic basis set and α_{high}, the parameter used to construct our basis set (taken from table 5.4). R_{atomic} is scaled so that $\alpha_{\text{min}} = \frac{1}{\sqrt{R_{\text{atomic}}}}$ for the helium atom.

Interestingly the behaviour of α_{min} and α_{high} across the set of elements follows that

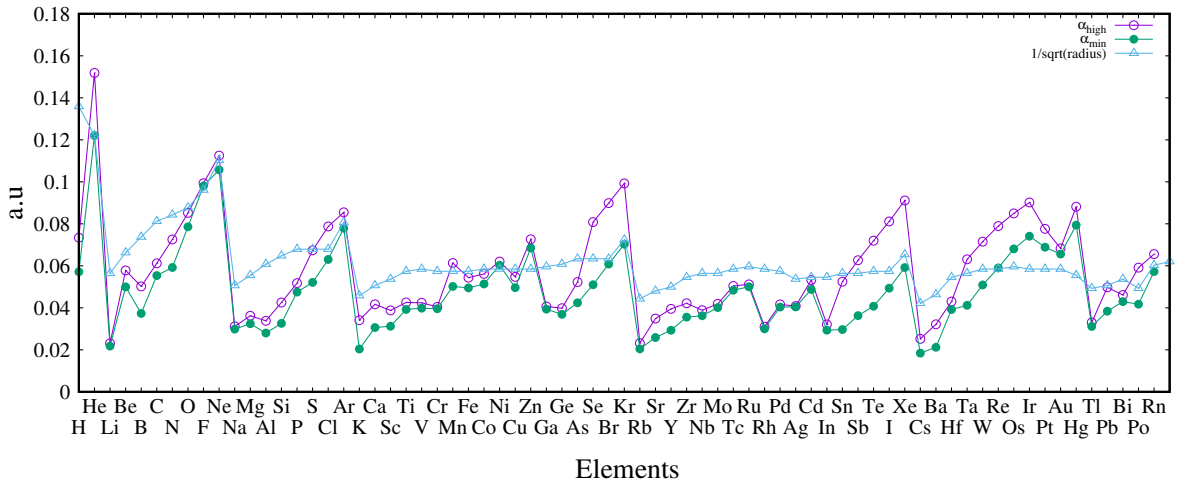

Figure 5.11: *Plot of the square root of the inverse atomic radius, α_{min} and α_{high} for the elements considered in the Δ-set.*

of the square root of the inverse atomic radius, albeit not exactly. Nevertheless the more pronounced features of the inverse atomic radius plot, such as the big drops from He to Li, Ne to Na and Ar to K which correspond to the increase in radius from fully filled electronic orbitals (for noble gases) to that of a valence orbital with one electron, are replicated by both α curves. A similar behaviour was reported in [53] for the first and second row elements (although only s-orbitals were considered in that particular plot).

Besides elucidating the overall trend for α with respect to the different elements, figure 5.11 demonstrates that our search for higher α has not destroyed the expected behaviour of α across the set of elements.

5.7 Summary

An uncontracted even-tempered primitive basis set has been generated for each atom in the Δ-set. These bases are large when compared with similar Gaussian basis sets, see table 5.3 for a comparison between our basis sets and that of Dunning for a few elements. The number of primitives in each of the basis sets generated here can be inferred from table 5.4. The same basis generation routine was used for each atom and we showed that the resulting basis set produces a ground state atomic energy that is only 1 meV away from a very well converged systematic calculation. It was demonstrated that our basis sets produces the set of even-tempered parameters with the highest α, which helps with both stability and efficiency. The large size of our basis sets offer a good starting point for contraction in a polyatomic KSDFT calculation. Furthermore the basis sets contain polarization primitives which might be tailored for the calculation at hand.

The next chapter will address the filtration step, here the very large number of primitive functions we have chosen (up to 240 for Cu) can be used to produce a manageable basis set for a full calculation.

Elements	Our basis set	Dunning (cc-pVTZ) [70]
H	18	8
C	60	18
Si	60	26
Cu	240	47

Table 5.3: *The number of primitives in our basis sets compared and a triple zeta Dunning basis set. The cc-pVTZ basis set were consulted in [2].*

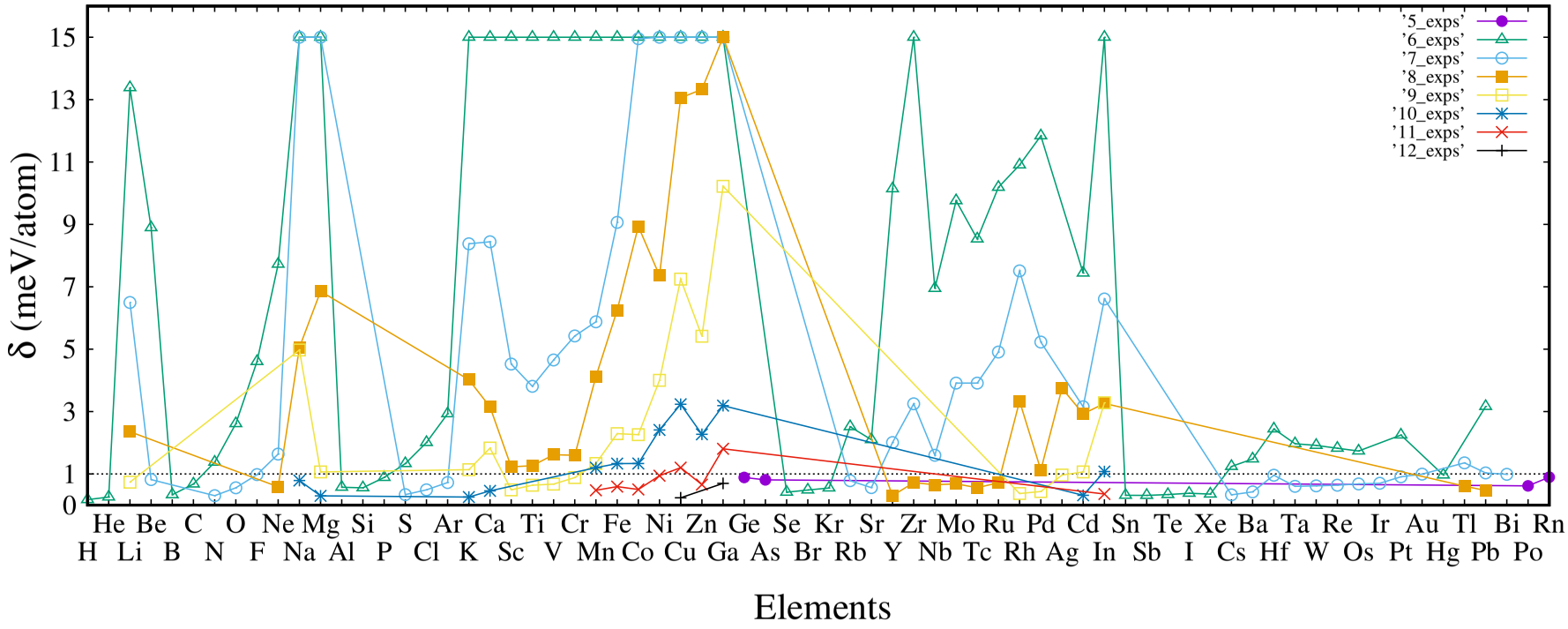

Figure 5.12: *Plot of individual δ_{min} obtained after simplex for each elements, each coloured line represents the simplex energies for different atoms obtained using the same number of exponents. The information relating the number of exponents (exps) and the colour is contained in the key. The dotted line represents the 1 meV line. Any $\Delta > 15.0$ meV has been reduced to 15 meV. For $n = 5$ only those points with $\Delta < 1.0$meV were plotted for simplicity sake.*

Element	α	β	n
H	0.07341	2.8252	6
He	0.15187	2.4966	6
Li	0.02312	2.2837	9
Be	0.05782	2.6962	7
B	0.05020	2.3588	6
C	0.06120	2.4860	6
N	0.07259	2.2304	7
O	0.08522	2.2739	7
F	0.09936	2.3019	7
Na	0.03119	2.0882	10
S	0.06738	1.9274	7
Mg	0.03621	2.1537	10
Al	0.03383	2.4059	6
Si	0.04255	2.0251	6
P	0.05177	2.1571	6
Cl	0.07873	1.9256	7
Ar	0.08549	1.9464	7
K	0.03411	1.9252	10
Ca	0.04167	1.9395	10
Sc	0.03876	2.3157	9
Ti	0.04258	2.0614	9
V	0.04241	2.0643	9
Cr	0.04047	2.1270	9
Fe	0.05436	1.8759	11

Element	α	β	n
Co	0.05618	1.8640	11
Ni	0.06205	1.8488	11
Cu	0.05473	1.8767	12
Zn	0.07263	1.8283	11
Ga	0.04064	1.8938	12
Ge	0.03985	2.8576	5
As	0.05228	2.6376	5
Se	0.08085	1.9961	6
Br	0.08986	2.0013	6
Kr	0.09924	2.0676	6
Rb	0.02319	2.4949	7
Sr	0.03489	2.4875	7
Y	0.03952	2.0914	8
Nb	0.03887	2.1645	8
Mo	0.04189	2.1606	8
Tc	0.05040	2.0983	8
Ru	0.05117	2.0991	8
Rh	0.03102	2.0435	9
Pd	0.04164	1.9637	9
Ag	0.04084	1.9698	9
Cd	0.05324	1.9015	10
In	0.03209	1.8902	11
Sn	0.05247	2.1300	6
Sb	0.06268	2.0995	6

Element	α	β	n
Sb	0.06268	2.0995	6
Te	0.07197	2.1080	6
I	0.08116	2.1056	6
Xe	0.09112	2.0718	6
Cs	0.02524	2.5266	7
Ba	0.03216	2.2760	7
Hf	0.04300	2.2826	7
Zr	0.04216	2.1100	8
Ta	0.06312	2.1627	7
W	0.07151	2.1179	7
Re	0.07893	2.1271	7
Ne	0.11249	2.1031	8
Re	0.07893	2.1271	7
Os	0.08499	2.1252	7
Ir	0.09019	2.1269	7
Pt	0.07762	2.1347	7
Au	0.06832	2.1834	7
Hg	0.08813	2.0527	6
Tl	0.03302	1.9418	8
Pb	0.04977	2.0787	8
Bi	0.04611	2.1456	7
Po	0.05914	2.3911	5
Rn	0.06557	2.4010	5

Table 5.4: *The parameters which define the uncontratcted even-tempered primitive basis set for each element considered in the* Δ*-test.*

Chapter 6

An updated filtration methodology tailored for large primitive basis sets

6.1 Introduction

Over the previous chapters an efficient method to build the KS Hamiltonian using GTOs was summarized and a procedure to generate high-quality GTOs was presented, all that remains now is to solve the GEP. Straightforward application of direct diagonalization to solve the GEP results in the cubic scaling of computational expenditure with respect to Hamiltonian matrix size (i.e. the size of the basis set). Efforts to reduce the computational effort in the diagonalization step can be adopted from linear algebra. Methods optimized for sparse matrices [77, 78] (when the problem at hand permits it) can be used, iterative diagonalization methods can also be implemented [79], or more modern techniques involving parallelization [80] can be used. One such iterative method used in regular `AIMPRO` can be found in [81]. If such methods are used the computational effort involved in solving the GEP and the respective scaling with respect to basis set size can be reduced from cubic to quadratic. However even with such a reduction in computer time large scale calculations are still very demanding.

Most KSDFT implementations discussed thus far do scale cubically $\mathcal{O}(N^3)$. The computer time required for a calculation can then be expressed, as a function of the number of atoms, as:

$$T = cN_{\text{atom}}^3 \tag{6.1}$$

Where c is a prefactor. Notwithstanding, the scaling involved in the other steps of a KSDFT calculation, typically for large-scale calculations the bottleneck with regards to timing resides in the scaling of the diagonalization step [14]. Current state-of-the-art Gaussian methods can tackle up to 500 atoms on a modern PC cluster [81]. However, KSDFT's success in solid-state physics and quantum chemistry has led to its spread to

other fields, such as nano-technology [82] and biology [83] (or even large-scale metallic calculations [84]) which require far more atoms, on the order of thousands or tens of thousands. To combat this a great deal of research, in the DFT field, has been done to develop algorithms with lower complexity, often called order-N ($\mathcal{O}(N)$), which provide linear scaling with respect to the number of atoms.

The overall CPU time of a calculation using low-complexity methods can be expressed as,

$$T = c_{\mathrm{l}} N_{\mathrm{atom}} \tag{6.2}$$

where c_{l} is the prefactor involved in the timing of linear-scaling calculations. The prefactors involved in the regular methods and linear-scaling are typically different, with c_{l} being often larger than c [14]. The point (number of atoms) at which the linear-scaling method is preferable to the regular cubic-scaling is known as the crossover point. For systems that are smaller than a particular code's crossover point, a regular cubically scaling code is faster as figure 6.1 indicates.

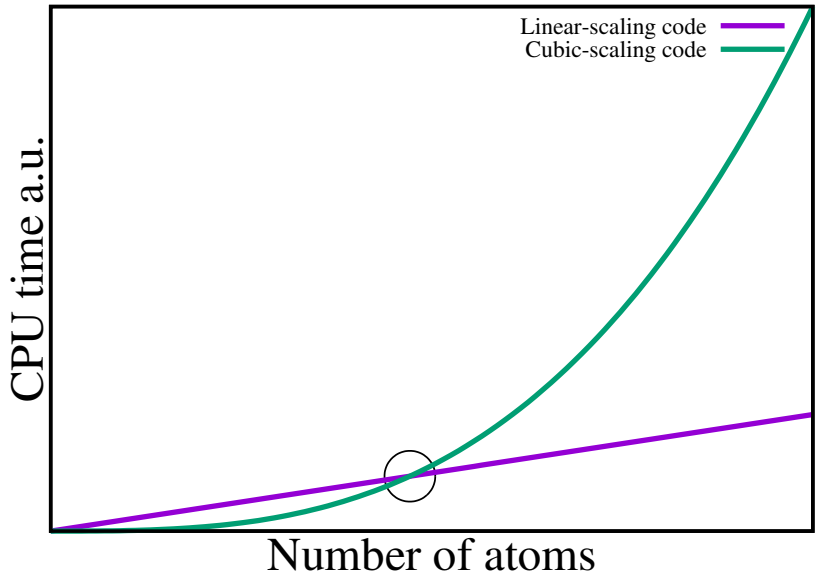

Figure 6.1: *Schematic illustrating the change in CPU time with respect to an increasing number of atoms for a linear and a cubic scaling code. The black circle indicates the crossover point. For systems with a smaller number of atoms than the one indicated by this point a cubic scaling code is preferred.*

Other methods exist which allow for calculations on large systems, force fields or semi-empirical methods such as density functional tight biding (DFTB) [85], can also handle large number of atoms, however such methods are not *ab-initio*. Particularly, tight-biding owes it speed due to its small Hamiltonian GEP (or OEP depending on the choice of basis sets) [86], in this regard it is similar to the filtration algorithm to be described in this chapter.

Unlike low-complexity DFT methods the filtration methodology does not rely on physical locality to perform fast calculations, it derives its computational saving by constructing a Hamiltonian with size comparable to that of a tight-binding calculation and performing the time consuming diagonalization in this space. In [16] the relaxed structure of a cell of 1728 silicon atoms was calculated using `AIMPRO`, both conventionally ($\mathcal{O}(n^3)$ scaling) and using the filtration methodology. It was found that even with a modest filtration strategy — good enough to provide filtration results which were within $\approx 10^{-4}$Å error of the conventional calculation — the filtration calculation was approximately 3 times faster. It is important to note that in these calcualtions and those presented in [5] the filtration calculations were compared with conventional `AIMPRO` runs. However, in this work we will be comparing our results with those obtained from plane wave implementations, a hard task for any GTO implementation. Furthermore unlike low-complexity methods the benefits of filtration extend to systems of all sizes there is no notion of a "cross-over" point.

In this section we will summarize the filtration methodology used in `AIMPRO` [5, 16], including recent changes to the algorithm.

6.2 Linear-scaling methods and locality

Although the locality responsible for many low-complexity implementations is not involved in filtration, it is worth briefly reviewing it here to differentiate it from other forms of locality, associated with spatial distribution, which do play a part in filtration.

As mentioned in the introduction most linear-scaling methods are conceptually linked to a fundamental feature of electronic structure, properties of a small region of atoms (in a big system) are weakly influenced by other atoms that are located, spatially, far away [87, 14, 15]. This is known as *locality* or *near-sightedness* [87].This is not necessarily related to the often labelled "locality" of a basis sets (spacial distribution), these are two separate, but relatable, topics. Indeed the "locality" of some real space implementations, often as a result particular choice of basis set, is often used to take advantage of the near-sightedness property of electronic structure and implement linear-scaling methods.

In science, particularly in Chemistry and Biology, the concept of locality is often tacitly assumed. For example when studying DNA molecules by breaking the molecule into pairs [88], or proving the bonding of large molecules by focusing on small subsets of said molecule [89] there is an underlying assumption that the physics of the overall system are only marginally affected by our focused analysis. It would seem natural then that in quantum mechanics (ultimately most of Biology and all of Chemistry is applied quantum mechanics) a certain degree of locality is to be expected.

The need to study large scale structures with DFT has resulted not just in the develop-

ment of linear-scaling algorithms but in addition it has lead to a deeper understanding of locality in quantum systems [87, 90]. In fact near-sightedness can be observed in some structures using regular DFT. For example, if one has a C_2H_6 chain and appends to it a CH_2 unit, one finds that the energy of this unit when calculated in the chain is very similar to the energy of a CH_2 unit calculated in a very long chain [14]. For an electron in a CH_2 unit then, the length of the C_nH_{2n+2} chain it inhabits has only a small effect on its perceived environment (after a certain length of C_nH_{2n+2} chain is constructed). For some systems we could be justified, for efficiency, in cutting out the interactions of a particular unit within that system with neighbouring units that are a certain distance away without a loss to the overall physics of the system. This near-sightedness property however does not imply that a particular problem can be broken down into smaller problems. Take for example the calculation of the conductivity of DNA using a linear-scaling DFT method [91, 92] 30 base pairs sufficed, however some problems involving kinks and DNA folding will most likely require more than 160 base pairs [93].

Most $\mathcal{O}(N)$ methods are built around localization regions, where outside of this region exponentially decaying terms are cut off [14]. It is therefore beneficial, for real space methods, that whatever basis sets one picks offers spatial locality. A good overview of the different sorts of linear-scaling methods and locality is given in [14] and [15]. Near-sightedness is not a universal concept [90]. Metals at a low temperature do not exhibit near-sightedness. Filtration, however, does not have any problems with systems which do not have any near-sightedness property, as we will see shortly.

When the term locality is used to describe a function it typically implies a small spatial distribution. Although there is no exact definition for what the locality of a function is we can deem a function $f(\mathbf{r})$ to be local if $f(\mathbf{r}-\mathbf{R}) \approx 0$ for $|\mathbf{r}-\mathbf{R}| > \mathbf{r}_c$, for some reasonable $\mathbf{r}_c$ where $\mathbf{R}$ is the "centre" of the function $f(\mathbf{r})$.

It is also possible to define the locality over coefficient (or Hamiltonian) space. If a function (Φ) is expanded over a space of functions (ϕ_i for $i = 1, 2, ...N$) we can define Φ to be local in coefficient space if,

$$\Phi = \sum_{i=1}^{N} c_i \phi_i \tag{6.3}$$

and c_i is finite only for a small number of functions ϕ_i in the space of functions..

I must stress that spacial and coefficient locality are pertinent to filtration, however, the near-sightedness is not.

6.3 Filtration

The filtration method summarized below differs slightly from previous implementations of the methodology [5, 40, 16]. However, the computational saving and the respective fast

calculations arise out of the same underlying principle, that of transforming the primitive GEP to a much smaller *filtered* GEP. Whilst previous work [5, 40, 16] has focused on the time saving aspect of filtration, in this thesis we are concerned with benchmarking and demonstrating its potential accuracy, which we aim to demonstrate can rival that of plane wave implementations. We will now summarize the filtration methodology and, where appropriate, highlight the current changes to the algorithm.

6.3.1 KSDFT summary

In order to visualize how the filtration algorithm acts we must briefly revisit the steps involved in a self-consistency loop of KSDFT calculation. Throughout this section we will be referring to the *primitive* space which is spanned by the primitive basis sets $\{\phi_i\}[i = 1, ..., N]$ (the uncontracted even-tempered GTOs from chapter 4). As before, a KS orbital is expanded in the primitive space as

$$\psi_\lambda(\mathbf{r}) = \sum_i c_{i\lambda}\phi_i(\mathbf{r}) \tag{6.4}$$

and the Hamiltonian and overlap matrices are constructed as described in chapter 4. A brief summary of the main steps involved in a KSDFT calculation is provided below with some extra information regarding timings.

1. The Hamiltonian matrix is built in the primitive space.

$$\begin{aligned} H_{ij} = &\int \phi_i(\mathbf{r})(-\frac{1}{2}\bigtriangledown^2 + V(\mathbf{r}))\phi_j(\mathbf{r})d\mathbf{r} \\ &+ \int\int \phi_i(\mathbf{r})V^{\mathrm{nl}}(\mathbf{r},\mathbf{r}')\phi_j(\mathbf{r}')d\mathbf{r}d\mathbf{r}' \end{aligned} \tag{6.5}$$

where $V(\mathbf{r})$ includes all the local terms: the local pseudopotential, the Hartree and the exchange-correlation potentials. $V^{\mathrm{nl}}(\mathbf{r},\mathbf{r}')$ is the non-local part of the pseudopotential. This non-locality of the pseudopotential does not affect the filtration method, given that it is short ranged. For small scale calculations this step is typically the most computationally expensive. An efficient Hamiltonian build was discussed in chapter 4.

2. Similarly the overlap matrix is constructed in the primitive space,

$$S_{ij} = \int \phi_i(\mathbf{r})\phi_j(\mathbf{r})d\mathbf{r} \tag{6.6}$$

and the GEP is formed,

$$\mathbf{Hc} = \mathbf{Sc\Lambda} \tag{6.7}$$

3. Solve the GEP (either by direct diagonalization or an iterative process), update the density matrix

$$b_{ij} = \sum_{\lambda}^{N} f_\lambda c_{i\lambda} c_{j\lambda} \tag{6.8}$$

and generate the new density,

$$n(\mathbf{r}) = \sum_{ij}^{N} b_{ij} \phi_i(\mathbf{r}) \phi_j(\mathbf{r}) \tag{6.9}$$

which we use to construct a new $V(\mathbf{r})$.

The Filtration method replaces step 3. Instead of solving the full (primitive space) GEP, $\mathbf{H}$ and $\mathbf{S}$ are expressed in a *contracted* space,

$$\mathbf{H}'\mathbf{c}' = \mathbf{S}'\mathbf{c}'\mathbf{\Lambda}' \tag{6.10}$$

Where,

$$\mathbf{k}^T \mathbf{H} \mathbf{k} = \mathbf{H}' \tag{6.11}$$

and $\mathbf{k}$ are contraction matrices. The GEP is then solved in the contracted space.

6.3.2 Contracted Basis sets

The contracted (or filtered) basis set $\{\tilde{\phi_I}\}[I = 1, .., \tilde{n}]$ is constructed using the underlying primitive basis set $\{\phi_i\}[i = 1, ..., N]$,

$$\tilde{\phi_I}(\mathbf{r}) = \sum_{i}^{N} k_{iI} \phi_i(\mathbf{r}); \quad I = 1, ..., \tilde{n} \tag{6.12}$$

where k_{iI} are the contraction coefficients and $\tilde{n} < N$. Contracted basis sets have been described previously in this thesis (chapter 4), however the contraction presented here is fundamentally different. Conventionally, such as in Pople [52] or Dunning [70], the matrix of contraction coefficients $\mathbf{k}_I$ is obtained from an isolated atomic calculation and the coefficients (k_{iI}) remain frozen throughout subsequent KSDFT calculations, whenever the basis set is used. This is one of the main reasons for the plethora of different basis sets existent today. In the case of filtration however using very high quality primitives we construct the contracted basis set on-the-fly for the system at hand. This allows us to tailor the contracted basis set to the current electronic environment, removing the need for countless different basis sets and system appropriate augmentations. This contraction (filtration) is done by filtering out components from high-energy eigenfunctions from the primitive basis, the resulting, much smaller, contracted basis sets spans the, useful, lower energy interval of the Hamiltonian.

6.3.3 Filtration

For simplicity, in the current discussion we assume an orthogonal basis. Once the filtration method is explained the case for non-orthogonal basis is described. Consider an $n \times n$ eigenvalue problem

$$\mathbf{H}\mathbf{c}_\lambda = \lambda \mathbf{c}_\lambda \tag{6.13}$$

if one is only interested in eigenvalues in a specific range $[\lambda_i < \lambda < \lambda_j]$ then solving equation (6.13) using direct diagonalization can be deemed wasteful, especially if the eigenvalue spectrum under consideration is small. To remedy this one could devise a function of the Hamiltonian $\mathbf{F}(\mathbf{H})$ that would filter out eigenvalues outside the desired spectrum,

$$\mathbf{F} = \sum_i |i\rangle \, f(\lambda_i) \, \langle i| \tag{6.14}$$

Where $f(\lambda_i)$ would select, mostly, the eigenvectors $|i\rangle$ for which λ_i is in the chosen spectrum. Operating with $\mathbf{F}$ on a trial function $|t_k\rangle$,

$$\mathbf{F} \, |t_k\rangle = \sum |i\rangle \, f(\lambda_i) \, \langle i|t_k\rangle = |t'_k\rangle \tag{6.15}$$

where $\{|i\rangle \, , \lambda_i\}$ are the eigenpairs of $\mathbf{H}$ and similarly $\{|i\rangle \, , f(\lambda_i)\}$ are the eigenpairs of $\mathbf{F}$ with $0 < f(\lambda_i) < 1$. By applying $\mathbf{F}$ to our trial function the resulting filtered function $|t'_k\rangle$ will have, mostly, components in the desired eigenvector range. This process is repeated and different filtered functions ($|t'_k\rangle$)are generated until the space is spanned adequately (say by $|t'_k\rangle \, [k = 1, .., m]$). A $m \times m$ GEP is constructed in the subspace of m functions,

$$\mathbf{H}'\mathbf{c}' = \mathbf{S}'\mathbf{c}'\mathbf{\Lambda}' \tag{6.16}$$

and diagonalized.

The accuracy of this method can always be increased by using a larger number of trial functions or constructing a lower temperature filtration function $f(\lambda)$, an example of the effect of chosing different temperatures for the filtration can be seen in figure 6.2.

For non-orthogonal primitives the filtration step, equation (6.15) becomes

$$\mathbf{c} f(\mathbf{\Lambda}) \mathbf{c}^T \mathbf{S} \, |t\rangle = \mathbf{F}\mathbf{S} \, |t\rangle = |t'\rangle \tag{6.17}$$

However, the underlying idea and outcome is the same as when orthogonal basis are used.

6.3.3.1 Filtration function

For our applications, given that we are interested in the lowest eigenpairs of the Hamiltonian, we use a modified high-temperature Fermi-Dirac distribution:

$$f(\lambda_i) = \left(e^{(\lambda_i - \mu)/kT} + 1\right)^{-1} \tag{6.18}$$

Where λ_i are the eigenvalues and μ is chosen based on the HOMO-LUMO gap of the atom, i.e. difference between the highest occupied atomic orbitalal and the lowest unocuppied atomic orbital. We shall refer to μ as the Fermi energy throughout this thesis when filtration is discussed. The Fermi energy can be increased to facilitate the inclusion of functions with higher angular momentum values than those present in the atom, as we can see in figure 6.2. The main body of work presented in this thesis was done so using a systematic assignment of μ for each atom. However a small number of atomic calculations required manual tweaking of this parameter, this will be discussed at end of the next section and in the future works.

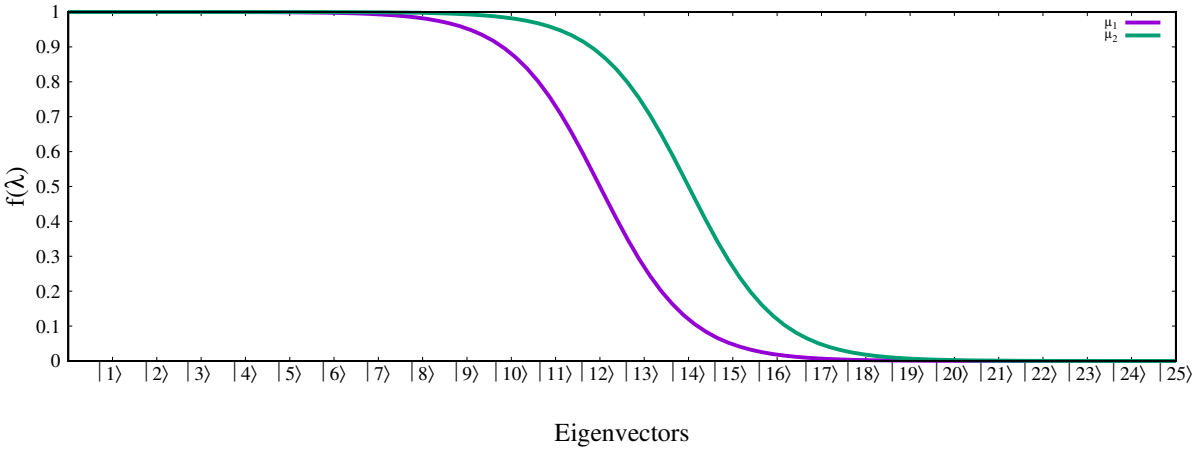

Figure 6.2: *Plot of two Fermi-Dirac functions, where $\mu_2 > \mu_1$. Recall that, the eigenvectors of the Hamiltonian for which $f(\lambda) \neq 0$ are included in the generation of the filtered basis. Increasing μ results in more eigenfucntions being included in the filtration stage, particularly those with a higher angular momentum than the highest filled KS orbital.*

6.4 Localization constraints

The localization constraints of the current filtration methodology differ slightly from the original implementation [5, 16]. Nevertheless, it is worthwhile to explain how the localization region was defined previously given that the newest method can be taken as an limiting case of the previous.

The filtration method as presented up until now does not offer any computational saving. Constructing the filtration matrix $\mathbf{F}$ requires the same computational effort as calculating the density (both require solving $\mathbf{H}$ in the primitive space). To remedy this, we impose localization constraints when constructing $\mathbf{F}$. For each atom in the system, at $\mathbf{R}_\alpha[\alpha = 1, .., N_{\text{atom}}]$, we construct a filtration matrix F_α using only the primitive basis of atoms located within a distance r^α_{cut} from the atom at R_α. That is the primitive functions of the atom at $\mathbf{R}_\beta$) are used to construct $\mathbf{F}_\alpha$ if $|\mathbf{R}_\beta - \mathbf{R}_\alpha| < r^\alpha_{\text{cut}}$. We shall refer to this method as *off-site* filtration.

In the filtration method used in this thesis, however, only the primitives from the atom at $\mathbf{R}_\alpha$ are used when generating $\mathbf{F}_\alpha$. A method which we refer to as *on-site* filtration. It is important to notice that the matrix elements used to construct the smaller filtred Hamiltonian are taken from the full Hamiltonian, so that this smaller space is contructed *in situ* in the environment of the full problem.

As mentioned above, a Fermi-Dirac function is used when constructing each $\mathbf{F}_\alpha$, the temperature is set to be high, assuring the localization of the filtered functions. However, it follows from this localization that more filtered functions are required to properly span the primitive space.

With regards to the locality referenced in this section it must be stressed that filtration is unlike low complexity methods which rely on the density matrix to attain linear-scaling. Particularly divide and conquer methods [94] where a system is divided in to smaller subsystems, and the respective densities of calculated there and then reformed into the whole system's density. At first glance this method appears similar to filtration, but it is more alike, in its theoretical foundation, to methods which use the locality of the density matrix to produce sparse matrices and attain linear-scaling [95, 96].

Filtration relies on the filtration matrix locality (eq. (6.15)), not the density matrix. Ultimately the Hamiltonian GEP is still diagonalized with cubic scaling but in a reduced space unlike low complexity methods. It follows that such methods might struggle with systems which do not exhibit near-sightedness such as low electronic temperature metallic systems [14]. Filtration, however, does not depend on any near-sightedness property and is therefore suitable for arbitrary systems [5].

6.4.1 Trial functions

The filtration method as described above places no constraints on the set of trial functions, $|t\rangle$, that are used to generate the filtered functions, $|t'\rangle$. The only caveat being that the set of trial functions should be localized in real space. Ideally, for each atom one would use a set of trial functions that adequately represent its different KS orbitals, particularly from the angular momentum point of view. In addition, one should include functions which

represent higher lying orbitals than that of the fully filled atom. For example, carbon has two electrons with p_x and p_y angular momentum channels, σ-orbital, thus one could be inclined to chose a set of trial functions which mimic the behaviour of these orbitals, however when carbon is in graphene it is well known that the π-orbital, constructed from the p_z angular momentum channel, is important for band structure calculations. Thus our initial guess for the trial functions would most likely miss out what, *a posteriori*, is an important angular momentum channel for carbon applications.

Gaussian functions are localized both in real and in primitive coefficient space making them great candidates for trial functions, in addition `AIMPRO`'s kernel is already optimized to handle them which greatly simplify their usage in filtration. Our set of trial functions is constructed from the underlying primitive basis set as described in the next section.

6.4.1.1 The number of primitives in the trial set

The number of primitives in the trial set is controlled by the positive basis-e_{cut} parameter, specified by the user. Once the atomic calculation is performed in the subspace, we count the atomic states, of angular momentum l, that have an energy below our chosen basis-e_{cut}. The total number of states for each angular momentum channel will determine the numbers of primitives, with the same angular momentum value l, in the trial set. The exponents of these primitives are given by an even-tempered distribution where the α is taken to be the same as the primitive set's, and β_{trial} is given by,

$$\beta_{\text{trial}} = \left(\frac{\alpha}{\alpha_{\text{end}}}\right)^{\frac{1}{N_{\text{l}}-1}} \tag{6.19}$$

where α_{end} is the largest exponent in the primitive set and N_{l} is the number of states with angular momentum l with energy less than basis-e_{cut}. N_{l} will also be the number of exponents in the trial set with angular momentum l, the primitives generated from these exponents take into account the degeneracies due to l. For example, If there are five s-states and four p-states with energy below a chosen basis-e_{cut}, the trial set will be constructed with five primitives (all with different exponents) with an angular momentum of $l = 0$, and four sets of 3 primitive (each with the same exponent) with angular momentum $l = 1$.

With a higher basis-e_{cut} we have $N_l = N$ for all values of l at which point the trial set becomes almost the same as the primitive set, at which point increasing basis-e_{cut} further will have no effect.

6.4.2 Computational method

Having described the filtration methodology, all that remains is to implement it inside an AIMPRO calculation. As mentioned before the filtration method replaces the direct diagonalization of a regular AIMPRO run. Therefore it is assumed here that both **H** and **S** have been constructed using the primitive basis. A linear-scaling build of the Hamiltonian was described in chapter 4.

6.4.2.1 Construction of the filtered basis

We will describe the method for on-site filtration. Let us assume that **H** and **S** have been built in the primitive space. We loop over and construct the filtered basis for each atom in the system. The steps presented below assume we are dealing with an atom at $\mathbf{R}_\alpha$.

1. Localization constraint : The set, call it $\{B_\alpha\}$, of n_α primitives from the atom at $\mathbf{R}_\alpha$ are used to generate a new atomic Hamiltonian $\bar{\mathbf{H}}$. Note that $n_\alpha <$ N and is independent of system size. The elements of the new Hamiltonian can actually be taken from the respective entries in the primitive Hamiltonian,

$$\bar{H}_{ij} = H_{ij}, \quad \text{if } i,j \in \{B_\alpha\} \tag{6.20}$$

2. The $n_\alpha \times n_\alpha$ subspace GEP, $\bar{\mathbf{H}}\bar{\mathbf{c}} = \bar{\mathbf{\Lambda}}\bar{\mathbf{S}}\bar{\mathbf{c}}$, is solved.

3. The respective columns of the filtration matrix, $\mathbf{f}(\bar{\mathbf{c}})\bar{\mathbf{S}}$, are formed,

$$|f_k(\bar{c})\rangle = \bar{\mathbf{c}}\mathbf{f}(\bar{\mathbf{\Lambda}})\bar{\mathbf{c}}^T\bar{\mathbf{S}}\,|t_k\rangle \tag{6.21}$$

4. The vector $|f_k(\bar{c})\rangle$ (with space size n_α) is mapped into the corresponding column of **k** (with space size N). This decompresses a vector of length n_α into a sparse N length vector, with the individual entries referring to the respective primitive basis. Looping over the set of trial functions provides $\tilde{n}_\alpha$ columns of the contraction matrix **k**, where $\tilde{n}_\alpha \ll n_\alpha$ is the number of trial functions, set by basis e_{cut}.

As each GEP in step 2 is independent of system size the generation of the filtered basis set scales linearly with system size. Furthermore this algorithm can be performed in parallel given that, for the purposes of filtration, each atom is independent.

The filtration step described here is performed in each self-consistent loop. The overall result of this is the construction of the contraction matrix (**k**) with size $N \times N_{\text{sub}}$, where

$$N_{\text{sub}} = \sum_{\alpha=1}^{N_{\text{atoms}}} \tilde{n}_\alpha \tag{6.22}$$

with $N_{\text{sub}} < N$.

6.5 Primitive to filtered space transformation.

Once the **k** matrix is formed filtered basis might be expressed as,

$$\tilde{\phi_I}(\mathbf{r}) = \sum_i^N k_{iI}\phi_i(\mathbf{r}); \quad I = 1, ..., \tilde{n} \tag{6.23}$$

we may now transform the original GEP in the primitive space to a much smaller GEP in the contracted subspace,

$$\begin{aligned} \tilde{H}_{IJ} &= \int \tilde{\phi}_I(\mathbf{r})\hat{H}\tilde{\phi}_J(\mathbf{r})d\mathbf{r} \\ &= \sum_i^N \sum_j^N k_{iI}k_{jJ} \int \phi_i(\mathbf{r})\hat{H}\phi_j(\mathbf{r})d\mathbf{r} \\ &= \sum_i^N \sum_j^N k_{iI}k_{jJ}H_{ij} \end{aligned} \tag{6.24}$$

where k_{iI} are the contraction coefficients obtained during the filtration step. Equation (6.24) can be rewritten as

$$\tilde{\mathbf{H}} = \mathbf{k}^T\mathbf{H}\mathbf{k} \tag{6.25}$$

and similarly for the overlap matrix,

$$\tilde{\mathbf{S}} = \mathbf{k}^T\mathbf{S}\mathbf{k} \tag{6.26}$$

We can then construct the subspace GEP,

$$\tilde{\mathbf{H}}\tilde{\mathbf{c}} = \tilde{\mathbf{S}}\tilde{\mathbf{c}}\tilde{\mathbf{\Lambda}} \tag{6.27}$$

which we then solve using direct diagonalization. The Hamiltonian matrix size is now $N_{\text{sub}} \times N_{\text{sub}}$. Whereas before generating the new density required N^3 operations (where N is the number of primitives) we have now reduced the computational expenditure by $(\frac{N}{N_{\text{sub}}})^3$. For small N_{sub} this provides large time savings [5].

6.6 Filtered to primitive subspace.

Once the subspace GEP has been solved and the density matrix ($\tilde{\mathbf{b}}$) constructed we can transform back to the original primitive space.

$$\begin{aligned} n(\mathbf{r}) &= \sum_{IJ}^{N_{\text{sub}}} \tilde{b}_{IJ}\tilde{\phi}_I(\mathbf{r})\tilde{\phi}_J(\mathbf{r}) \\ &= \sum_{IJ}^{N_{\text{sub}}} \sum_{ij}^{N} k_{iI}k_{jJ}\tilde{b}_{IJ}\phi_i(\mathbf{r})\phi_j(\mathbf{r}) \\ &= \sum_{ij}^{N} b_{ij}\phi_i(\mathbf{r})\phi_j(\mathbf{r}) \end{aligned} \tag{6.28}$$

It follows from equation (6.28) that elements in b_{ij} which are finite in $\mathbf{S}$ can be constructed from elements in $\tilde{b}_{IJ}$ which are finite in $\tilde{\mathbf{S}}$. Thus the density matrix $\mathbf{b}$ in the primitive space can be build from the subspace density matrix as,

$$\mathbf{b} = \mathbf{k}\tilde{\mathbf{b}}\mathbf{k}^T \tag{6.29}$$

After the subspace to primitive transformation the calculation then proceeds as in the regular `AIMPRO` implementation. Due to the sparsity of the matrices both primitive space $\rightarrow$ subspace and subspace $\rightarrow$ primitive space transformation scale linearly with respect to system size.

6.7 Summary

Figure 6.3 summarizes the different steps performed to generate a density from a GEP using filtration and direct diagonalization. Although the method presented here is slightly different than previous filtration implementations, the potential time savings still arise out of the same concept. This aspect of filtration has have already been discussed and demonstrated in [5, 16]. Essentially, the main difference from previous methodology to the one presented here is that we are producing, effectively, a new primitive set and the current work focus on the potential gains in accuracy and stability by means of filtration rather than speed. Algorithm wise the main difference between the two methodologies is the on-site (current) vs off-site (previous) filtration.

Unlike low complexity algorithms where the benefit of linear scaling methods only becomes prominent for very large calculations. Filtration is a multi-purpose "tool", not only does it allow for systems of 10,000 atoms to be analysed on a desktop but also, as we will demonstrate, for very accurate basis set to be performed.

Having generated high quality uncontracted basis sets which would be unusable in

regular AIMPRO (save for an isolated atom) we can now use them regularly with filtration, setting the stage for calculations close to the basis set limit. In addition this accuracy can be attained in a systematic way by increasing the size of trial functions, therefore giving us systematic convergence.

The accuracy of our methodology and basis sets will now be assessed using a recent benchmark [3], which distils the results of an almost periodic-table wide test set into a single value, named the Δ-value.

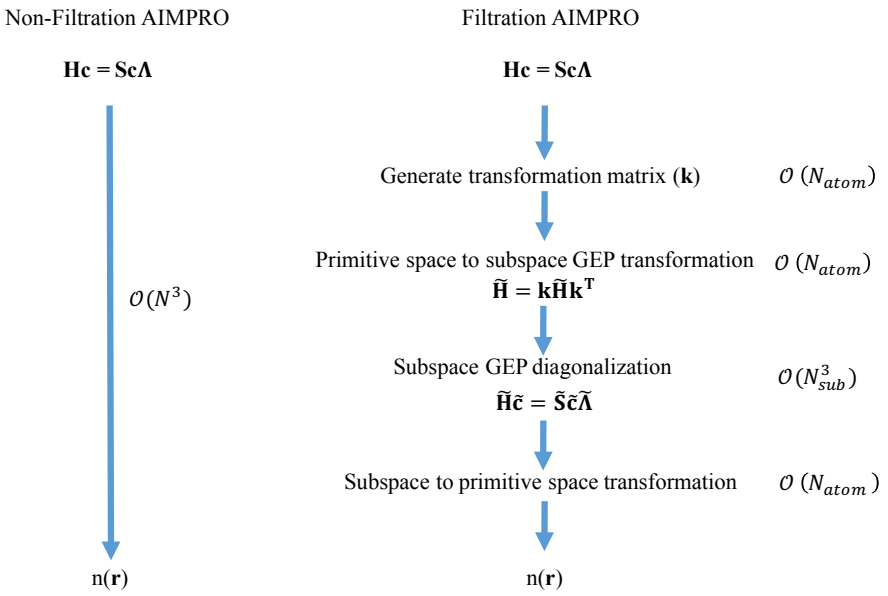

Figure 6.3: *Comparison between the steps involved in generating a density from a primitive GEP between a filtration and regular calculations. The scaling refer to the steps directly to the left.*

Chapter 7

The Δ benchmark as an assessment of the filtration methodology

7.1 Introduction

Recall, from the introductory chapters, that although DFT is in principle exact some approximations were made before arriving at a solvable set of Kohn-Sham equations, particularly:

- The Born-Oppenheimer approximation (immovable nuclear charge).
- Approximations to the exact exchange-correlation functional.

These approximations will contribute error to any property calculated with DFT. With the choice of exchange-correlation being responsible for most of the deviation between DFT predictions and experimental results (for ground state properties). Minimising the error associated with a choice of exchange-correlation functional or understanding the limitations of a particular functional is common to any KSDFT implementation and it is a topic of active research [97, 98], typically benchmark studies focus on providing a measure of this error. Both of the aforementioned errors are shared by all DFT implementations. To separate these kinds of errors — shared by all implementations — to those particular to a specific code they are labelled *intrinsic errors* [6]. It follows then that, having specified an exchange-correlation and using a state-of-the-art all electron code [99] (taken to be the most accurate kind of DFT codes [100]) these errors are responsible for the code-to-experiment deviation, i.e. the *accuracy* of the result predicted by DFT.

Barring the intrinsic errors, all DFT implementations should predict identical results for a given choice of exchange-correlation functional. However the numerical implementation of the KSDFT formalism leads to code specific deviations related to the particular kernel of the code. The choice of basis sets, pseudopotential or even how numerical operations are performed will lead to a scatter of predicted results. This can be thought as

affecting the *precision* of a code, that is how far does the result deviate from that of a well-converged all-electron calculation (a code-to-code measure).
Lejaeghare et al. label these errors as *numerical errors* [6], of which the two biggest sources are:

- Basis sets.
- Pseudopotentials.

The implementation of relativistic effects, particularly for heavier atoms, can be another source of *numerical* deviation. However this is more noticeable in all-electron calculations where this must be treated explicitly, than for codes using pseudopotentials in which the relativistic effects are treated during their generation.

A recipe to quantify both numerical and intrinsic errors is given by the recently developed Δ-benchmark [6, 3]. Although the Δ-benchmark does provide a recipe to ascertain the quality of an exchange-functional (the accuracy), the novel, and important, procedure to provide a comprehensive check of the precision of a code and indicating it with a single value (the Δ-value) is the main focus of the present chapter. Particularly we are interested in assessing the error introduced by the filtration and our uncontracted basis sets when compared with similar calculations (same pseudopotential) and those performed using the all-electron codes.

7.1.1 The Δ-benchmark

The Δ-benchmark is a pairwise code comparison involving calculations of root-mean-squared (r.m.s.) difference between the equations-of-state — for the 71 ground-state elemental crystals — of two different methods (the method one wishes to evaluate and a reference). We will only be using 70 elements since there is no pseudopotential for Lu (for Mathias Krack's pseudopotentials [39]). Amongst the set of 70 ground-state elemental crystals, there is a wide range of crystal structures which vary from simple hexagonal and cubic to low symmetry monoclinic cells, an overview of the different structures and the number of atoms is presented in figure 7.1. In addition ground-state crystals for elements which require spin polarization calculations are also included: O, Cr, Mn (antiferromagnetic) and Fe, Co, Ni (ferromagnetic), these correspond to the grey entries in figure 7.1. Such a diverse array of materials and structures allowed for comprehensive calculations which are considered to "establish statistically justified intrinsic error estimates" for the PBE functional [6].

The procedure to generate a code's Δ-value uses the same elements and almost the same structures (the elemental crystals for Mn and S are changed for purposes of efficiency) as the intrinsic error evaluation. Here too the diversity of the Δ elemental crystals set

H																	He
194																	194
hR9																	hP2
Li	Be											B	C	N	O	F	Ne
166	194											166	194	205	12	15	225
hR9	hP2											hR36	hP4	cP8	mS4	mS8	cF4
Na	Mg											Al	Si	P	S	Cl	Ar
166	194											225	227	64	166	64	225
hR9	hP2											cF4	cF8	o58	hR3	oS8	cF4
K	Ca	Sc	Ti	V	Cr	Mn	Fe	Co	Ni	Cu	Zn	Ga	Ge	As	Se	Br	Kr
229	225	194	194	229	229	225	229	194	225	225	194	64	227	166	152	64	225
cI2	cF4	hP2	hP2	cI2	cI2	cF4	cL2	hP2	cF4	cF4	hP2	oS8	cF8	hR6	hP3	oS8	cF4
Rb	Sr	Y	Zr	Nb	Mo	Tc	Ru	Rh	Pd	Ag	Cd	In	Sn	Sb	Te	I	Xe
229	225	194	194	229	229	194	194	225	225	225	194	139	227	166	152	64	225
cI2	cF4	hP2	hP2	cI2	cI2	hP2	hP2	cF4	cF4	cF4	hP2	tI2	cF8	hR6	hP3	oS8	cF4
Cs	Ba		Hf	Ta	W	Re	Os	Ir	Pt	Au	Hg	Tl	Pb	Bi	Po		Rn
229	229		194	229	229	194	194	225	225	225	139	194	225	166	221		225
cI2	cI2		hP2	cI2	cI2	hP2	hP2	cF4	cF4	cF4	tI2	hP2	cF4	hR6	cP1		cF4

Figure 7.1: *The ground-state crystal structures for all the 70 elements considered in this thesis used in the Δ-set test. The grey background indicates elements which require a spin-polarized calculation. The first number in each element box corresponds to the space group, whilst the xYN entry is the Pearson symbol, with x standing for the Crystal family, Y for the lattice and N for the number of atoms.*

allows for a "broad and comprehensive" test for precision, so that an acceptable Δ-value is (currently) the best pass/fail indicator of a code's quality [3].

7.1.2 The Δ-test

Typically the Δ-benchmark calls for the reference calculations to be performed with all-electron codes, however any type of code can be used. The ability to choose different reference codes allows us to tailor the benchmark to study specific numerical errors of interest. This will be discussed at the end of this section.

For simplicity let us define the following notation when referring to different types of Δ-values:

$$\Delta_y^i \tag{7.1}$$

where the presence of a i superscript indicates the Δ-value of a particular *element* (where i can be the element's symbol), or if i is absent it indicates an average of the individual Δ^i (i.e. the code's Δ-value). The y subscript indicates, if present, which code we use as a reference (i.e. Δ_{ABINIT} implies the Δ-value was calculated using ABINIT as a reference). If only Δ is present this indicates the standard Δ-test, where each individual Δ^i was calculated with respect to an all-electron calculation. Using this notation we can write

AIMPRO's Δ_{ABINIT} as,

$$\Delta_{\text{ABINIT}} = \frac{\sum_{i=1}^{\text{N}} \Delta^i_{\text{ABINIT}}}{\text{N}} \tag{7.2}$$

where N is the number of elements considered.

The Δ^i of an element is defined as a difference between the equation of state (EOS) (for the ground-state elemental crystal) calculated using the code in question and that of a reference code:

$$\Delta^i = \frac{\int \Delta E^2(V) dV}{\Delta V} \tag{7.3}$$

where $\int \Delta E^2(V) dV$, plotted in figure 7.2, is the r.m.s. difference between the two code's EOS,

$$\int \Delta E^2(V) dV = \int_{V_i}^{V_f} (E_1(V) - E_2(V))^2 dv \tag{7.4}$$

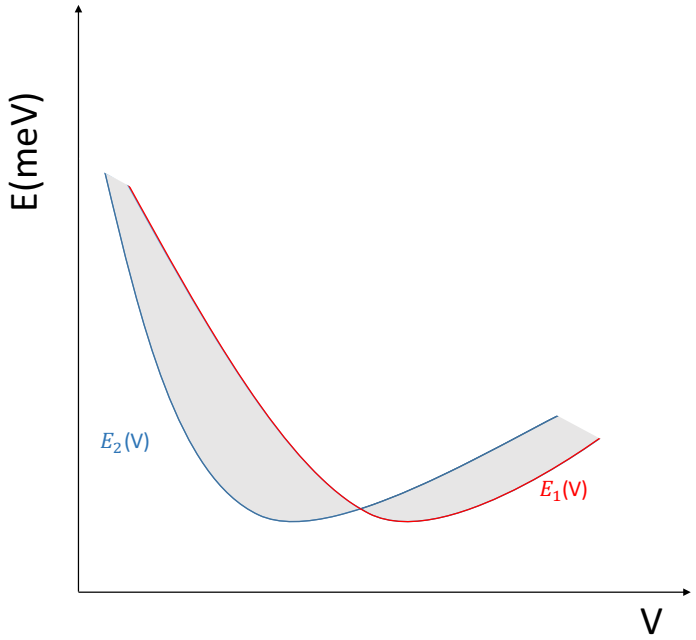

Figure 7.2: *A comparison of two EOS obtained from two codes: Code 1 (red) and code 2 (blue), the integral difference is indicated by the grey area between the two curves. This integral is always calculated between an initial volume (V_i) and a final volume (V_f). Where, conventionally, V_i and V_f are 94% and 106% of the VASP optimized equilibrium volume.*

and $\Delta V = V_f - V_i$, where V_i and V_f are drescribed in figure 7.2. The equations of

state $E_1(V)$ and $E_2(V)$ are Birch-Murnaghan EOS given by:

$$E(V) = E_0 + \frac{9V_0B}{16}\left(\left[\left(\frac{V_0}{V}\right)^{\frac{2}{3}} - 1\right]^3 B_1 + \left[\left(\frac{V_0}{V}\right)^{\frac{2}{3}} - 1\right]^2\left[6 - 4\left(\frac{V_0}{V}\right)^{\frac{2}{3}}\right]\right) \tag{7.5}$$

where E_0 is the energy per atom of the compound we are investigating, V_0 the equilibrium volume, B_0 the bulk modulus and B_1 the pressure derivative of the bulk-modulus (evaluated at the V_0),

$$B_1 = \left.\frac{\partial B}{\partial P}\right|_{V_0} = \left.\frac{\partial}{\partial P}\left(V\frac{\partial^2 E}{\partial V^2}\right)\right|_{V_0} \tag{7.6}$$

Note that in evaluating (7.5) all structural lengths are scaled as the volume is changed (including atomic positions). The E_0, V_0, B and B_1 values do not directly give us any insight into the numerical errors, however they can be used to ascertain the quality of a functional (intrinsic errors), since experimental values of these quantities can be found in literature for the ground-state elemental crystals considered in the set [6].

For the evaluation of numerical errors the minimum energy E_0 is not used when calculating Δ^i. The benchmark calls for the minima of both code's EOS to be the same, i.e. $\min[E_1(V)] = \min[E_2(V)]$. Only V_0, B, B_1 are used to define both code's EOS, equation 7.5, and by extension the integral in equation 7.4. It follows that the Δ^i of an element is then dependent on two sets of EOS parameters (V_0, B, B_1), one for the reference code and another for the code we wish to study. For each code, and particular element, the parameters (V_0, B, B_1) are found by fitting the total energy obtained from well converged (with respect to any internal parameters) KSDFT calculations of the ground-state energy of the elemental crystal at 7 separate volumes, without any geometry optimization. The volumes in these calculations range from $0.94V_e$ to 1.06 V_e in steps of 0.02 V_e, where V_e is the equilibrium volume of the structure calculated using VASP. The fitting procedure is provided in the Δ-benchmark package. It is written in python and requires 7 sets of $(V, E(V))$ data, generated as I have described above. A pictorial representation of the fitting is shown in figure 7.3.

In conclusion, to calculate the overall Δ for a code each EOS must be found for all elements in the set. In our case this translates into 490 (7×70) calculations, typically the parameters, (V_0, B, B_1), for the reference code's EOS equations are given by the benchmark package (otherwise 980 calculations).

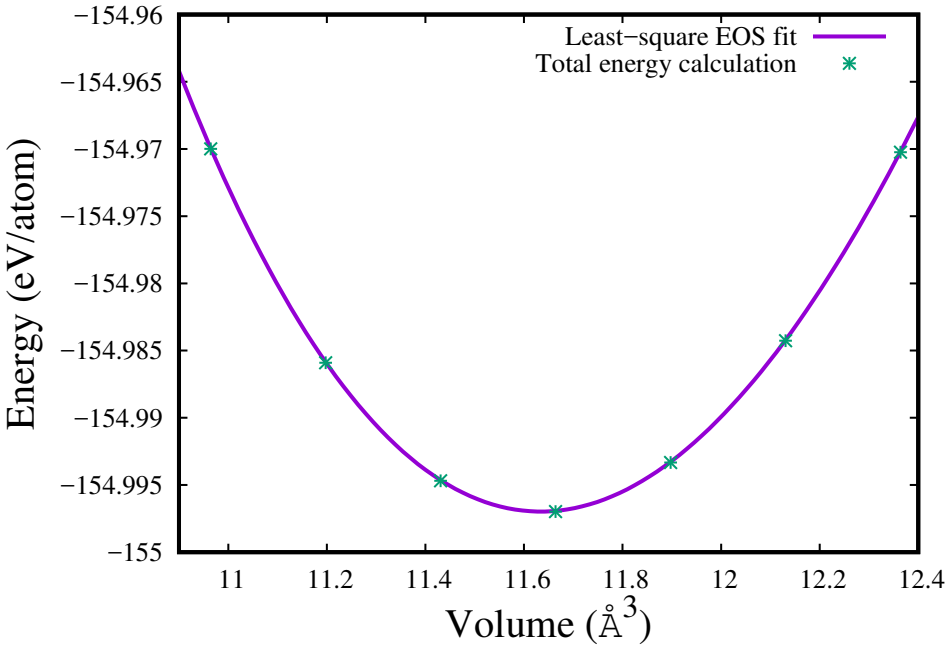

Figure 7.3: *A least-square fit of the Birch-Murnaghan EOS to seven different energies obtained from KSDFT calculations of the Carbon ground-state crystal structure with different volumes using* `AIMPRO`*. The resulting parameter set, which defines the EOS, is* $V_0 = 11.63396$ Å^3 *,* $B = 205.52326$ *GPa and* $B_1 = 3.544$*.*

7.2 Methodology

The structure and accepted equilibrium volume is provided in the Δ-benchmark website [1]. Note that this volume is only used to determine the specimen volumes at which E(V) is evaluated. Each code evaluates its V_0 by fitting to the Birch-Murnaghan EOS.

Due to the large number of calculations required to produce a Δ-value, we have completely automated the process to generate it using several scripts written in Perl and Bash. This automation includes the process of generating a basis set and subsequent file handling, setting and running the different `AIMPRO` calculations and collating all results to be used by the benchmark package. This not only removes any human error that could appear whilst handling the data files but it also streamlines the process of generating a Δ so that any change to either the implementation (`AIMPRO`), or the choice of pseudopotential and exchange-correlation, which could potential affect numerical errors can be easily assessed. The different stages involved in generating a Δ-value from a choice of pseudopotential performed in this thesis are shown in figure 7.4.

A suggested list of settings to run the calculations, such as the number of *k-points* and *temperature factor*, etc... are specified in the supplementary material of [6]. Our chosen settings will be discussed in the next few chapters.

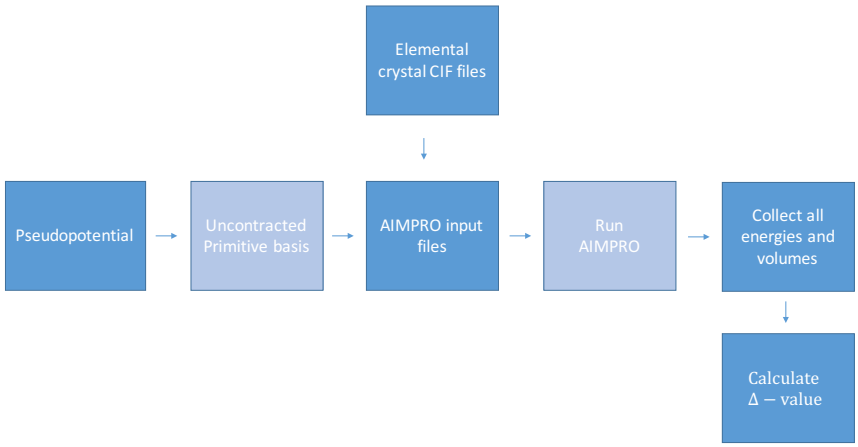

Figure 7.4: *A plot highlighting the different stages involved in generating a* Δ*-value using* `AIMPRO`*. Each arrow indicates a perl script. The lighter blue squares indicate stages where DFT calculations are run, here bash scripts are also used to manage the different calculations efficiently.*

7.3 Standard Δ-values

Before proceeding to present `AIMPRO`'s Δ-value we must first expand on what can be considered a "good" value of Δ. As a first step into establishing a typical value of Δ, Lejaeghere et al took high quality experimental measurements for the equations of state for Cu, Au and Ag [101, 102] and applied the r.m.s. formalism described above to find an average $\Delta_{\text{exp}} = 1$ meV/atom between the different experiments [3]. For the same set of elements the respective EOS were calculated using several all-electron codes [103, 104, 105, 106, 107, 108, 99], using the process described above. Doing this we find an average $\Delta_{\text{code}} = 0.8$ meV/atom among all the different all-electron codes [3]. It follows that for this particular set of elements the precision of all-electron codes outperformed that of the experiments.

A broader overview of the current precision for all-electron codes can be found using the 71 elements in the Δ-benchmark [3]. Generating the EOS equations for this set of elements using the different all-electron codes referenced above and calculating the Δ-values using all the permutations of code-to-be-evaulated and reference code, table 7.1, we find an average $\Delta_{\text{a.e.}}$=0.6 meV/atom, with the highest code-to-code Δ-value being elk's $\Delta_{\text{FPLO}} = 1$ meV/atom (or vice-versa). It was then asserted by Lejaeghere et all [3] - given that the benchmark call for an all-electron code to be used but not specifying which - that codes with a $\Delta \approx 1$ meV/atom, or even 2 meV/atom, produce almost identical EOS.

	elk	exciting	FHI-aims	Fleur	FPLO	RSPt	WIEN2k
elk		0.3	0.3	0.6	1.0	0.9	0.3
exciting	0.3		0.1	0.5	0.9	0.8	0.2
FHI-aims	0.3	0.1		0.5	0.9	0.8	0.2
FLEUR	0.6	0.5	0.5		0.8	0.6	0.4
FPLO	1.0	0.9	0.9	0.8		0.9	0.9
RSPt	0.9	0.8	0.8	0.6	0.9		0.8
WIEN2k	0.3	0.2	0.2	0.4	0.9	0.8	

Table 7.1: *Comparison between all electron codes, using the Δ formalism, which have their EOS parameters available in the Comparison website [1]. The Δ-values in this table have units of meV/atom. If two Δ-values are available for the same code, the parameters which yield the lowest Δ are used. Data taken from the supplementary materials available in [1], the details pertaining to the specific calculations can be found therein. Further information regarding this comparison can also be found in [3].*

7.4 Results

In this section the results obtained using the Δ-benchmark package as a method to assess the filtration methodology and our basis sets are presented and analysed.

7.4.1 Convergence of the energy with respect to basis-e_{cut}

In figure 7.5 the convergence of the total energy calculated (with `AIMPRO`) with respect to basis-e_{cut} for two elements (C and Y) (belonging to the set considered here) is shown. For these calculations the respective lattices were taken from the Δ-set and the VASP optimized volume was used. In this plot the y-axis corresponds to,

$$\delta(x) = E(x) - E(\text{highest}) \tag{7.7}$$

where $E(x)$ is the total energy per atom calculated with a particular basis-e_{cut}, which we label x, and E(highest) is the total energy per atom calculated with the highest basis-e_{cut} for which the calculation ran without instability. For C the E(highest) $= -155.02856$ eV/atom and basis-e_{cut} $= 400$ eV (which corresponds to 46 filtered functions out of 60 primitives) and for Y we have E(highest) $= -1042.7468$ eV/atom and basis-e_{cut} $= 200$ eV (which corresponds to 104 filtered functions out of 160 primitives).

Indeed from figure 7.5 we see that as basis-e_{cut} is increased (and corresponding number of filtered functions) the energy of the system converges. This is a marked difference from other GTO basis sets where convergence is not a straightforward property.

As highlighted in chapter 5, the primitive basis set considered here is very large which would make their usage in regular `AIMPRO` very inefficient, and most often, infeasible. Similarly at certain high values of basis-e_{cut} which are system dependent and most likely

correspond to a large number of filtered functions and/or high angular momentum the calculation for certain systems might fail. For the Δ-benchmark calculations presented over the next sections the highest basis-e_{cut} for which the calculation ran without instability is chosen. Given that we are trying to assess potential gains in accuracy using the filtration methodology this assignment corresponds to using the highest number of functions possible in the filtered set and thus our most accurate. This method leads to different basis-e_{cut} values over the set of elements considered, these are shown in figure 7.10.

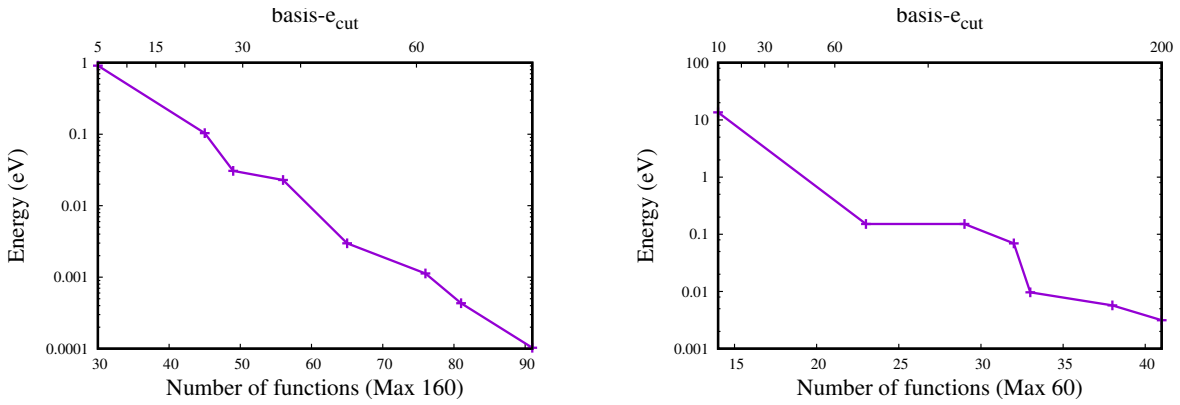

(a) Y **(b)** C

Figure 7.5: *Convergence with respect to basis-e_{cut} for the total energy (per atom) of the ground state elemental crystals for Y (a) and C (b) at the VASP equilibrium volume. The bottom axis indicates the number of filtered basis functions used whilst the top axis indicates its corresponding basis-e_{cut}. The y-axis contains the difference in energy with respect to the highest basis-e_{cut}. For Y the total number of functions in the underlying primitive basis set is 160, whilst for C it is 60. Filtration produces filtered basis sets with up to 160 and 60 functions for Y and C respectively (the size of the respective underlying primtive basis sets), where the basis-e_{cut} parameter controls the number of functions in the filtered set.*

7.4.2 `AIMPRO`'s standard Δ-value

Figure 7.10 contains the individual $\Delta^{i}_{\text{WIEN2k}}$ calculated using `AIMPRO` and the respective basis-e_{cut} (and corresponding number of filtered functions), for reasons which will be expanded upon in section 7.6 we include only 66 elements out of the 70 available in our overall Δ. The set of parameters which define the individual EOS calculated using `AIMPRO` are given in table 7.5. For the calculations which yielded these EOS curves (and respective Δ-values) the Brillouin zone is spanned using grids generated according Monkhorst-Pack [48]. The individual k-point meshes used for each elemental system considered here are shown in table 7.6. These k-point meshes are taken to produce converged

results (with respect to the number of k-points) according to the additional information in [1]. For purposes of stability each calculation uses a Fermi-Dirac smearing function with a temperature of 0.01 eV. The reasoning behind these choices will be detailed in the next section.

Averaging the different Δ^i_{WIEN2k} (figure 7.10) we obtain AIMPRO's overall $\Delta_{\text{WIEN2k}} = 2.245$ meV/atom. Initially, it would appear that this value is higher than the 1 meV/atom (or 2 meV/atom) discussed in the previous section and for some elements the individual Δ^i also appear to be high. However, recall that the calculations performed with AIMPRO use Krack pseudopotentials, which as discussed previously adds pseudization errors. Comparing our Δ-value with that of ABINIT, where the results are well converged, for the same group of elements (and respective pseudopotentials) we find that ABINIT $\Delta_{\text{WIEN2k}} = 2.112$ meV/atom, which is very close to ours. Furthermore comparing individual Δ^i_{WIEN2k} from both codes, figure 7.9, we find that for the most elements AIMPRO's Δ^i_{WIEN2k} curve follows that of ABINIT, particularly the region of high Δ^i_{WIEN2k}. Thus it is likely that great part of AIMPRO's Δ_{WIEN2k} is mostly due to the use of pseudopotentials. It is important to stress at this point, that ABINIT's Δ calculations were performed with an plane wave energy cut-off of 250 Ry, an atypically high value. So that the ABINIT points in figure 7.9 correspond to very accurate (and computationally expensive) plane wave calculations.

As we will see below the flexibility of the benchmark, however, allows us to properly assess the accuracy of our methodology as well.

7.4.3 Δ-value with respect to systematic basis sets

To understand the nature of our standard Δ-value (i.e. whether it is dominated by pseudization error, basis set error or something else entirely) we can approximately break down the intrinsic errors, considered by the Δ-benchmark, into constituent parts. Let us assume the following relation for AIMPRO's Δ-value (it would work similarly for any code, but for simplicity let us use AIMPRO),

$$\Delta_{\text{WIEN2k}} = f(\text{pp,bs,numerical}) \tag{7.8}$$

where pp is as the error associated with using a pseudopotential, bs is the error associated with basis sets (in our case GTOs) and the numerical term contains any numerical errors not associated with the previous two terms. If instead of an all-electron method we perform AIMPRO's Δ-test with respect to a KSDFT code with systematic convergence,

say ABINIT, using the same pseudopotentials, we can then rewrite equation 7.8 as,

$$\Delta_{ABINIT} = f(\text{numerical,bs}) \tag{7.9}$$

this is a reasonable assumption since specifying a pseudopotential and the exchange-correlation defines the KS Hamiltonian and we would expect two well-converged codes to yield similar results. Any error resulting from a pseudopotential would be related to how the pseudopotential is implemented and thus not *pseudization* error, it would instead be part of the *numerical* term. We must have the *pp* term be 0. Furthermore assuming that the plane wave calculations have been converged with respect to e_{cut} we can assume that most of the *bs* error is due to `AIMPRO`'s use of GTOs. Having homogeneity in the calculation settings between `AIMPRO`'s and that of the new reference code – such as k-point sampling method and grid, smearing function and temperature, etc... – ensures that the errors due to the *numerical* term are minimized (with respect to the reference code) for different calculation settings. *Numerical* errors can be further minimized by ensuring that other code specific calculation settings are set to very accurate values, doing so one could further approximate equation 7.9 as,

$$\Delta_{\text{ABINIT}} \approx f(\text{bs}) \tag{7.10}$$

where the Δ-value (calculated with the reference code described above) is now a good estimate of the error associated with the basis sets and filtration methodology, and by virtue of the comprehensive nature of the Δ-benchmark the best single assessment of our method.

It must be noted that assessing `AIMPRO`'s methodology error, as described here, can not be done by subtracting its standard Δ_{WIEN2k} from the standard ABINIT Δ_{WIEN2k} in the following manner,

$$\texttt{AIMPRO}\Delta_{\text{ABINIT}} \neq \texttt{AIMPRO}\Delta_{\text{WIEN2k}} - \text{ABINIT}\Delta_{\text{WIEN2k}} \tag{7.11}$$

given that the Δ-benchmark uses a r.m.s method to construct the individual Δ^i.

7.4.3.1 Drawback of using just the standard Δ-test

A potential hidden danger, particularly with regards to non-systematic type basis sets (for this discussion, GTOs) can arise if only the standard Δ-test is used as figure 7.6 illustrates.

Let us assume that we have found a particular EOS with a GTO which we label $E_{bs1}(V)$, in addition assume that we have calculated in a like-to-like calculation for the same structure, as described above, another EOS $E_{\text{bs2}}(V)$ using a well converged plane

wave code. Even if we find the standard $\mathrm{bs1}\Delta^i_{\mathrm{WIEN2k}} \approx \mathrm{bs2}\Delta^i_{\mathrm{WIEN2k}}$ this does not imply $E_{\mathrm{bs1}}(V) \approx E_{\mathrm{bs2}}(V)$ as figure 7.6 illustrates. Both areas (salmon and light blue) in 7.6 have a similar size which would be indicative of similar standard Δ^i however the predicted equilibrium volumes are different. Furthermore $\mathrm{bs1}\Delta^i_{\mathrm{bs2}}$, which as discussed above indicates the GTO error, is higher than their individual $\Delta^i_{\mathrm{WIEN2k}}$. Thus the standard Δ-test is in fact a misrepresentation of the true GTO error. Other constructions of hypothetical EOS can be performed which highlight the same scenario only now B_0 and B_1 are changed lead to the same conclusion. This ambiguity can lead to erroneous conclusions regarding the quality of a basis set if only the standard Δ-test is used. However this can be eliminated by a more exhaustive application of the Δ-formalism as we demonstrated in section 7.4.3.

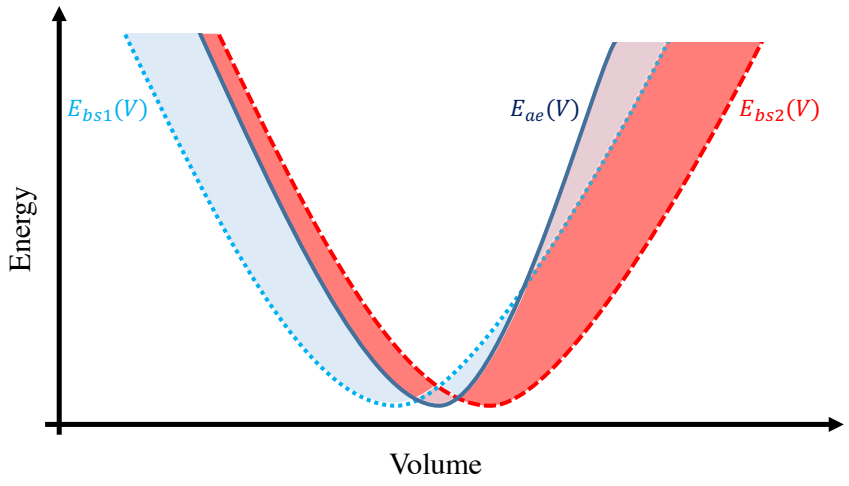

Figure 7.6: *Illustration of a possible pitfall to the uniformed usage of the Δ-benchmark. In this figure $E_{\mathrm{bs1}}(V)$ represents the EOS resulting from well converged calculations which uses pseudopotentials, E_{ae} is the EOS calculated by an all-electron code and let E_{bs2} be another EOS calculated by a different code using the same pseudopotential as E_{bs1}. Using the standard Δ test one finds that the blue area and the red area, and therefore the resulting Δ^i, are similar. However $E_{\mathrm{bs1}} \not\approx E_{\mathrm{bs2}}$.*

7.4.3.2 `AIMPRO` Δ_{ABINIT}

It follows from the two previous sections, that using well converged EOS obtained from ABINIT and performing the Δ-test with respect to them is a more accurate assessment of our methodology than just a standard all-electron comparison.

The reasoning for our choice of calculation settings in section 7.4.2 is now clear, we intended for the respective EOS to be used in a like-to-like comparison with ABINIT. The settings used by ABINIT can be found in the supplementary material available in [1], they are the same as the ones used with `AIMPRO`. We can then just use ABINIT's

published EOS parameters (available in [1]) to perform the analysis described in section 7.4.3. Doing so we find that AIMPRO $\Delta_{\text{ABINIT}} = 0.401$ meV/atom an excellent result. Furthermore the individual Δ^i_{ABINIT} are plotted in figure 7.11, which are, also, all excellent results (note the different scale on the vertical axes when compared with fig. 7.9). From these result it follows, according to the Δ-benchmark, that the filtration methodology implemented in AIMPRO generates results which are practically indistinguishable from similar well converged plane wave results, in a much shorter time scale.

7.5 Precision of the filtration methodology

Similar to the analysis presented above which lead to a measure of the precision of all-electron codes, we can perform a comparison using the Δ-benchmark between codes that use a chosen pseudopotential, in our case semicore Krack pseudopotential [39]. This sort of comparison should improve the accuracy of the approximation made in (7.10) i.e. that performing AIMPRPO's Δ with respect to a systematic basis set reference, gives a good indication of the basis set error.

As before we should expect $\Delta_{\text{code}} < 1$ meV/atom among the different codes, given that we are just making a code-to-code comparison. In this instance not all codes will necessarily have the same calculation settings. Using the results posted online [1], we can extract a set of 29 elements for which calculations were performed using the same Krack pseudopotentials for two different codes ABINIT and BigDFT. BigDFT [24] uses wavelets and, like ABINIT, offers systematic convergence with respect to basis sets. Its standard Δ-test is calculated using a mixture of Krack pseudopotentials (29 elements) and in-house developed pseudopotentials. However for the purposes of our discussion we are only interested in results using Krack pseudopotentials.

Table 7.2 contains the Δ_{code} for AIMPRO, ABINIT and BigDFT calculated with respect to each other. We find, as we expected, that all Δ_{code} are less than 1 meV/atom. Therefore, according to the standards set by Lejeghaere [3] indicates practically indistinguishable EOS and we find, as before, that very accurate AIMPRO calculations using filtration (performed with the highest basis-e_{cut} permissable) have an accuracy comparable to that of systematic basis sets.

7.5.1 Analysis of individual Δ^i

Plotting the elemental Δ^i_{code}, figure 7.7, obtained from the calculations involved in constructing table 7.2, we can observe one of the drawbacks, highlighted in section 7.4.3, of the standard Δ test. The elements Ti, V, Fe and Co all present an unusual high BigDFT Δ^i_{code} with respect to both ABINIT and AIMPRO. Note that for most of the other

	BigDFT	AIMPRO	ABINIT
BigDFT		0.878	0.689
AIMPRO	0.878		0.260
ABINIT	0.689	0.260	

Table 7.2: *Comparison between ABINIT, AIMPRO and BigDFT, using the Δ formalism, for a set of elements that use the same Krack pseudopotentials. The values show in this table have units of eV/atom. For ABINIT and BigDFT their EOS parameters are available in the comparison website [1]. The details pertaining to each calculation can be found in the supplementary materials in [1].*

elements the individual Δ^i_{code} are almost always within 1 meV/atom of each other. The discrepancy for those 4 elements most likely indicates a problem with the calculation for these particular elements with BigDFT. Indeed, consulting the supplementary materials regarding BigDFT Δ-value calculation (available in [1]) we find that the temperature used in their calculation differs from ABINIT (and by construction AIMPRO). In addition for some elements, Fe and Co in particular, the k-point grid used was smaller than that of the corresponding calculations with AIMPRO and ABINIT. These discrepancies indicate a need for ensuring that all the calculations submitted to the comparison website are converged with respect to any code parameters, and ideally should use similar k-point meshes or smearing functions. Similarly a precision test such as the one performed above should be done and individual Δ^i checked to ensure that there are no underlying apparent sources of *numerical* errors which could be corrected by a more exhaustive application of the formalism. Although calculation settings are suggested in the original paper [6] I believe, as the analysis above shows, that this is not enforced strictly. However, the reasons for this particularly discrepancy are not fundamentally important for this discussion as opposed to the resulting conclusions.

The pertinent point regarding figure 7.7 with respect to the standard Δ-test becomes apparent when one observes the Δ^i_{WIEN2k} for these particular elements. In table 7.3 the standard Δ^i_{WIEN2k} obtained, for all the elements with high Δ^i_{code} in figure 7.7 are shown.

Let us take Cobalt (Co) as an example, from the application of the standard Δ-test

	BigDFT	ABINIT	AIMPRO
Ti	2.595	0.590	0.662
V	3.956	0.892	0.955
Fe	2.666	5.148	6.017
Co	2.689	2.682	2.849

Table 7.3: *Standard Δ^i_{WIEN2k} (meV/atom) for the elements with the highest error in figure 7.7.*

(comparison with all-electron codes) one could deduce that BigDFT $\Delta^{\text{Co}}_{\text{WIEN2k}}$ is compa-

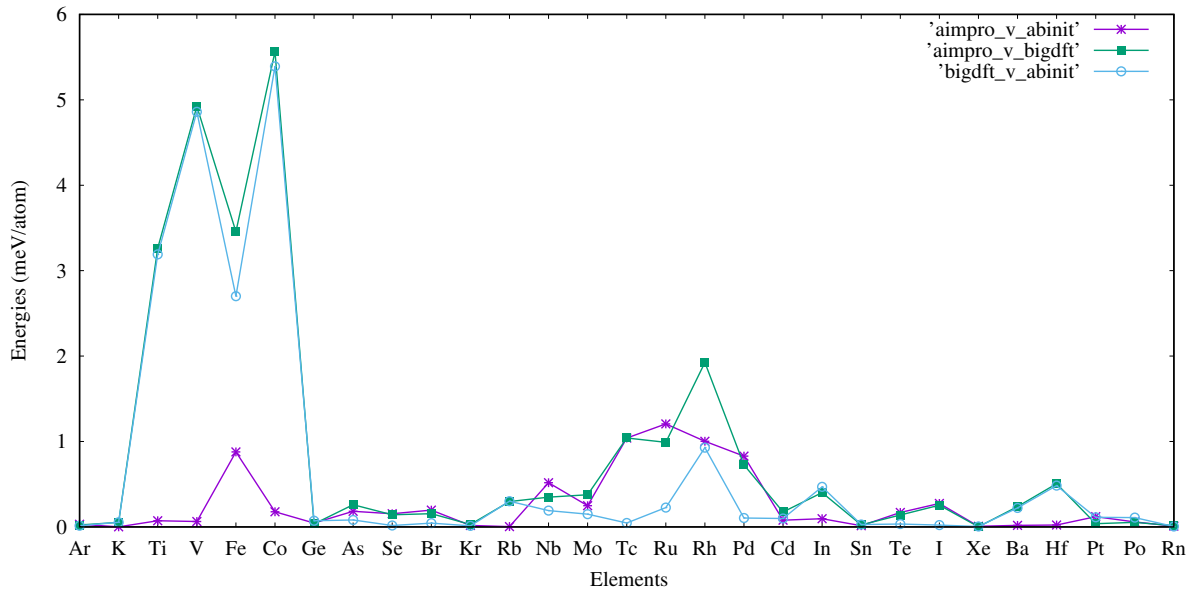

Figure 7.7: *Individual $\Delta^i WIEN2k$ for a set of 30 elements calculated by* `AIMPRO`*, ABINIT and BigDFT using Krack pseudopotentials. The individual EOS parameters for ABINIT and BigDFT can be found in [1].*

rable to that of ABINIT (or `AIMPRO`), table 7.3, and thus conclude that as far as the benchmark is concerned, whatever parameters or basis sets one used for Co are justified. However performing the Δ-test with respect to another code which uses the same pseudopotential and provides very accurate results, table 7.4, disagrees with that assessment. As discussed in section 7.4.3 the Δ^i_{code} obtained by comparing like-to-like calculation should provide a more accurate assessment of calculations involving pseudopotentials, such as the present Cobalt one, unlike the all-electron comparison. Indeed comparing the values shown in red (which involve a BigDFT calculation) and those shown in green (involve only ABINIT and/or `AIMPRO`) in both tables 7.3 and 7.4, we see evidence of the problems highlighted in section 7.4.3.1. That is, BigDFT $\Delta^{\text{Co}}_{\text{code}}$ calculated with respect to both `AIMPRO` and ABINIT (red values in table 7.4) are much higher than `AIMPRO` $\Delta^{\text{Co}}_{\text{ABINIT}}$ (green value in table 7.4), however we have from table 7.7,

$$\texttt{AIMPRO}\Delta^{\text{Co}}_{\text{WIEN2k}} \approx \text{ABINIT}\Delta^{\text{Co}}_{\text{WIEN2k}} \approx \text{BigDFT}\Delta^{\text{Co}}_{\text{WIEN2k}} \tag{7.12}$$

which is ambiguous. This becomes even more apparent when we plot Cobalt's EOS calculated with the different codes, fig. 7.8.

	BigDFT w.r.t. ABINIT	BigDFT w.r.t. AIMPRO	AIMPRO w.r.t. ABINIT
Co	5.392	5.565	0.177

Table 7.4: *Calculated Δ^i_{code} for Cobalt comparing codes which use Krack pseudopotential.*

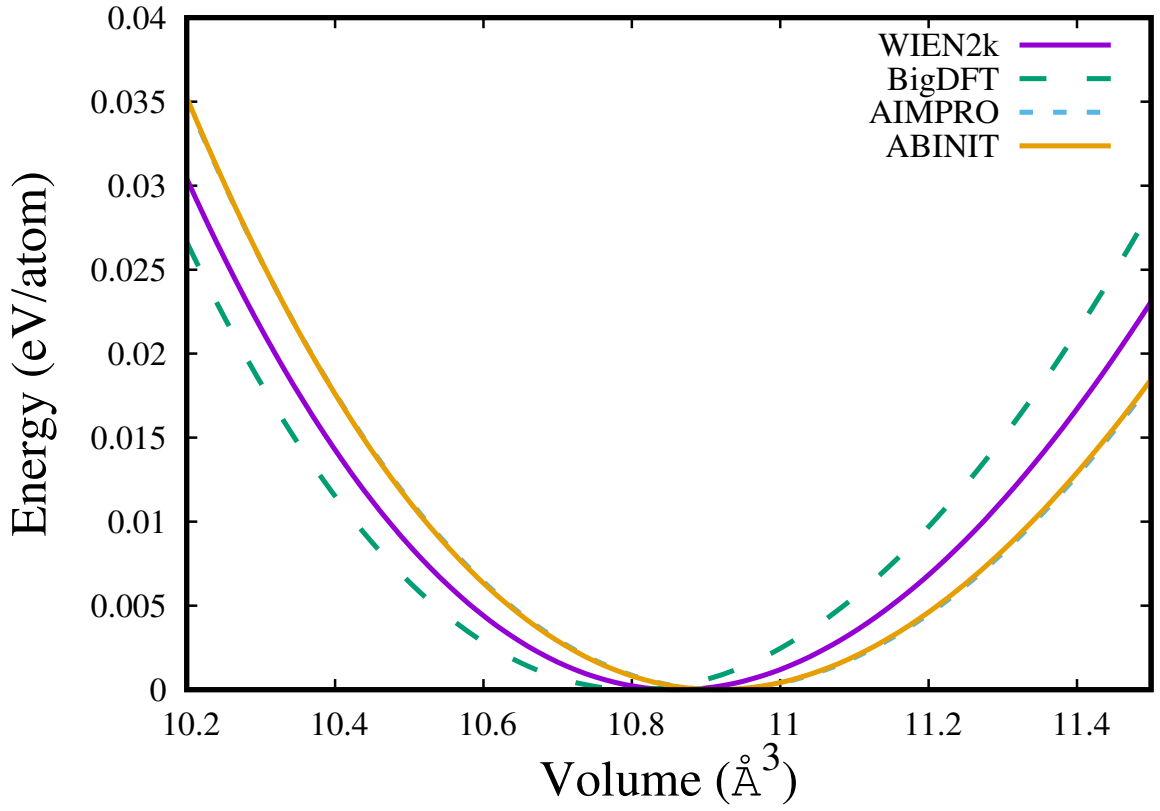

Figure 7.8: *Cobalt EOS calculated with WIEN2k, BigDFT, ABINIT and* `AIMPRO`*. For the calculations performed using the last 3 codes referenced above, the same pseudopotentials were used. Each Birch-Murnaghan has been modified such that the minimum energy is set to zero.*

In figure 7.8 we see that, for Co, both `AIMPRO` and ABINIT yield similar EOS thus we would be justified in presenting and drawing any conclusions from their respective standard Δ^i. Whilst the EOS calculated by BigDFT differs from both however, fortuitously, it predicts just enough of an erroneous volume as to yield an acceptable standard Δ^i.

When one considers BigDFT, or any code with systematic convergence, the disparity between the standard Δ-test and that of a like-to-like comparison most likely indicates an unconverged calculation or different calculation settings, which does not point to any particular fault within the code, but nevertheless confusing and unnecessary. If instead we were using GTOs such disparities could be caused by a bad basis set and — if we are not careful with the application of the Δ-formalism — lead us to accept an otherwise unacceptable basis set. It is in such cases, like ours, were a Δ-value calculated with respect to a well converged like-to-like calculation becomes imperative, or more so several such comparisons like in the precision test above.

This analysis lends further credence to our assessment regarding filtration high accuracy. Not only have we demonstrated that `AIMPRO`'s (using filtration and our basis set) standard Δ-value is close to that of ABINIT's and dominated mostly by pseudopotential

error, but in addition comparison between AIMPRO and different systematic implementations yield almost indistinguishable results.

7.6 Elements which required variation in the filtration parameters

The work presented thus far used the same internal settings which control the filtration step, such as the temperature which controls the fictitious Fermi-Dirac function. It is remarkable that so much of the periodic table – in our case 66 elements out of the original 70 for which there are pseudopotentials – yielded good Δ^i values with the only varying parameter, with regards to filtration, being basis e_{cut}. However out of the 70 elements for which we generated a basis set the heavy atoms Ir, Tl, Pb and Hg incurred some instabilities which resulted in failures in the filtration calculation. The primary reason for this stems from the process of choosing the correct Fermi energy for the Fermi-Dirac filtration function. Particularly for heavier atoms where the "$l + 1$" policy leads to the inclusion of functions with an angular momentum value of g. Such functions might not be present at the atomic level with a low Fermi level energy Fermi-Dirac function. This leads to instabilities if one tries to generate a filtered (contracted) function with "g" angular momentum, given their absence from the available functions to filter from. See section 6.3.3.1 and figure 6.2.

Indeed manually tweaking the Fermi energy upwards, i.e.increasing μ (section 6.3.3.1), removes this class of problems. For example, considering Hg and increasing the Fermi level energy we obtain, with basis-e_{cut}=50 eV, a $\Delta^{Hg}_{\text{ABINIT}} = 0.936$ meV/atom. Before, the calculation ran with instabilities only for a basis-$e_{cut} < 10.0$ eV.

In addition to the type of instabilities referenced above, for some elements with low first exponent (i.e. α) the filtered basis KSDFT calculation can fail due to ill conditioned matrices (discussed in chapter 5 but with respect to primitive basis). As before, this type of instability manifests itself more often on heavier atoms where g angular momentum functions might be used (potentially adding instability on top of that which arises out of the correct setting of the Fermi energy value). For instance Ir has $\alpha \approx 0.050$, Pb has $\alpha \approx 0.046$ and Tl has $\alpha \approx 0.033$. Calculations for the aforementioned elements failed even for small basis-e_{cut}. A potential solution will be discussed in the future works, however we have found that this class of problems can be overcome with a careful choice of trial functions. Typically increasing the α used to generate the trial functions to a value higher than that present in the primitive set whilst at the same time increasing the Fermi energy, to account for the type of instability discussed above, removes this type of problem. Following this we Increased Ir's α to 0.13, Pb's α to 0.38 and Tl's

α to 0.390 (for functions in the trial basis with"f" and "g" angular momentum). In addition the Fermi energy was manually increased. The calculations performed with these settings yielded $\Delta^{Ir}_{\text{ABINIT}} = 0.123$ meV/atom, $\Delta^{Pb}_{\text{ABINIT}} = 0.047$ meV/atom and $\Delta^{Tl}_{\text{ABINIT}} = 0.594$ meV/atom, all excellent values.

Due to our, self-imposed, requirement for a systematic setting of filtration parameters we decided to discuss these 4 elements (Hg, Pb, Ir and Tl) separately and provide both a discussion on the difficulties encountered with filtration and potential solutions. More on this will be discussed in the future work section. On a side note it is important to note that the Δ^i benchmark package does not call for all the elements to be included in the overall Δ-value calculation and some codes miss out some elements for undisclosed reasons. In this work we have presented filtration Δ^i values for all possible elements, 66 of which had systematic filtration settings (basis-e_{cut} will undoubtedly change depending on the type element and system.) and 4 of which required a small manual shift of parameters.

Having discussed some failures due to instability we can address Cl, an element for which our calculations were stable but we have a $\Delta^{Cl}_{ABINIT} = 2.7$ meV/atom. This value, although acceptable according to [3], is an outlier when compared with other elemental Δ^i.This value is well converged with a basis-$e_{cut} = 400$ eV and thus it does not suffer from the instabilities described in the previous paragraphs, however it is indirectly related to it. Using an uncontracted basis set, constructed as described in the previous chapter but with an angular momentum value two above the highest filled orbital in the atom we obtain a $\Delta^{Cl}_{ABINIT} = 0.536$ meV/atom with a basis-e_{cut} of 100 eV, an excellent result this time. Similarly for other atoms the uncontracted basis set could be constructed with an angular momentum that is two above its highest filled atomic orbital and we would expect smaller Δ^i, however in practice more elements would develop instabilities due to the difficulty in choosing the respective Fermi energy level (discussed above) arising from the inclusion of even higher lying angular momentum functions. In addition such inclusion would lead to an heavier computational load arising in the filtration step. A more thorough discussion on this will also be included in the future work section.

7.7 Conclusion

It has been demonstrated elsewhere [5, 16] that filtration can considerably speed up localised basis sets calculations. However, an added benefit of contracting the basis set *in situ* and *in vivo* is the possibility of using large uncontracted primitive basis sets and attain plane wave accuracy in a systematic manner using GTOs. It was demonstrated in this chapter, using a modern state-of-the-art benchmark package, that for a wide range of elements with different structures we were able to produce results which are practically indistinguishable from like-to-like calculations using a plane wave implementation ABINIT.

Doing so we found that AIMPRO's $\Delta_{\mathrm{ABINIT}} = 0.401$ meV/atom, an excellent result which indicates that AIMPRO's calculation were practically identical to the respective plane waves ones. Furthermore, it is important to note that ABINIT's results were calculated with an e_{cut} of 250 Ry, which is an uncommon large value considering typical calculations. In addition performing AIMPRO's Δ test with respect to like-to-like plane wave calculations revealed that most of our standard $\Delta_{\mathrm{WIEN2k}} = 2.245$ meV/atom resulted from the use of pseudopotentials.

A further and more exhaustive precision test where we compared Δ^i for a smaller subset of elements among three different codes (AIMPRO being one of them) which all used the same pseudopotentials lead to similar conclusions regarding the accuracy of filtration. This result also strengthened our assumption that performing the Δ-test with respect to systematic basis sets was a good assessment of our primitive basis sets and filtration.

In conclusion the filtration methodology coupled with the large uncontracted primitive basis set presented in this thesis has indeed allowed us to perform very accurate calculations using GTO's. Such basis sets are too large to be considered in regular AIMPRO calculations. This has enabled calculations to be converged across the whole periodic table, the first time this has been achieved with AIMPRO.

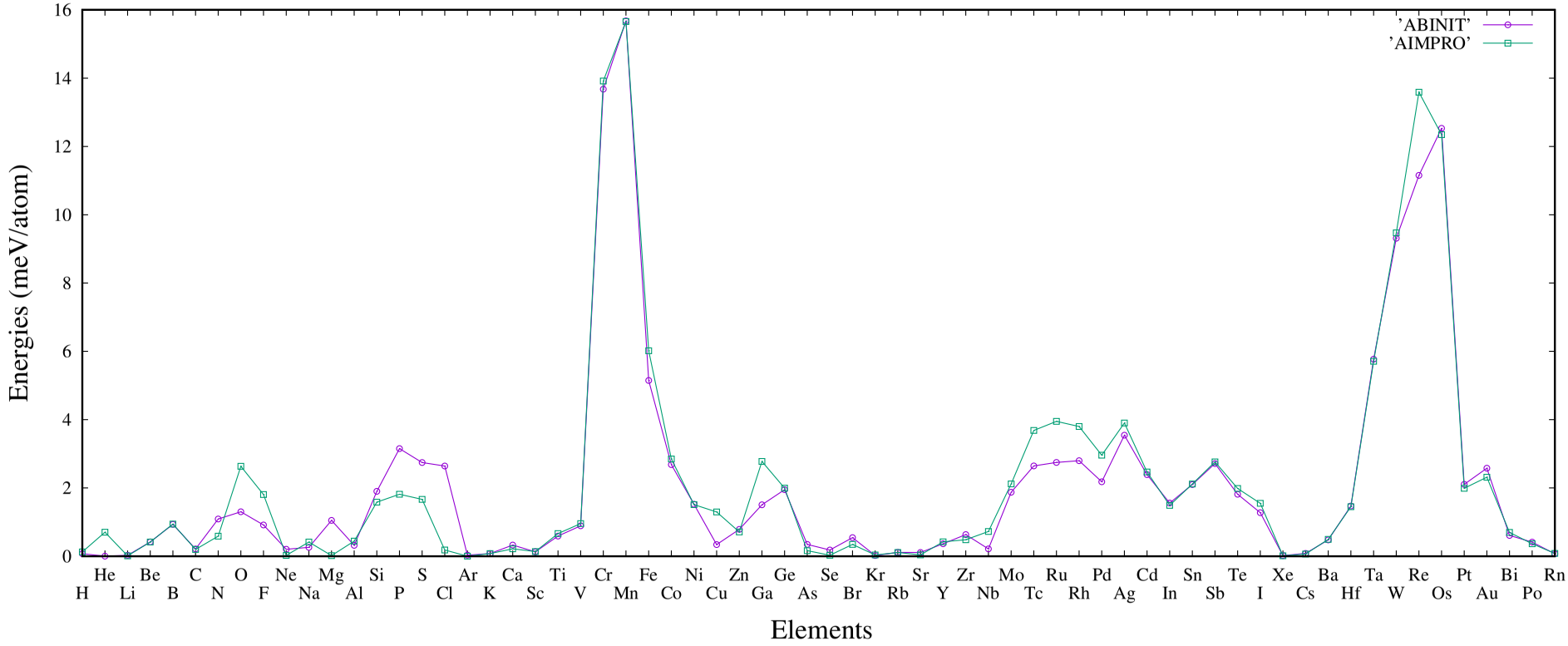

Figure 7.9: *Plot of individual* $\Delta^{i}_{\mathrm{WIEN2k}}$ *calculated with ABINIT and* `AIMPRO` *for the 66 elements which have a Krack pseudopotential, semi-core if available. The parameters which specify the different EOS calculated by ABINIT can be found in [1].*

H																	He
0.125																	0.703
400																	400
Li	Be											B	C	N	O	F	Ne
0.012	0.417											0.943	0.199	0.588	2.633	1.807	0.024
200	400											200	400	400	400	400	400
Na	Mg											Al	Si	P	S	Cl	Ar
0.415	0.019											0.443	1.584	1.814	1.666	0.183	0.002
20	40											100	100	400	400	400	400
K	Ca	Sc	Ti	V	Cr	Mn	Fe	Co	Ni	Cu	Zn	Ga	Ge	As	Se	Br	Kr
0.078	0.217	0.136	0.662	0.955	13.917	15.659	6.017	2.849	1.512	1.296	0.712	2.776	1.995	0.164	0.03	0.347	0.038
60	60	100	60	60	40	60	40	40	40	20	20	10	100	100	200	400	400
Rb	Sr	Y	Zr	Nb	Mo	Tc	Ru	Rh	Pd	Ag	Cd	In	Sn	Sb	Te	I	Xe
0.111	0.04	0.422	0.483	0.724	2.118	3.685	3.949	3.798	2.96	3.901	2.468	1.491	2.115	2.763	1.985	1.548	0.014
100	200	200	100	60	60	60	60	20	15	20	100	10	200	200	400	400	400
Cs	Ba		Hf	Ta	W	Re	Os		Pt	Au				Bi	Po		Rn
0.065	0.495		1.45	5.707	9.471	13.589	12.345		1.989	2.315				0.698	0.366		0.082
400	100		100	60	30	20	30		30	30				60	60		400

Figure 7.10: *The standard Δ^i obtained from calculating the EOS for the different elemental crystal using AIMPRO and applying the Δ formalism. As before the grey background indicates elements which required a spin-polarized calculation. The first number in each element box corresponds to Δ^i in (meV/atom), whilst the second entry is the respective basis-e_{cut} used.*

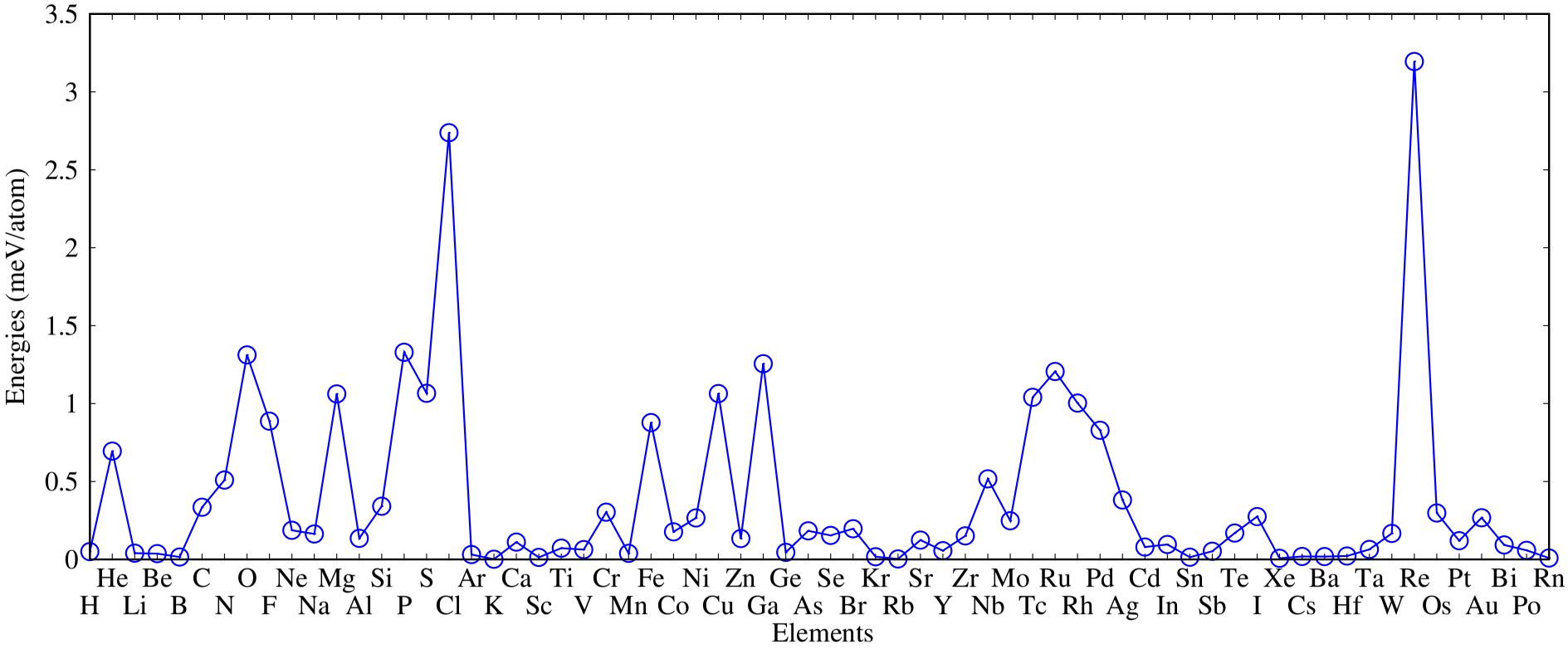

Figure 7.11: *Individual AIMPRO Δ^{i}_{ABINIT} for 66 elements which have a Krack pseudopotential, semi-core if available. The parameters which specify the different EOS calculated by ABINIT can be found in [1].*

H																	He
0.050																	0.695
400																	400
Li	Be											B	C	N	O	F	Ne
0.040	0.417											0.015	0.335	0.509	1.312	0.887	0.187
200	400											200	400	400	400	400	400
Na	Mg											Al	Si	P	S	Cl	Ar
0.163	1.062											0.031	0.341	1.329	1.066	2.738	0.031
20	40											100	100	400	400	400	400
K	Ca	Sc	Ti	V	Cr	Mn	Fe	Co	Ni	Cu	Zn	Ga	Ge	As	Se	Br	Kr
0.001	0.111	0.013	0.072	0.063	0.303	0.039	0.878	0.177	0.266	1.064	0.134	1.256	0.045	0.183	0.154	0.197	0.017
60	60	100	60	60	40	60	40	40	40	20	20	10	100	100	200	400	400
Rb	Sr	Y	Zr	Nb	Mo	Tc	Ru	Rh	Pd	Ag	Cd	In	Sn	Sb	Te	I	Xe
0.003	0.124	0.056	0.151	0.517	0.248	1.040	1.206	1.003	0.829	0.381	0.079	0.096	0.014	0.052	0.169	0.275	0.007
100	200	200	100	60	60	60	60	20	15	20	100	10	200	200	400	400	400
Cs	Ba		Hf	Ta	W	Re	Os		Pt	Au				Bi	Po		Rn
0.019	0.018		0.022	0.064	0.167	3.159	0.298		0.120	0.267				0.093	0.058		0.009
400	100		100	60	30	20	30		30	30				60	60		400

Figure 7.12: *AIMPRO individual Δ^i_{ABINIT} obtained as described in section 7.4.3. The first number in each element box corresponds to Δ^i in (meV/atom), whilst the second entry is the respective basis-e_{cut} used.*

El.	V_0	B_0	B_1
H	17.445	10.237	2.691
He	15.109	1.634	6.403
Li	20.223	13.860	3.305
B	7.223	234.338	3.421
Be	7.894	122.023	3.381
C	11.640	206.753	3.556
N	28.838	53.296	3.681
F	19.412	33.484	4.012
O	18.798	50.267	3.899
Na	37.724	7.413	3.862
P	21.350	68.097	4.224
Cl	38.927	18.441	4.379
S	17.094	83.081	4.069
Mg	22.936	36.089	4.044
Al	16.453	78.133	4.635
Si	20.367	87.018	5.099
Ar	52.371	0.742	7.327
K	73.599	3.595	3.817
Ca	42.249	17.466	3.416
Sc	24.631	54.474	3.450
Ti	17.417	111.704	3.624
V	13.475	182.452	3.956
Cr	12.185	133.928	7.219
Mn	12.004	119.266	6.187
Fe	11.486	172.527	8.036

El.	V_0	B_0	B_1
Co	10.919	211.086	5.009
Ni	10.921	198.719	5.252
Cu	11.993	141.520	4.840
Zn	15.224	75.702	5.164
Ga	20.574	47.432	5.115
Ge	24.075	57.603	4.762
As	22.578	68.588	4.211
Se	29.741	47.153	4.443
Kr	65.985	0.645	7.293
Br	39.376	22.507	4.851
Rb	91.054	2.796	3.756
Sr	54.510	11.326	4.704
Y	32.890	41.150	3.109
Sb	31.981	50.130	4.525
Nb	18.154	166.057	3.426
Te	35.179	44.717	4.724
Mo	15.823	259.633	4.456
Tc	14.493	300.755	4.405
Ru	13.821	312.033	4.778
Rh	14.108	256.700	5.225
Pd	15.392	165.945	5.566
Ag	18.043	89.099	5.765
Cd	22.878	44.639	6.868
In	27.650	36.230	5.331
Sn	37.096	34.135	4.720

El.	V_0	B_0	B_1
I	50.615	18.491	5.045
Xe	86.768	0.549	7.099
Cs	116.884	1.957	3.376
Ba	63.435	8.732	2.265
Hf	22.471	107.036	3.367
Zr	23.361	93.878	3.270
Ta	18.152	193.322	3.625
W	15.996	303.039	4.205
Re	14.791	345.449	3.692
Os	14.140	400.023	4.597
Ne	24.352	1.196	8.414
Pt	15.605	253.789	5.501
Au	17.897	143.327	6.001
Bi	36.982	42.602	4.554
Po	37.622	45.695	4.947
Rn	93.431	0.531	7.222

Table 7.5: *The parameters which define the EOS for the 66 ground state crystals which are used in our Δ test. V_0 is the equilibrium volume per atom (Å^3/atom), B_0 the bulk module (GPa) and B_1 the derivative of the bulk modulus.*

El.	kpts
H	$28 \times 28 \times 20$
He	$40 \times 40 \times 22$
Li	$38 \times 38 \times 38$
Be	$52 \times 52 \times 28$
B	$26 \times 26 \times 24$
C	$48 \times 48 \times 12$
N	$16 \times 16 \times 16$
F	$16 \times 28 \times 14$
O	$26 \times 24 \times 24$
Na	$22 \times 22 \times 22$
P	$30 \times 8 \times 22$
Cl	$12 \times 24 \times 12$
S	$38 \times 38 \times 38$
Mg	$36 \times 36 \times 20$
Al	$24 \times 24 \times 24$
Si	$32 \times 32 \times 32$
Ar	$16 \times 16 \times 16$
K	$20 \times 20 \times 20$
Ca	$18 \times 18 \times 18$
Sc	$34 \times 34 \times 20$
Ti	$40 \times 40 \times 22$
V	$34 \times 34 \times 34$
Cr	$36 \times 36 \times 36$
Mn	$28 \times 28 \times 28$
Fe	$36 \times 36 \times 36$

El.	kpts
Co	$46 \times 46 \times 24$
Ni	$28 \times 28 \times 28$
Cu	$28 \times 28 \times 28$
Zn	$44 \times 44 \times 20$
Ga	$22 \times 12 \times 22$
Ge	$30 \times 30 \times 30$
As	$30 \times 30 \times 10$
Se	$26 \times 26 \times 20$
Kr	$16 \times 16 \times 16$
Br	$12 \times 24 \times 12$
Rb	$18 \times 18 \times 18$
Sr	$16 \times 16 \times 16$
Y	$32 \times 32 \times 18$
Sb	$26 \times 26 \times 8$
Nb	$30 \times 30 \times 30$
Te	$26 \times 26 \times 16$
Mo	$32 \times 32 \times 32$
Tc	$42 \times 42 \times 22$
Ru	$42 \times 42 \times 24$
Rh	$26 \times 26 \times 26$
Pd	$26 \times 26 \times 26$
Ag	$24 \times 24 \times 24$
Cd	$38 \times 38 \times 18$
In	$30 \times 30 \times 20$
Sn	$26 \times 26 \times 26$

El.	kpts
I	$12 \times 22 \times 10$
Xe	$14 \times 14 \times 14$
Cs	$16 \times 16 \times 16$
Ba	$20 \times 20 \times 20$
Hf	$36 \times 36 \times 20$
Zr	$36 \times 36 \times 20$
Ta	$30 \times 30 \times 30$
W	$32 \times 32 \times 32$
Re	$42 \times 42 \times 22$
Os	$42 \times 42 \times 24$
Ne	$22 \times 22 \times 22$
Pt	$26 \times 26 \times 26$
Au	$24 \times 24 \times 24$
Bi	$26 \times 26 \times 8$
Po	$30 \times 30 \times 30$
Rn	$14 \times 14 \times 14$

Table 7.6: *The k-point mesh used to span the Brillouin zone for the individual Δ^i calculations.*

Chapter 8

Defect formation energy

The study of defects such as vacancies using DFT is greatly improved by methods, such as filtration, which can perform calculations more efficiently than regular DFT implementations, given that accurate calculations might require the use of very large simulation cells to remove spurious defect-defect interactions [109, 110, 111]. In addition for comparisons with experiments the results should be converged with respect to system size [110] which adds yet more overhead to what is already a highly demanding calculation.

It is clear then that very accurate and fast KSDFT implementations, such as filtration, can be a tremendous tool to study defects. Having established filtration as an accurate method in the previous chapter here we demonstrate that the somewhat artificial definition of the Δ-value comes across into real world application by calculating the ideal vacancy formation energy for some elements and comparing it to well converged plane wave results.

8.1 Constructing supercells

As detailed before in this thesis, periodic boundary conditions are well suited to represent a crystal. However, the introduction of defects in a calculation which uses periodic boundary conditions results in a periodic repetition of defects. This can result in unwanted defect-defect interactions which could lead to some error in the prediction of isolated defect formation energies when compared with experiment [112, 110]. Such errors can be minimized by constructing a supercell where the unit lattice of the system (without defect) is repeated periodically to construct a much larger cell (supercell) and then the defect is then introduced in this supercell, as figure 8.1 shows. The reasoning for this being that after a certain size of supercell is reached, the defects will be spaced so far apart that the defect-defect interaction will be negligible.

When a comparison with respect to experimental values is to be performed the va-

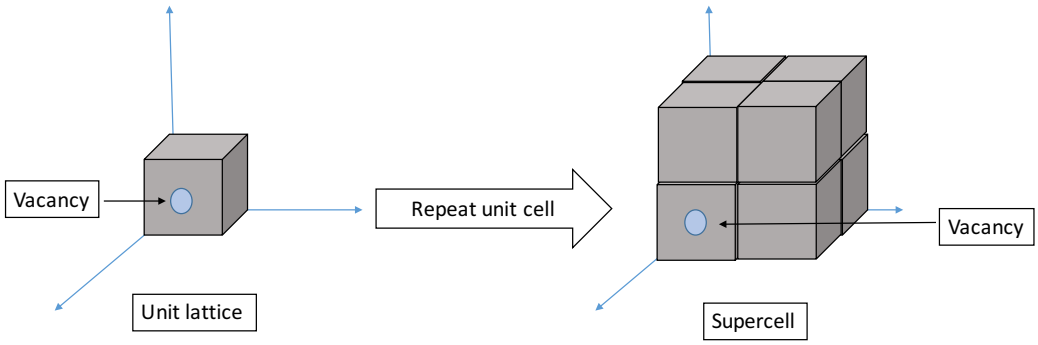

Figure 8.1: *To create a supercell the unit cell is appended multiple times in the the x,y and z directions to form a supercell. The defect is then introduced in one of the unit cells. Constructing increasing larger supercells will eventually minimize defect-defect interactions to an acceptable level.*

cancy calculation should then be converged with respect to the size of the supercell, which is typically expressed by the number of atoms within it [113]. For instance, to calculate the vacancy formation energies in Aluminum one particular study performed calculations using supercells with up to 1372 atoms [112] to ensure convergence with respect to lattice size. Similar calculations in a different study used supercells with the number of Aluminium atoms in the range of 1000 - 10,000 [114]. In another study where the vacancy formation energy of Silicon was investigated, supercells with up to 1000 atoms were considered [111]. In this study, however, we are only concerned with accuracy, that is a theory vs theory comparison, and so a much smaller supercell can be used. There is no need to minimize defect-defect interaction as we are not comparing with experiment.

8.2 Ideal vacancy calculations

In this work we will only consider vacancy formation energy (E_{v}), i.e. the energy required to remove one atom from a supercell. This can be defined as [110],

$$E_{\mathrm{v}} = E_{\mathrm{N}-1} - \left(\frac{N-1}{N}\right) E_{\mathrm{N}} \tag{8.1}$$

where E_{N} is the total energy of the N atom supercell (without vacancy) and $E_{\mathrm{N}-1}$ is the energy of the $N-1$ atom supercell with the vacancy, that is the supercell where an atom has been removed at any of the nuclear positions.

For a comparison with experiment the total energy of the supercell with the vacancy, $E_{\mathrm{N}-1}$, should be calculated with relaxed atomic positions. However for the purposes of theory to theory comparison we may perform the calculation without relaxing the atomic positions in the vacancy supercell, if this is the case the energy obtained using equation 8.1 but without relaxing the atomic positions in the vacancy supercell is sometimes referred to as *unrelaxed* or ideal vacancy formation energy [110]. In this chapter we will compare like-to-like ideal vacancy formation energy calculations for C, Ge and Al using `AIMPRO` with filtration against well converged ABINIT results. However, the ability to produce very accurate relaxed structures with filtration has been previously demonstrated [5].

For the calculations presented here it is enough to sample the Brillouin zone using only Γ-point for C and Ge, however for Al we will be using a $10 \times 10 \times 10$ k-point grid for reasons which will be explained in section 8.2.3. As before in this thesis the calculations were performed using the filtration methodology with PBE [41], Krack pseudopotentials [39] and using the uncontracted basis sets introduced in Chapter 5. No manual adjustment was made to any of the filtration parameters for the calculations in this chapter.

8.2.1 Equilibrium lattice constant calculations

Before constructing the different supercells we calculated the lattice constants of the respective unit cells using ABINIT, which we will report in this section. The conventional lattice for both C and Ge is simple cubic with 8 atoms, whilst Al conventional lattice is simple cubic with 4 atoms. For these calculations the k-point mesh and plane wave e_{cut} which resulted in well converged results (less than 1 meV/atom) are shown in table 8.1.

	C	Ge	Al
e_{cut}	80	60	100
k-point	$6 \times 6 \times 6$	$6 \times 6 \times 6$	$26 \times 26 \times 26$

Table 8.1: *The k-point mesh size and respective e_{cut} (Ha) which resulted in well converged calculations and were subsequently used to find the equilibrium lattice constant.*

We found the lattice constants by fitting an EOS (Birch-Murhagan) to energies calculated at different volumes ($E(V)$) using the settings found in table 8.1, similar to what is done in the Δ-benchmark. The calculated lattice constants are shown in table 8.2.

	C	Ge	Al
This work	3.573	5.775	4.039
PBE	3.575	5.769	4.019
Experimental	3.544	5.639	4.019

Table 8.2: *Equilibrium lattice constants a_0 (Å) for C (diamond), Ge(diamond) and Al (fcc) unit cells. The PBE (theory) and experimental values were taken from [4].*

The lattice constants generated with ABINIT using Krack pseudopotentials [39] and PBE [41] differs only slightly from previous PBE calculations [4]. Regardless, given that we will be comparing like-to-like ideal vacancy formation energy calculations, such small differences will not affect the overall comparison and resulting discussion.

8.2.2 C and Ge un-relaxed ideal vacancy energy

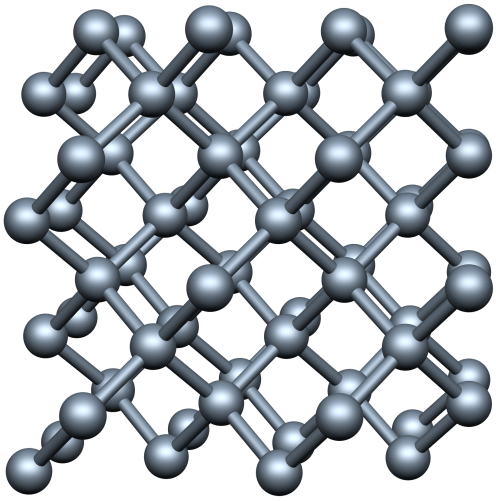

Figure 8.2: *A 64 atom supercell obtained from a $2 \times 2 \times 2$ repetition of the 8 atom conventional lattice. Both C and Ge supercell have this structure, with different lattice constants and respective (scaled) atomic distances.*

The supercell for C and Ge contains 64 atoms, figure 8.2, which is constructed from a $2 \times 2 \times 2$ repetition of the 8 atom conventional lattice. Both E_v calculations (C and Ge) we will be performed at the Γ point in the Brillouin zone.

For E_v calculations using ABINIT our tolerance for convergence with respect to plane wave e_cut is set at 0.01 eV (a similar tolerance is used in [110]), that is if

$$|E_\mathrm{v}^i - E_\mathrm{v}^{i+1}| < 0.01 \text{ eV} \tag{8.2}$$

where i and $i+1$ indicate successive and higher values of e_cut our plane wave E_v calculation

is taken to be converged. This tolerance will also serve as a guideline when AIMPRO's E_v results are compared with that of ABINIT's.

For C and Ge we found that $e_{\text{cut}} = 120$ Ha and $e_{\text{cut}} = 40$ Ha, respectively, was enough to provide a converged E_{v} with ABINIT, these values yielded the E_{v} shown in table 8.3. It should be noted that both plane wave cut-offs used to produce these results are large compared to values used in typical (i.e. non-Δ-value) calculations.

For AIMPRO's E_{v} calculations the results are shown in table 8.3, these were obtained with a basis-$e_{\text{cut}} = 180$ eV and basis-$e_{\text{cut}} = 80$ eV, for C and Ge respectively.

	ABINIT	AIMPRO	Difference
C	6.77390	6.76401	0.0099
Ge	1.00748	1.00677	0.0007

Table 8.3: *Vacancy formation energies for C and Ge calculated using ABINIT and AIMPRO in eV. The third row contains the difference of the previous two values (eV).*

From table 8.3 we find that for both C and Ge the difference in calculated E_{v} between ABINIT and AIMPRO was smaller than 0.01 eV, which is less than the tolerance used during ABINIT's e_{cut} convergence stage. This indicates that filtration was able to produce an ideal vacancy formation that is within the cut-off tolerance of a converged plane wave result, thus we might take AIMPRO's calculation to be as accurate as ABINIT's.

8.2.3 Al un-relaxed ideal vacancy energy

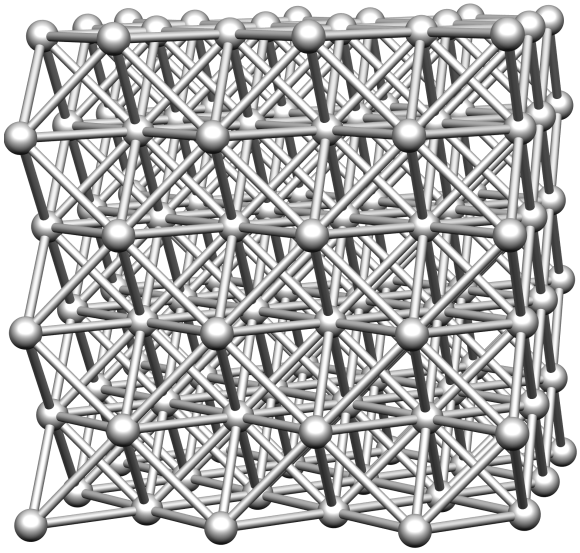

Figure 8.3: *The Aluminium supercell used in the vacancy formation energy calculation.*

The Al supercell, figure 8.3 consist of 108 atoms a $3 \times 3 \times 3$ repetition of the 4 atoms conventional cell.

For Aluminium – and similarly other metals – it is important to choose a reasonable temperature to overcome instabilities that could arise during the self-consistent calculations without temperature smearing (Chapter 3) [113, 115]. Such considerations must also be taken when performing vacancies formation energies calculation [116, 117]. For the work presented here an electronic a Fermi-Dirac smearing function with an electronic temperature of 0.05 eV was used in both ABINIT and `AIMPRO`. Previous research on Al have found the vacancy formation energy calculations to be very sensitive with regards to k-point sampling [118]. A $3 \times 3 \times 3$ k-point mesh has been used in calculations supercell of similar size [119, 119]. For the results presented here, E_{v} is calculated (in ABINIT and `AIMPRO`) over a $10 \times 10 \times 10$ k-point grid.

For ABINIT a plane wave cut-off of 100 Ha was found to produce a converged result, table 8.4. For `AIMPRO` a basis-e_{cut} of 60 eV was used to produced the result shown in table 8.4.

	ABINIT	`AIMPRO`	Difference
Al	0.63932	0.645186	0.0059

Table 8.4: *Vacancy formation energy (eV) for Al calculated using ABINIT and `AIMPRO` using the same calculation settings. The difference between these two values is shown in the third row.*

Here too `AIMPRO's` E_{v} is within 0.01 eV of ABINIT. This further demonstrates filtration ability to provide accurate results for real world applications. Note that here too the plane wave e_{cut} required to converge ABINIT's result is high.

8.3 Conclusion

In this chapter ideal vacancy formation energies (E_{v}) for 3 different structures (with varied electronic properties) were calculated with `AIMPRO` (using filtration) and compared with well converged ABINIT results. We found that `AIMPRO`'s results when compared with ABINIT are within typical tolerance values used to ensure convergence with respect plane wave cut-off in vacancy formation energy calculations. This indicates, as before, the possibility for highly accurate calculations using filtration.

Particularly with respect to the calculation of defects the results presented here, which again show the potential gains in accuracy afforded by filtration, coupled with the large scale efficiency demonstrated elsewhere [5, 16] show the great power of filtration to tackle demanding calculations efficiently and accurately.

It must be noted that achieving results with the level of accuracy presented here required very large plane wave cut-offs. Such values would be impractical for large scale

calculations. However for AIMPRO this is routinely achievable. Essentially we are getting plane wave accuracy at a cost of an efficient GTO implementation. Eventually, as it will be discussed in the future work, we will aim to bring this cost further down. So that large scale calculations could potentially be performed with an accuracy that is characteristic of much smaller systems using plane waves.

Chapter 9

Conclusions and future work

The aim of this work was to demonstrate the potential gains in accuracy that could be obtained by using the filtration methodology in AIMPRO a GTO KSDFT code. Whereas the gains in speed have been previously demonstrated [5], this work has shown for the first time that calculations using filtration can be performed at plane wave like accuracy for a comprehensive set of elements in the periodic table.

First, high quality uncontratcted GTO basis sets, for 70 elements of the periodic table, were generated that yielded an atomic energy (for the respective pseudo-atom) to within 1 meV of the complete basis set limit. In addition these basis sets were generated with properties that made them favourable for an efficient use within the filtration formalism. Particularly, it was shown that our basis set generation routine found the highest α — used to generate the uncontracted even-tempered primitives — for which our atomic tolerance was met. The gains in efficiency and stability which occur from this choice were summarized therein.

An updated filtration methodology, to be used with the basis sets generated in this work, was summarized. Essentially the methodology used here produces a new contracted basis by performing on-site filtration. The parameters which govern this construction are systematically chosen so that for the main results presented here only a single parameter basis-e_{cut} was changed across the different elements. Because of this, from the stand point of a user, the quality of the basis sets is controlled using only one parameter the basis-e_{cut}, which controls the number of contracted functions to be used in the KSDFT calculation.

A recently developed benchmark [3] was used to assess AIMPRO's quality, using the basis sets presented here and filtration. In addition some examples were provided where application of the standard Δ-test can lead to misjudging the quality of a particular atomic calculation, and likely perturbing the resulting overall Δ-value as well. By performing the comparison present in the benchmark with respect to like-to-like well converged plane wave calculations (or other systematic codes), we demonstrated that such problems can be resolved. Particularly, for the work shown in this thesis such a comparison resulted in a

fair assessment of the filtration methodology and our newly developed basis set. We found that AIMPRO's Δ-value calculated with respect to ABINIT was 0.401 meV/atom, which is typically taken to imply that AIMPRO's calculations were indistinguishable from ABINIT. It follows from this that our standard $\Delta_{WIEN2k} = 2.245$ meV/atom was mostly due to pseudization error. This value compares well with ABINIT $\Delta_{WIEN2k} = 2.1$ meV/atom, which required an atypically high plane wave cut-off of 250 Rydberg to reach such accuracy. Essentially demonstrating that with our new basis sets and filtration we are getting very well converged plane wave accuracy at a cost of GTO. At the time of writing no other GTO implementation has a Δ_{WIEN2k} published in [1]. Making AIMPRO's $\Delta_{WIEN2k} = 2.245$ meV/atom the first of its kind.

Unrelaxed vacancy formation energy calculations were performed for supercells of C, Ge and Al. Here it was found that AIMPRO's results were within the tolerance used to ascertain convergence with respect to plane wave cut-off e_{cut} for a plane wave implementation. This once more demonstrates that plane-wave-like accuracy is made possible by our high quality basis set and filtration, only in this instance a real world class of problems were attempted, rather than just a benchmark. For ideal vacancy formation energies reaching a convergence of 0.01 eV with respect to energy cut-off with plane waves required high cut-off values which are computational demanding and would certainly not be used in typical "production" calculations. This once more demonstrates the many possibilities of the current filtration methodology and our basis sets.

In short we have demonstrated that combining filtration with a high quality underpinning basis set has resulted in plane wave accuracy at a much reduced computational cost. With the added benefit, from a user's point of view, that said accuracy can be obtained systematically using the same GTO basis set.

9.1 Future work

This study has shown that filtration can perform calculations with plane wave accuracy at a fraction of it's computational cost. We hope that in the future filtration will be used to tackle a great variety of problems, which would otherwise be computationally expensive even at moderate accuracies.

Although a tremendous success, the current filtration methodology can be further improved in both its accuracy and speed. Current AIMPRO development aims to handle basis sets with h and i angular momentum values at little added cost when compared to the implementation used in this work. Once this newer version of AIMPRO is available the uncontracted primitives can be generated with an angular momentum value 2 (or even 3) above the respective highest angular momentum value present in the atom. This would

enormously reduce any residual error associated with the primitive basis set, a conclusion that seems clear form the discussion of Cl in the previous chapter.

Once such basis sets begin to be used within filtration it is likely that the Fermi energy, which controls the filtration function, will need to be systematically integrated with basis-e_{cut} to avoid instabilities during the filtered basis KSDFT calculation. Some work was done in the previous chapter where the Fermi energy was manually tweaked and indeed some types of instabilities for just 4 atoms were resolved in this manner. Furthermore for primitive basis sets with very large angular momentum the lowest exponent of the trial basis will probably need to be increased, particularly for trial functions with very large angular momentum. Some work has also been done in this area during this project, which should be revisited once the updated version of `AIMPRO` is available.

Whilst the discussion in this thesis is focused on attaining plane wave like accuracy, originally filtration was introduced as a method to speed up the calculations considerably whilst maintaining reasonable accuracy. However the speed factor can be reintroduced in the current methodology whilst retaining the quality of the results presented here. This will be accomplished by having multi step filtration, that is performing a second stage filtration (or more) after the first one is performed within the same calculation. This will likely hide the overhead that one incurs by dealing with such large primitive basis. Most likely this will also help with the stability of the overall calculation.

As it was demonstrated here, most of `AIMPRO`'s standard Δ value could be attributed to the use of pseudopotentials. Given GTOs natural flexibility in handling harder pseudopotentials, it stands to reason that if they are generated we could get `AIMPRO`'s Δ to be within the range obtained using all electron results. Such accuracy would most likely be very expensive to attain with regular plane wave codes.

Finally, relativistic effects could be incorporated besides the averaged way in which they are handled in pseudopotentials. This would contribute to an even lower standard Δ-value, and we would expect that the individual Δ^i for heavier elements would benefit significantly from this, and codes used to "define" a standard Δ use approximations to relativistic theory.

If these further developments are made, there is no reason why `AIMPRO` can not have a standard Δ-value of 0-0.5 meV/atom together with an asymptotic speed similar to tight-binding or semi-empirical quantum chemistry approaches. This would be a very impressive end point to this investigation.

References

[1] Comparing solid state DFT codes, basis sets and potentials. [Online]. Available: https://molmod.ugent.be/deltacodesdft

[2] C. for Multi-scale Chemical Science (CMCS) project. Basis set exchange. [Online]. Available: https://bse.pnl.gov/bse/portal

[3] K. Lejaeghere *et al.*, "Reproducibility in density functional theory calculations of solids," *Science*, vol. 351, no. 6280, 2016.

[4] P. Haas, F. Tran, and P. Blaha, "Calculation of the lattice constant of solids with semilocal functionals," *Phys. Rev. B*, vol. 79, no. 8, p. 085104, 2009.

[5] M. J. Rayson and P. R. Briddon, "Highly efficient method for Kohn-Sham density functional calculations of $500 - 10\,000$ atom systems," *Phys. Rev. B*, vol. 80, p. 205104, 2009.

[6] K. Lejaeghere *et al.*, "Error estimates for solid-state density-functional theory predictions: An overview by means of the ground-state elemental crystals," *Crit. Rev. Solid State Mater. Sci.*, vol. 39, 04 2012.

[7] J. Sakuray, *Modern Quantum Mechanics*. Addison-Wesley Publishing Company, 1994.

[8] J. D. Griffiths, *Introduction to quantum mechanics*. Cambridge University Press, 2005.

[9] P. Tipler and R. A. Llewellyn, *Modern Physics*. W. H. Freeman, 2000.

[10] E. Merzbacher, *Quantum Mechanics*. Wiley, 1970.

[11] P. Hohenberg and W. Kohn, "Inhomogeneous electron gas," *Phys. Rev.*, vol. 136, pp. B864–B871, 1964.

[12] M. Levy, "Electron densities in search of Hamiltonians," *Phys. Rev. A*, vol. 26, pp. 1200–1208, 1982.

[13] T. L. Gilbert, "Hohenberg-Kohn theorem for nonlocal external potentials," *Phys. Rev. B*, vol. 12, pp. 2111–2120, 1975.

[14] S. Goedecker, "Linear scaling electronic structure methods," *Rev. Mod. Phys.*, vol. 71, pp. 1085–1123, 1999.

[15] D. R. Bowler and T. Miyazaki, "$\mathcal{O}$(n) methods in electronic structure calculations," *Rep. Prog. Phys.*, vol. 75, no. 3, p. 036503, 2012.

[16] P. R. Briddon and M. J. Rayson, "Accurate Kohn-Sham DFT with the speed of tight binding: Current techniques and future directions in materials modelling," *Phys. Status Solidi B*, vol. 248, no. 6, pp. 1309–1318.

[17] D. M. Ceperley and B. J. Alder, "Ground state of the electron gas by a stochastic method," *Phys. Rev. Lett.*, vol. 45, pp. 566–569, 1980.

[18] J. P. Perdew and A. Zunger, "Self-interaction correction to density-functional approximations for many-electron systems," *Phys. Rev. B*, vol. 23, pp. 5048–5079, 1981.

[19] J. P. Perdew and Y. Wang, "Accurate and simple analytic representation of the electron-gas correlation energy," *Phys. Rev. B*, vol. 45, pp. 13 244–13 249, 1992.

[20] U. von Barth and L. Hedin, "A local exchange-correlation potential for the spin polarized case: I," vol. 5, no. 13, pp. 1629–1642, 1972.

[21] J. Grotendorst, S. Blugel, and D. Marx, Eds., *Computational Nanoscience: Do It Yourself!* NIC series, vol. 31.

[22] P. Briddon and R. Jones, "LDA calculations using a basis of Gaussian orbitals," *Phys. Status Solidi B*, vol. 217, no. 1, pp. 131–171, 2000.

[23] M. Springborg, R. C. Albers, and K. Schmidt, "Fractional occupancies and temperature in electronic-structure calculations," *Phys. Rev. B*, vol. 57, pp. 1427–1435, 1998.

[24] L. Genovese *et al.*, "Daubechies wavelets as a basis set for density functional pseudopotential calculations," *J. Chem. Phys.*, vol. 129, no. 1, p. 014109, 2008.

[25] "An alternative way of linearizing the augmented plane-wave method," *Solid State Communications*, vol. 114, no. 1, pp. 15–20, 2000.

[26] J. C. Slater, "Atomic shielding constants," *Phys. Rev.*, vol. 36, pp. 57–64, 1930.

[27] T. Kato, "On the eigenfunctions of many-particle systems in quantum mechanics," *Commun. Pure Appl. Math.*, vol. 10, no. 2, pp. 151–177, 1957.

[28] X. Gonze *et al.*, "ABINIT: First-principles approach to material and nanosystem properties," *Comput. Phys. Commun.*, vol. 180, pp. 2582–2615, 2009.

[29] R. Car and M. Parrinello, "Unified approach for molecular dynamics and density-functional theory," *Phys. Rev. Lett.*, vol. 55, pp. 2471–2474, 1985.

[30] R. Car, M. Parrinello, and S. Baroni, "Conjugate gradient minimization of the energy functional: A new method for electronic structure calculation," *Phys. Rev. B*, vol. 39, pp. 4997–5004, 1989.

[31] M. Segall *et al.*, "First-principles simulation: ideas, illustrations and the CASTEP code," *J. Phys. Condens. Matter*, vol. 14, pp. 2717–2744, 2002.

[32] M. J. Rayson, "Lagrange-Lobatto interpolating polynomials in the discrete variable representation," *Phys. Rev. E*, vol. 76, p. 026704, 2007.

[33] S. Obara and A. Saika, "Efficient recursive computation of molecular integrals over Cartesian Gaussian functions," *J. Chem. Phys.*, vol. 84, no. 7, pp. 3963–3974, 1986.

[34] J. C. Phillips and L. Kleinman, "New method for calculating wave functions in crystals and molecules," *Phys. Rev.*, vol. 116, pp. 287–294, 1959.

[35] E. Antonick, "Approximate formulation of the orthogonalized plane-wave method," *J. Phys. Chem. Solids*, vol. 10, no. 4, pp. 314–320, 1959.

[36] D. R. Hamann, M. Schlluter, and C. Chiang, "Norm-conserving pseudopotentials," *Phys. Rev. Lett.*, vol. 43, pp. 1494–1497, 1979.

[37] G. Bachelet, D. R. Hamann, and M. Schlüter, "Pseudopotentials that work: From H to Pu," *Phys. Rev. B*, vol. 26, pp. 4199–4228, 1982.

[38] S. Goedecker, M. Teter, and J. Hutter, "Separable dual-space Gaussian pseudopotentials," *Phys. Rev. B*, vol. 54, pp. 1703–1710, 1996.

[39] M. Krack, "Pseudopotentials for H to Kr optimized for gradient-corrected exchange-correlation functionals," *Theor. Chem. Acc.*, vol. 114, no. 1, pp. 145–152, 2005.

[40] M. Rayson, "Rapid filtration algorithm to construct a minimal basis on the fly from a primitive Gaussian basis," *Comput. Phys. Commun.*, vol. 181, no. 6, pp. 1051–1056, 2010.

[41] J. P. Perdew, K. Burke, and M. Ernzerhof, "Generalized gradient approximation made simple," *Phys. Rev. Lett.*, vol. 77, pp. 3865–3868, 1996.

[42] J. P. Perdew *et al.*, "Atoms, molecules, solids, and surfaces: Applications of the generalized gradient approximation for exchange and correlation," *Phys. Rev. B*, vol. 46, pp. 6671–6687, 1992.

[43] J. P. Perdew and W. Yue, "Accurate and simple density functional for the electronic exchange energy: Generalized gradient approximation," *Phys. Rev. B*, vol. 33, pp. 8800–8802, 1986.

[44] J. A. White and D. M. Bird, "Implementation of gradient-corrected exchange-correlation potentials in Car-Parrinello total-energy calculations," *Phys. Rev. B*, vol. 50, pp. 4954–4957, 1994.

[45] A. Baldereschi, "Mean-value point in the Brillouin zone," *Phys. Rev. B*, vol. 7, pp. 5212–5215, 1973.

[46] D. J. Chadi, "Special points for Brillouin-zone integrations," *Phys. Rev. B*, vol. 16, pp. 1746–1747, 1977.

[47] P. E. Blöchl, O. Jepsen, and O. K. Andersen, "Improved tetrahedron method for brillouin-zone integrations," *Phys. Rev. B*, vol. 49, pp. 16 223–16 233, 1994.

[48] H. J. Monkhorst and J. D. Pack, "Special points for Brillouin-zone integrations," *Phys. Rev. B*, vol. 13, pp. 5188–5192, 1976.

[49] F. Jensen, "Polarization consistent basis sets: Principles," *J. Chem. Phys.*, vol. 115, no. 20, pp. 9113–9125, 2001.

[50] T. Helgaker and P. R. Taylor, *Gaussian basis sets and molecular integrals*, 1994.

[51] J. G. Hill, "Gaussian basis sets for molecular applications," *Int. J. Quantum Chem.*, vol. 113, no. 1, pp. 21–34, 2012.

[52] R. Ditchfield, W. J. Hehre, and J. A. Pople, "Self-consistent molecular-orbital methods. ix. An extended Gaussian-type basis for molecular-orbital studies of organic molecules," *J. Chem. Phys.*, vol. 54, no. 2, pp. 724–728, 1971.

[53] M. W. Schmidt and K. Ruedenberg, "Effective convergence to complete orbital bases and to the atomic Hartree-Fock limit through systematic sequences of Gaussian primitives," *J. Chem. Phys.*, vol. 71, no. 10, pp. 3951–3962, 1979.

[54] S. Wilson, "Universal systematic sequence of even-tempered Gaussian primitive functions in electronic correlation studies," *Theor. Chim. Acta.*, vol. 58, no. 1, pp. 31–40, 1980.

[55] R. D. Bardo and K. Ruedenberg, "Even-tempered atomic orbitals. VI. Optimal orbital exponents and optimal contractions of Gaussian primitives for hydrogen, carbon, and oxygen in molecules," *J. Chem. Phys.*, vol. 60, pp. 918–931, 1974.

[56] E. Papajak*et al.*, "Perspectives on basis sets beautiful: Seasonal plantings of diffuse basis functions," *J. Chem. Theory Comput.*, vol. 7, no. 10, pp. 3027–3034, 2011.

[57] R. C. Raffenetti, "General contraction of Gaussian atomic orbitals: Core, valence, polarization, and diffuse basis sets; molecular integral evaluation," *J. Chem. Phys.*, vol. 58, no. 10, pp. 4452–4458, 1973.

[58] G. A. Petersson *et al.*, "On the optimization of Gaussian basis sets," *J. Chem. Phys.*, vol. 118, no. 3, pp. 1101–1109, 2003.

[59] F. Jensen, "The basis set convergence of the Hartree-Fock energy for h_3^+, li_2 and n_2." *Theor. Chem. Acc.*, vol. 104, no. 6, pp. 484–490, 2000.

[60] E. S. Kryachko and S. Wilson, "Generation of systematic sequences of even-tempered basis sets: Empirical generating formulae," *Int. J. Quantum Chem.*, vol. 93, no. 2, pp. 112–120, 2003.

[61] D. M. Silver and W. Nieuwpoort, "Universal atomic basis sets," *Chem. Phys. Lett.*, vol. 57, no. 3, pp. 421–422, 1978.

[62] S. Wilson and D. M. Silver, "Universal basis sets in molecular calculations," *Chem. Phys. Lett.*, vol. 63, pp. 367–369, 1979.

[63] F. Jensen, "Atomic orbital basis sets," *Wiley. Interdiscip. Rev. Comput. Mol. Sci.*, vol. 3, no. 3, pp. 273–295, 2013.

[64] H. W. Jones and B. Etemadi, "Multicenter molecular integrals using harmonic expansions of Slater-type orbitals and numerical integrations," *Int. J. Quantum Chem.*, vol. 38, no. 24, pp. 405–410, 1990.

[65] S. F. Boys and A. C. Egerton, "Electronic wave functions - I. A general method of calculation for the stationary states of any molecular system," vol. 200, no. 1063, pp. 542–554, 1950.

[66] F. Jensen *et al.*, "The elephant in the room of density functional theory calculations," *J. Phys. Chem. Lett.*, vol. 8, no. 7, pp. 1449–1457, 2017.

[67] J. S. Binkley, J. A. Pople, and W. J. Hehre, "Self-consistent molecular orbital methods. 21. Small split-valence basis sets for first-row elements," *J. Am. Chem. Soc.*, vol. 102, no. 3, pp. 939–947, 1980.

[68] M. S. Gordon *et al.*, "Self-consistent molecular-orbital methods. 22. Small split-valence basis sets for second-row elements," *J. Am. Chem. Soc.*, vol. 104, no. 10, pp. 2797–2803, 1982.

[69] K. Faegri and H. J. Speis, "Basis set quality vs size. approximate Gaussian type orbital (GTO) wave functions for first row transition metal atoms," *J. Chem. Phys.*, vol. 86, no. 12, pp. 7035–7040, 1987.

[70] T. H. Dunning Jr., "Gaussian basis sets for use in correlated molecular calculations. i. The atoms boron through neon and hydrogen," *J. Chem. Phys.*, vol. 90, no. 2, pp. 1007–1023, 1989.

[71] K. A. Peterson and T. H. Dunning Jr., "Accurate correlation consistent basis sets for molecular core-valence correlation effects: The second row atoms Al-Ar, and the first row atoms B-Ne revisited," *J. Chem. Phys.*, vol. 117, no. 23, pp. 10 548–10 560, 2002.

[72] F. Weigend, F. Furche, and R. Ahlrichs, "Gaussian basis sets of quadruple zeta valence quality for atoms HâĂŞKr," *J. Chem. Phys.*, vol. 119, no. 24, pp. 12 753–12 762, 2003.

[73] J. A. Nelder and R. Mead, "A simplex method for function minimization," *Comput. J.*, vol. 7, no. 4, pp. 308–313, 1965.

[74] M. J. D. Powell, "On search directions for minimization algorithms," *Math. Program.*, vol. 4, no. 1, pp. 193–201, 1973.

[75] H. W. Press *et al.*, *Numerical Recipes in Fortran 77: The Art of Scientific Computing*. Cambridge University Press, 1992.

[76] L. A. Curtiss *et al.*, "Assessment of Gaussian-2 and density functional theories for the computation of enthalpies of formation," *J. Chem. Phys.*, vol. 106, no. 3, pp. 1063–1079, 1997.

[77] R. B. Morgan, "Generalizations of Davidson's method for computing eigenvalues of large nonsymmetric matrices," *J. Comput. Phys.*, vol. 101, no. 2, pp. 287–291, 1992.

[78] A. Stathopoulos and C. F. Fischer, "A Davidson program for finding a few selected extreme eigenpairs of a large, sparse, real, symmetric matrix," *Comput. Phys. Commun.*, vol. 79, no. 2, pp. 268–290, 1994.

[79] A. V. Knyazev and K. Neymeyr, "Efficient solution of symmetric eigenvalue problems using multigrid preconditioners in the locally optimal block conjugate gradient method," vol. 15, pp. 38–55, 2003.

[80] I. Nebot-Gil, "Diagonalization of large matrices: A new parallel algorithm," *J. Chem. Theory Comput.*, vol. 11, no. 2, pp. 472–483, 2015.

[81] M. J. Rayson and P. R. Briddon, "Rapid iterative method for electronic-structure eigenproblems using localised basis functions," *Comput. Phys. Commun.*, vol. 178, pp. 128–134, 2008.

[82] C. D. Reddy, Z. G. Yu, and Y.-W. Zhang, "Two-dimensional Van der Waals C60 molecular crystal," *Sci. Rep.*, vol. 5, 2015.

[83] R. Z. Khaliullin, J. VandeVondele, and J. Hutter, "Efficient linear-scaling density functional theory for molecular systems," *J. Chem. Theory Comput.*, vol. 9, no. 10, pp. 4421–4427, 2013.

[84] J. Aarons *et al.*, "Perspective: Methods for large-scale density functional calculations on metallic systems," *J. Chem. Phys.*, vol. 145, no. 22, p. 220901, 2016.

[85] B. Aradi, B. Hourahine, and T. Frauenheim, "Dftb+, a sparse matrix-based implementation of the dftb method," *J. Phys. Chem. A*, vol. 111, no. 26, pp. 5678–5684, 2007.

[86] P. Koskinen and V. Mäkinen, "Density-functional tight-binding for beginners," *Comput. Mater. Sci.*, vol. 47, no. 1, pp. 237–253, 2009.

[87] W. Kohn, "Density functional and density matrix method scaling linearly with the number of atoms," *Phys. Rev. Lett.*, vol. 76, pp. 3168–3171, 1996.

[88] I. Turel and J. Kljun, "Interactions of metal ions with DNA, its constituents and derivatives, which may be relevant for anticancer research," *Current topics in medicinal chemistry*, vol. 11, no. 21, pp. 2661–2687, 2011.

[89] L. A. Hardegger *et al.*, "Systematic investigation of halogen bonding in protein-ligand interactions," *Angew. Chem. Int. Ed.*, vol. 50, no. 1, pp. 314–318, 2011.

[90] E. Prodan and W. Kohn, "Nearsightedness of electronic matter," *Proc. Natl. Acad. Sci. U.S.A.*, vol. 102, no. 33, pp. 11 635–11 638, 2005.

[91] E. Artacho *et al.*, "Linear-scaling ab-initio calculations for large and complex systems," *Phys. Status Solidi B*, vol. 215, no. 1, pp. 809–817, 1999.

[92] E. Artacho *et* al., "Electrons in dry DNA from density functional calculations," *Mol. Phys.*, vol. 101, no. 11, pp. 1587–1594, 2003.

[93] J. S. Mitchell, C. A. Laughton, and S. A. Harris, "Atomistic simulations reveal bubbles, kinks and wrinkles in supercoiled DNA," *Nucleic Acids Res.*, vol. 39, no. 9, pp. 3928–3938, 2011.

[94] W. Yang, "Direct calculation of electron density in density-functional theory," *Phys. Rev. Lett.*, vol. 66, pp. 1438–1441, 1991.

[95] N. Hine *et al.*, "Linear-scaling density-functional theory with tens of thousands of atoms: Expanding the scope and scale of calculations with ONETEP," *Comput. Phys. Commun.*, vol. 180, no. 7, pp. 1041–1053, 2009.

[96] G. E. Scuseria, "Linear scaling density functional calculations with Gaussian orbitals," *J. Phys. Chem. A*, vol. 103, no. 25, pp. 4782–4790, Jun 1999.

[97] N. Mardirossian and M. Head-Gordon, "Thirty years of density functional theory in computational chemistry: An overview and extensive assessment of 200 density functionals," *Mol. Phys.*, vol. 115, no. 19, pp. 2315–2372, 2017.

[98] H. S. Yu, S. L. Li, and D. G. Truhlar, "Perspective: Kohn-Sham density functional theory descending a staircase," *J. Chem. Phys.*, vol. 145, no. 13, p. 130901, 2016.

[99] P. Haas, F. Tran, and P. Blaha, "Calculation of the lattice constant of solids with semilocal functionals," *Phys. Rev. B*, vol. 79, p. 085104, 2009.

[100] A. Gulansand, A. Kozhevnikov, and C. Draxl, "Microhartree precision in density functional theory calculations," *Phys. Rev. B*, vol. 97, p. 161105, 2018.

[101] C. Kittel, *Introduction to Solid State Physics.* Wiley, 2005.

[102] W. B. Holzapfel, M. Hartwig, and W. Sievers, "Equations of state for Cu, Ag, and Au for wide ranges in temperature and pressure up to 500 GPa and above," *J. Phys. Chem. Ref. Data*, vol. 30, no. 2, pp. 515–529, 2001.

[103] K. Dewhurst *et al.* The Elk FP-LAPW code. [Online]. Available: http://elk.sourceforge.net/

[104] A. Gulans *et al.*, "exciting: a full-potential all-electron package implementing density-functional theory and many-body perturbation theory," *J. Phys. Condens. Matter*, vol. 26, no. 36, p. 363202, 2014.

[105] V. Blum *et al.*, "Ab initio molecular simulations with numeric atom-centered orbitals," *Comput. Phys. Commun.*, vol. 180, no. 11, pp. 2175–2196, 2009.

[106] S. Blügel *et al.* FLEUR: The Jülich FLAPW code family. [Online]. Available: http://www.flapw.de/pm/index.php?n=Main.HomePage

[107] K. Koepernik and H. Eschrig, "Full-potential nonorthogonal local-orbital minimum-basis band-structure scheme," *Phys. Rev. B*, vol. 59, pp. 1743–1757, 1999.

[108] RSPt. [Online]. Available: http://www.physics.uu.se/research/materials-theory/ongoing-research/code-development/rspt-main/

[109] N. D. M. Hine *et al.*, "Linear-scaling density-functional simulations of charged point defects in Al2O3 using hierarchical sparse matrix algebra," *J. Chem. Phys.*, vol. 133, no. 11, p. 114111, 2010.

[110] M. I. J. Probert and M. C. Payne, "Improving the convergence of defect calculations in supercells: An ab initio study of the neutral silicon vacancy," *Phys. Rev. B*, vol. 67, p. 075204, 2003.

[111] F. Corsetti and A. A. Mostofi, "System-size convergence of point defect properties: The case of the silicon vacancy," *Phys. Rev. B*, vol. 84, p. 035209, 2011.

[112] G. Ho *et al.*, "Energetics and kinetics of vacancy diffusion and aggregation in shocked aluminium via orbital-free density functional theory," *Phys. Chem. Chem. Phys.*, vol. 9, pp. 4951–4966, 2007.

[113] M. J. Gillan, "Calculation of the vacancy formation energy in aluminium," *J. Phys. Condens. Matter*, vol. 1, no. 4, p. 689, 1989.

[114] B. Radhakrishnan and V. Gavini, "Effect of cell size on the energetics of vacancies in aluminum studied via orbital-free density functional theory," *Phys. Rev. B*, vol. 82, p. 094117, 2010.

[115] B. Grabowski, T. Hickel, and J. Neugebauer, "Ab initio study of the thermodynamic properties of nonmagnetic elementary fcc metals: Exchange-correlation-related error bars and chemical trends," *Phys. Rev. B*, vol. 76, p. 024309, 2007.

[116] T. R. Mattsson and A. E. Mattsson, "Calculating the vacancy formation energy in metals: Pt, Pd, and Mo," *Phys. Rev. B*, vol. 66, p. 214110, 2002.

[117] T. Korhonen, M. J. Puska, and R. M. Nieminen, "Vacancy-formation energies for fcc and bcc transition metals," *Phys. Rev. B*, vol. 51, pp. 9526–9532, 1995.

[118] D. E. Turner *et al.*, "Energetics of vacancy and substitutional impurities in aluminum bulk and clusters," *Phys. Rev. B*, vol. 55, pp. 13 842–13 852, 1997.

[119] T. Angsten *et al.*, "Elemental vacancy diffusion database from high-throughput first-principles calculations for fcc and hcp structures," *New J. Phys.*, vol. 16, no. 1, 2014.